1. Přílohy

Kopie recenzovaných odborných článků publikovaných v časopisech s impakt faktorem související s tématem disertační práce

1.1. **P1**

Novakova V., Zimcik P., Miletin M., VACHOVA L., Kopecky K., Lang K., Chabera P., Polivka T.: Ultrafast intramolecular charge transfer in tetrapyrazinoporphyrazines controls the quantum yields of fluorescence and singlet oxygen. *Phys. Chem. Chem. Phys*., **2010**,12, 11, 2555-2563. IF_{2016} 4,123.

(Tato práce vznikla za použití dat z mé diplomové práce. Není proto uplatněna jako podklad pro získání titulu Ph.D.)

Ultrafast intramolecular charge transfer in tetrapyrazinoporphyrazines controls the quantum yields of fluorescence and singlet oxygen†

Veronika Novakova,[a] Petr Zimcik,*[a] Miroslav Miletin,[a] Lenka Vachova,[a] Kamil Kopecky,[a] Kamil Lang,*[b] Pavel Chábera[c] and Tomáš Polívka[c]

Received 9th September 2009, Accepted 18th November 2009
First published as an Advance Article on the web 21st January 2010
DOI: 10.1039/b918546a

A series of octasubstituted zinc(II) tetrapyrazinoporphyrazines (TPyzPz), aza-analogues of phthalocyanines, differing in the number of peripheral *N*,*N*-diethylamino (n = 0–8) and *tert*-butylsulfanyl substituents ($m = 8 - n$) has been synthesized. All possible congeners were characterized including adjacent and opposite isomers. Steady-state (UV-vis, fluorescence) and time-resolved (fluorescence, femtosecond transient absorption) spectroscopies, redox and photochemical (singlet oxygen formation) properties were investigated and compared. The peripheral tertiary amino substituents (donor) induce a new competitive relaxation pathway to fluorescence and intersystem crossing due to the mixing of the first excited state S_1 of the TPyzPz macrocycle with a nearby intramolecular charge transfer (ICT) state. The fluorescence quantum yield and fluorescence lifetime of **6Zn** bearing one *N*,*N*-diethylamino substituent (n = 1, m = 7) decreased with increasing solvent polarity, while the same observables of **5Zn** with no donor centre (n = 0, m = 8) were not affected. Protonation of the *N*,*N*-diethylamino substituent in **6Zn** led to a strong increase of the fluorescence intensity. The cyclic voltammetry data, the steady-state and time-resolved emission and transient absorption studies revealed strong electronic coupling between the TPyzPz moiety and *N*,*N*-diethylamino substituents. ICT is an extremely rapid process occurring with a time constant of 10 ps and 7 ps in **6Zn** (n = 1, m = 7) and **11Zn** (n = 8, m = 0) in pyridine, respectively. The ICT efficiency decreased in non-polar solvents. The presence of two *N*,*N*-diethylamino substituents in **7Zn** (n = 2, m = 6) considerably quenched the S_1 states in pyridine (polar, coordinating), toluene (non-polar, non-coordinating) and toluene–1% pyridine (v/v) (non-polar, coordinating). The photophysical properties of compounds with more donor substituents on the periphery ($n > 2$, $m < 6$) were similar to those of **7Zn**.

Introduction

In recent years, tetrapyrazinoporphyrazines (TPyzPz), phthalocyanine (Pc) aza-analogues, have steadily attracted the attention of researchers due to the interesting photochemical, photophysical and electrochemical properties.[1–7] Our previous work has focused on the synthesis of TPyzPz derivatives and description of their photophysical and photochemical properties related to photodynamic therapy. The intense absorption bands above 650 nm, fluorescence and high singlet oxygen quantum yields are advantageous for this application.[8] We have formulated structure–activity relationships for alkyl-heteroatom substituted TPyzPz and demonstrated that heteroatoms connecting the peripheral chain to the macrocyclic core play an essential role.[9] Thus, the derivatives with the sulfur or oxygen linkages have high quantum yields of fluorescence and singlet oxygen, while the presence of nitrogen heteroatoms decreases these parameters almost to zero. This is consistent with observations that the quantum yields strongly decrease when a nitrogen atom is a part of a peripheral[10] or central aliphatic substituent[11] suggesting that the excited states of alkylamino TPyzPz and Pc undergo competitive nonradiative decay processes. A plausible explanation is intramolecular photoinduced electron transfer (PET) occurring between the donor (lone pair on the peripheral nitrogen) and the acceptor (the macrocyclic system) separated from the donor by an aliphatic bridge. As a consequence, the photoexcited macrocycle is reductively quenched.

A photoexcited macrocycle can act as a donor or acceptor in the PET processes. Mostly, Pc acts as a donor, *i.e.*, undergoes the oxidative quenching. The constructs usually employ Pc–fullerene conjugates due to the readiness of fullerenes to accept electrons and are widely investigated as artificial light-harvesting systems for solar energy conversion.[12–17]

[a] *Department of Pharmaceutical Chemistry and Drug Control, Faculty of Pharmacy in Hradec Kralove, Charles University in Prague, Heyrovskeho 1203, Hradec Kralove, 50005, Czech Republic. E-mail: petr.zimcik@faf.cuni.cz; Fax: +420 495067167; Tel: +420 495067257*
[b] *Institute of Inorganic Chemistry of the Academy of Sciences of the Czech Republic, v.v.i., 250 68 Řež, Czech Republic. E-mail: lang@iic.cas.cz*
[c] *Institute of Physical Biology, University of South Bohemia, Zámek 136, 373 33 Nové Hrady, Czech Republic*

† Electronic supplementary information (ESI) available: Synthesis and characterization of compounds; experimental details for thin layer chromatography; UV-vis spectra; fluorescence spectra; titration of toluene solutions with pyridine; dependence of fluorescence quantum yields on the number of donor centers; titration with sulfuric acid. See DOI: 10.1039/b918546a

Pc–perylenes,[18,19] Pc–flavin[20] and Pc–porphyrins[21] also showed interesting electron-transfer properties. Only a few examples of dyads or triads utilize the Pc macrocycles as electron acceptors.[22–25] Daraio *et al.* showed that excited Pc singlet and triplet states are quenched by aliphatic and aromatic amines in cationic micelles due to intermolecular PET.[26,27] Based on their findings we have suggested that a similar process can be responsible for quenching of excited states in alkylamino TPyzPz.[28]

To study the photophysical properties of TPyzPz we have designed a derivative bearing a single donor *N*,*N*-diethylamino substituent (**6Zn**, Chart 1) and compared its properties with model compound **5Zn** having eight *tert*-butylsulfanyl substituents. As nitrogen atoms are conjugated with the macrocycle, the first excited S_1 state of the macrocycle is transformed to a nearby intramolecular charge transfer (ICT) state. In this non-fluorescent state an electron is transferred from the *N*,*N*-diethylamino substituent to the TPyzPz macrocycle. One donor substituent may not be enough to observe changes and that is why compound **11Zn** with eight donor centres was prepared (Chart 1). The bulkiness of peripheral substituents reduced aggregation caused by π–π interactions of planar macrocycles (H-aggregates) to a minimum. Generally, aggregation decreases the fluorescence and singlet oxygen quantum yields of porphyrinoid compounds due to new nonradiative relaxation channels of the excited states[8,29] and would misrepresent the experimental results. Metal-free Pc and TPyzPz have low fluorescence and singlet oxygen quantum yields and therefore the changes induced by competitive ICT would not be well observable. In this respect, metallation by zinc (II) is advantageous because it significantly increases fluorescence and lengthens the triplet state lifetimes.[29,30]

The first part of the work is devoted to the quantification of relaxation processes within **5Zn**, **6Zn** and **11Zn** compounds including the characterization of the ICT state. In the second part, the photophysical and photochemical properties of a series of compounds **5Zn–11Zn** (Chart 1) are complemented and the influence of the number of donor centres is described in detail.

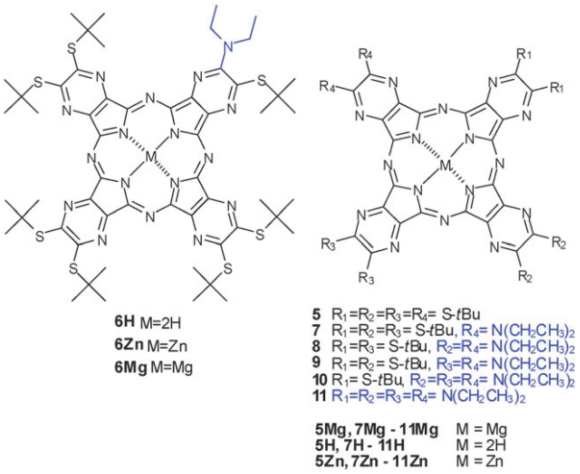

Chart 1 Structures of compounds.

Results and discussion

Synthesis

TPyzPz are usually synthesized by cyclotetramerization of appropriate pyrazinedicarbonitriles. Precursors **1**,[31] **3**[32] and **4**[33] were prepared according to the published procedures. Compound **2** was synthesized by nucleophilic substitution of chlorine atom in **1** by *tert*-butylthiolate in a good yield (Scheme 1).

There are several ways for the preparation of unsymmetrical TPyzPz.[34] Among them, statistical condensation of precursors A and B followed by column chromatography is the most often used method, especially if all possible congeners (AAAA, AAAB, AABB, ABAB, ABBB, BBBB) are of interest.[35–37]

Our first attempts to prepare zinc complexes **5Zn–11Zn** directly by heating precursors in DMF with zinc acetate as a template failed. Cyclotetramerization proceeded well, however, we were not able to separate congeners because of an extensive tailing on TLC plates (see the ESI, Fig. S1†). As symmetrical metal-free compounds **5H** and **11H** have well-separated retention factors and the spots are of an ideal round shape with no significant tailing, we modified the synthetic sequence as follows: the preparation of magnesium (II) complexes **5Mg–11Mg**, removal of central magnesium to get **5H–11H**, separation of congeners, and finally metallation of isolated macrocycles with zinc(II) cation (Scheme 1).

The distribution of congeners in statistical condensation strongly depends on the reactivity and the ratio of precursors used for cyclization.[34,38] The reactivity of both **2** and **3** is similar, thus, three equivalents of **3** with one equivalent of **2** shifted the reaction equilibrium toward **6Mg** (Scheme 1, Reaction A). The reactivity of **3** and **4** is also very similar,

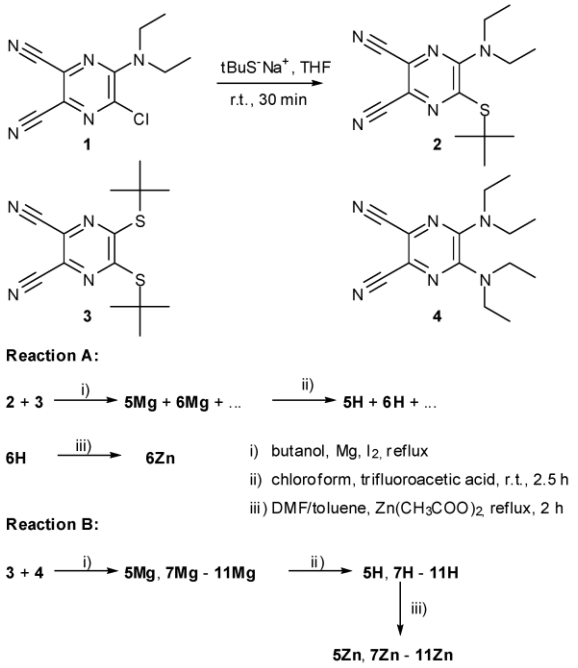

Scheme 1 Synthesis of investigated compounds.

that is why the ratio 1 : 1 was used to ensure reasonable yields of congeners **5Mg**, **7Mg–11Mg** in a one-pot reaction (Scheme 1, Reaction B).

The treatment of magnesium TPyzPz complexes with trifluoroacetic acid yielded a mixture of metal-free TPyzPz. After demetallation, the congeners were separated by column chromatography on silica using a step-gradient elution followed by the repurification of each congener by column chromatography (see the ESI†). Using this methodology we succeeded in the rarely achieved isolation of two positional isomers—opposite **8H** (ABAB type) and adjacent **9H** (AABB type).[39 41] Pure compounds **5H–11H** were then treated with anhydrous zinc acetate in pyridine to obtain corresponding **5Zn–11Zn** followed by final repurification by column chromatography on silica. All synthetic procedures are described in detail in the ESI† including the complete characterization of all compounds.

UV-vis absorption

The absorption spectra of prepared **5Zn–11Zn** in coordinating solvents like tetrahydrofuran or pyridine exhibited typical features of monomeric TPyzPz with no aggregation tendency even at high concentrations (measured up to 1×10^{-4} M). The Q-bands and Soret bands in pyridine are between 657–664 nm and 380–385 nm, respectively. There is also a small red shift of the Q-bands in the series from **5Zn** to **11Zn** (Table 1, Fig. 1) as a consequence of the increasing number of *N*,*N*-diethylamino substituents. Although the splitting of the Q-band can be expected for **6Zn–10Zn** due to the loss of the macrocycle symmetry, only the Q-band of **8Zn** exhibits considerable splitting with two resolved peaks at about 657 and 670 nm (Fig. 1). Similar observations have been already described for other TPyzPz derivatives[35,42] and are in accordance with the fact that the strongest splitting of the Q-band is observed for congeners of the ABAB type[43,44] (*i.e.*, in our case **8Zn**). Ground-state charge transfer interactions in substituted TPyzPz, especially in **10Zn** and **11Zn**, are manifested by broad absorption bands within 520–540 nm in pyridine, well separated from other electronic transitions. The CT absorption is not observed in solutions of **5Zn**.

In non-coordinating solvents (*e.g.*, toluene), the spectra of **9Zn–11Zn** gained a broad and flat character with two additional maxima at about 636 and 702 nm (see ESI, Fig. S6–S8†). This behaviour is attributed to the formation of slipped *J*-dimers after the coordination of the central Zn with the peripheral *N*,*N*-diethylamino substituent of an adjacent macrocycle.[28] More specifically, extended *J*-dimerization occurs with compounds bearing *N*,*N*-diethylamine substituents on two proximal isoindole units. The presence of the *J*-dimers of **9Zn** and **10Zn** was confirmed by NMR, UV-vis and fluorescence spectroscopy similarly to **11Zn**.[28] The dynamic equilibrium between monomer and dimer in toluene is indicated by the residual monomer absorption band in UV-vis spectra and by the absence of the monomer band in fluorescence excitation spectra recorded at the emission maxima of dimer (see ESI, Fig. S9†). The contribution of the monomer decreases in the series **9Zn**, **10Zn** and **11Zn** indicating that the dynamic equilibrium is influenced by the number of *N*,*N*-diethylamino substituents available for the coordination of the central metal of the adjacent molecule.

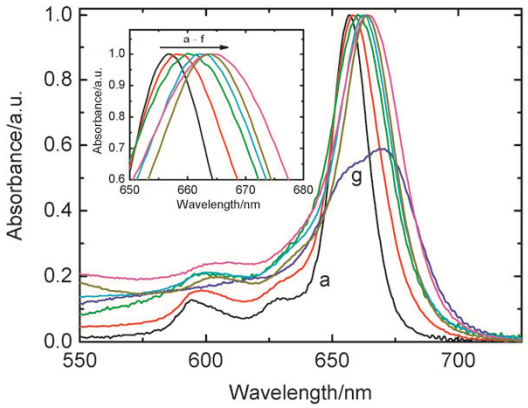

Fig. 1 Normalized absorption spectra of **5Zn** (a), **6Zn** (b) **7Zn** (c), **8Zn** (g), **9Zn** (d), **10Zn** (e) and **11Zn** (f) in pyridine. Arrow indicates the shift of the Q-band maxima with the increasing number of *N*,*N*-diethylamino groups.

For comparison, the absorption spectrum of **5Zn** practically does not change in toluene when compared with pyridine solution and the spectra of **6Zn–8Zn** show only a small absorbance increase above 680 nm indicating the negligible contribution of aggregates (see ESI, Fig. S2–S5†).

Dimers in toluene can be monomerized by the addition of a pyridine that coordinates to a central metal (see ESI, Fig. S10†). Titration of **9Zn**, **10Zn** and **11Zn** toluene solutions with pyridine revealed that complete monomerization is reached at 0.05, 0.25 and 0.36% v/v, respectively, showing again that less stable *J*-dimers of **9Zn** and **10Zn** are easier monomerized than **11Zn**. Based on these titrations, some of the following measurements in toluene were performed with 1% v/v pyridine to achieve full monomerization.

Fluorescence and solvent polarity

The photophysical behaviour of **5Zn** and **6Zn** was investigated using steady-state fluorescence in different solvents. Table 2 summarizes the fluorescence maxima (λ_{max}) and quantum yields (Φ_F) in solvents of increasing polarity and Fig. 2 shows fluorescence emission spectra. The energy levels of the singlet excited states E_{00} were estimated from the intersection of the normalized *Q*-band absorption and emission spectra, giving 1.88 and 1.87 eV for **5Zn** and **6Zn** in pyridine, respectively (for comparison, E_{00} = 1.85 eV for **11Zn**). The spectra of **5Zn** with one dominant band are typical of TPyzPz[42] and exhibit a slight solvatochromism with maxima varying from 655 nm in tetrahydofuran to 665 nm in DMSO. The spectra of **6Zn** are red-shifted by several nm when compared to **5Zn** corresponding to the shift of the *Q*-band in the absorption spectra. The fact that the excitation spectra superimposed the absorption spectra confirms the identity of the fluorescence.

While the Φ_F values for **5Zn** remained practically unchanged in all solvents, the Φ_F values of **6Zn** bearing one donor centre on the macrocycle periphery generally decrease with increasing solvent polarity (Table 2). The time-resolved fluorescence features track those of the steady-state

Table 1 Absorption maxima of the *Q*-bands (λ_{max}), quantum yields of singlet oxygen formation (Φ_Δ) and fluorescence quantum yields (Φ_F) of **5Zn–11Zn**

		Pyridine		Toluene		Toluene with 1% pyridine (v/v)	
Compound	λ_{max} (pyridine)	Φ_Δ[a]	Φ_F[a]	Φ_Δ[a]	Φ_F[a]	Φ_Δ[a]	Φ_F[a]
5Zn	657	0.66	0.31	0.55	0.25	0.70	0.25
6Zn	658	0.13	0.0025	0.59	0.080	0.69	0.13
7Zn	661	0.01	0.0011	0.04	0.0019	0.05	0.0027
8Zn	657; 670	0.01	<0.0005	0.10	0.0053	0.10	0.0050
9Zn	663	0.01	<0.0005	0.05	0.0011	0.04	0.0015
10Zn	664	0.02	<0.0005	0.13	0.0037	0.05	0.0040
11Zn	664	0.02	<0.0005	0.29	0.0071	0.07	0.0041

[a] Three independent measurements, estimated error ±15%.

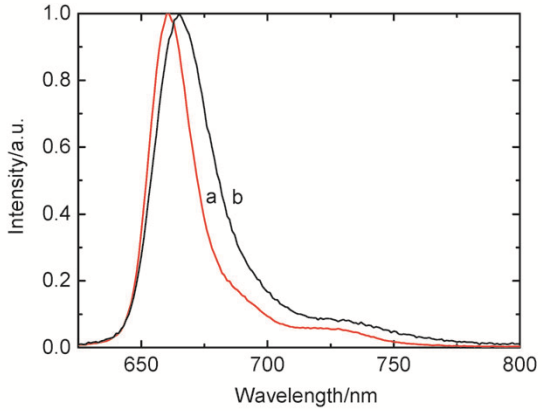

Fig. 2 Normalized emission spectra of **5Zn** (a) and **6Zn** (b) in toluene.

Table 2 Fluorescence quantum yields (Φ_F) together with the fluorescence maxima (λ_{max}) of **5Zn** and **6Zn** in solvents of different polarity. The Φ_F values are the mean of three independent measurements, estimated error ±15%

Solvent	ε_r	Φ_F **5Zn** (λ_{max})	Φ_F **6Zn** (λ_{max})
Toluene	2.4	0.25 (661)	0.080 (665)
Toluene–1% pyridine	~2.4	0.25 (661)	0.13 (665)
Chloroform	4.7	0.25 (660)	0.024 (666)
Tetrahydrofuran	7.4	0.32 (655)	0.013 (660)
Dichloromethane	8.9	0.25 (661)	0.0043 (665)
Pyridine	12.3	0.31 (663)	0.0025 (671)
Acetone	20.7	0.29 (656)	0.022 (661)
N,*N*-Dimethylformamide	36.7	0.23 (660)	0.0043 (667)
Acetonitrile	37.5	0.26 (658)	0.0013 (661)
Dimethylsulfoxide	48.9	0.26 (665)	0.00072 (667)

measurements. Both model compounds had a mono-exponential decay. The fluorescence lifetime of **5Zn** in pyridine is 2.61 ns and did not change in toluene–1% pyridine (v/v) (the presence of 1% pyridine ensures strictly monomeric state). In contrast, the lifetime of **6Zn** in toluene–1% pyridine (v/v) was only 1.71 ns together with lower Φ_F of 0.13 and the lifetime in pure pyridine is even much shorter than the time resolution of the instrument (~300 ps). It is reflected by very low Φ_F of 0.0025 (Table 2). These results indicate the occurrence of an excited-state quenching event that could occur either by energy transfer or ICT. In the absence of any appreciable new absorption of **6Zn** in the emission wavelength region, energy transfer can be eliminated. The most likely mechanism of fluorescence quenching is ICT between the peripheral *N*,*N*-diethylamino substituent and the singlet excited state localized at the TPyzPz moiety to give an ICT state. As the thermodynamic feasibility of ICT increases in polar solvents, the quenching of excited states becomes more effective that is corroborated by the significant decrease of fluorescence quantum yields.[12,45,46] Together with nearly no influence of the solvent polarity on fluorescence of **5Zn**, this observation can be considered as the indirect confirmation of ICT.

The rate constant for the formation of the ICT state in **6Zn** in toluene–1% pyridine (v/v) was determined using the observables. The radiative rate constants k_F in **5Zn** and **6Zn** can be calculated *via* $k_F = \Phi_F/\tau_F$ and are 9.6×10^7 s^{-1} and 7.6×10^7 s^{-1}, respectively. With the assumption that the shorter fluorescence lifetime of **6Zn**, relative to that of **5Zn**, is entirely due to ICT, the rate constant k_{ICT} is given by $k_{ICT} = 1/\tau_F(\mathbf{6Zn}) - 1/\tau_F(\mathbf{5Zn}) - k_F(\mathbf{6Zn}) - k_F(\mathbf{5Zn})$. It gives a k_{ICT} of 2.2×10^8 s^{-1}. The process is much faster in pure pyridine on a picosecond time scale. The ultrafast ICT in **6Zn** and also **11Zn** was directly confirmed by femtosecond transient absorption measurements (see below).

Protonation of donor centre

The amine donor centres, generally, can be blocked by protonation.[47,49] However, the interpretation of absorption and fluorescence changes in the case of TPyzPz macrocycles is complex because azomethine and pyrazine nitrogens are also protonated.[50,52] The titrations were performed in DMSO solutions of **5Zn** and **6Zn** with the stepwise addition of concentrated sulfuric acid. No significant changes in the absorption spectra were observed up to approximately 6% v/v sulfuric acid (Fig. 3A,B, Fig. S12†). Above this concentration, the *Q*-band absorption at 658 nm considerably decreased with a concomitant absorption increase at 700 nm. These changes are caused by protonation of one azomethine nitrogen of the TPyzPz macrocycle.[50,53]

The fluorescence emission spectra were recorded using an excitation wavelength of 599 nm. The initial fluorescence intensity of **6Zn** was very weak and steeply increased upon the addition of sulfuric acid up to 12% v/v (Fig. 3B). Further titration led to a decrease of fluorescence intensity. The

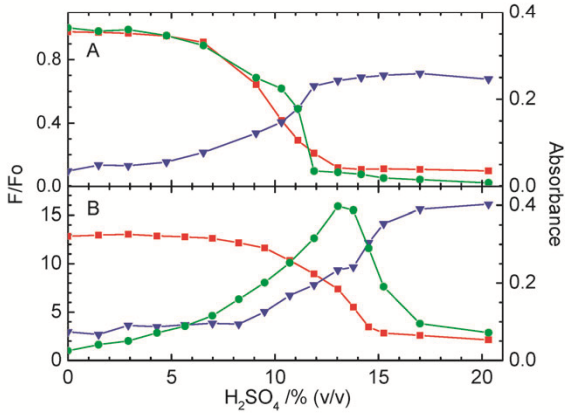

Fig. 3 Absorbance and emission intensity changes of DMSO solutions of **5Zn** (A) and **6Zn** (B) upon the addition of sulfuric acid: absorbance of the neutral form at 658 nm (■) and of the monoprotonated form at 700 nm (×10) (▼); ratio F/F_0, where F and F_0 are fluorescence intensities at 667 nm after the addition and without sulfuric acid, respectively (●).

compound **5Zn** showed a moderate intensity decrease up to approx. 6% v/v sulfuric acid and a steep decrease up to about 12% v/v sulfuric acid. The course of fluorescence intensity of **5Zn** is closely followed by the absorbance changes at 658 nm (Fig. 3A).

We have previously shown that one azomethine nitrogen of **5Zn** is easily protonated[50] as indicated by a decrease of the neutral form absorption band at 658 nm and an increase contribution of the monoprotonated form peaking at 700 nm. Focusing on the fluorescence intensity, the protonation of azomethine nitrogen in **5Zn** leads to a significant decrease of emission intensity. These observations are in good agreement with Beeby *et al.*[51] who showed that protonation of azomethine nitrogens of phthalocyanine macrocycles considerably decreases their fluorescence quantum yields.

As shown in our previous study, peripheral *N*,*N*-diethylamino nitrogens in **11Zn** are the most basic sites.[50] Therefore, the *N*,*N*-diethylamino substituent in **6Zn** is protonated first, and this protonation is not accompanied by changes in the absorption spectra. The considerable increase in fluorescence intensity (up to 7 times) during the addition up to 6% v/v sulfuric acid (Fig. 3B) can be attributed solely to the partial blocking of ICT. Protonation of the *N*,*N*-diethylamino substituent is completed at larger additions of sulfuric acid (above 6% v/v) as evidenced by the further considerable increase of fluorescence intensity. At the same time (starting from 6% v/v) protonation of azomethine nitrogens takes place as detected by the absorption changes of **5Zn** and **6Zn**. Although the protonation of azomethine nitrogen decreases the fluorescence intensity as shown for **5Zn** (Fig. 3A), the effect of the ICT blocking is much stronger, which is manifested by a further fluorescence intensity increase up to 12% v/v sulfuric acid. At larger additions, the effect of azomethine protonation prevails, resulting in a strong decrease of fluorescence. These experiments prove the substantial importance of the free electron pair of the *N*,*N*-diethylamino substituent for the formation of the ICT state.

Electrochemistry

As ICT-based quenching is of oxido-reductive character, the electrochemistry of TPyzPz macrocycles can help in understanding of the whole process. The electrochemistry of representative derivatives synthesized in this work was studied by cyclic voltammetry (CV) in pyridine solution at room temperature. The main focus was on an oxidation process involving the TPyzPz periphery and a reduction process ascribable to the TPyzPz core (Fig. 4). Compound **5Zn** shows two reversible reductions characterized by the half-wave potentials $E_{1/2}$ of −0.58 and −0.98 V *vs.* SCE that can be assigned to the first and second one-electron reduction of the TPyzPz ring system.[4] No oxidation occurs below 1.0 V *vs.* SCE. Although **11Zn** is an analogous compound, the reduction processes are substantially shifted to negative values, namely, the first reduction is at $E_{1/2}$ = −0.79 V *vs.* SCE and the second reduction at $E_{1/2}$ = −1.18 V *vs.* SCE. A relatively large negative shift in the reduction potentials by 20 mV when compared with **5Zn** indicates an interaction between electron-donating *N*,*N*-diethylamino substituents and the TPyzPz core. Noticeably, the potential differences between the first and second reduction potentials of both compounds are the same (0.40 and 0.39 V for **5Zn** and **11Zn**, respectively), and are very close to the reported average separation of 0.37 V for structurally similar zinc(II) TPyzPz derivative.[4] In contrast to **5Zn**, compound **11Zn** undergoes an irreversible oxidation best characterized by a half-peak potential $E_{p/2}$ of 0.77 V *vs.* SCE. Compared with the redox behaviour of anilines typically having an irreversible oxidation step, *e.g.*, $E_{1/2}$ = 0.76 V *vs.* SCE for diethylaniline in acetonitrile,[54] the process can be attributed to the oxidation of the peripheral *N*,*N*-diethylamino substituents.

Excited state dynamics

Excited state dynamics may bring a more detailed view on the behaviour of the studied TPyzPz and unequivocally confirm ICT. Transient absorption spectra in pyridine obtained after excitation into the Soret band at 395 nm are shown in Fig. 5. The transient absorption spectrum of **5Zn** at 0.4 ps after excitation exhibits typical features of the first excited singlet states (S_1) of porphyrinoid compounds (Fig. 5a). It consists of

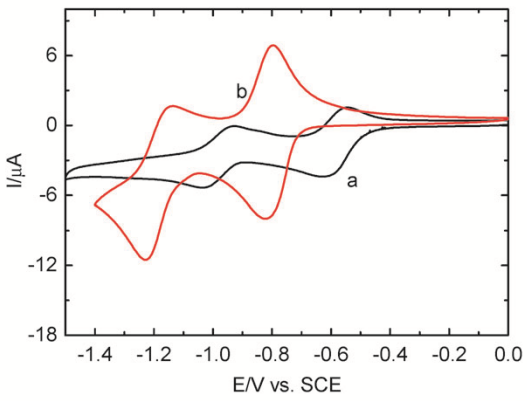

Fig. 4 Cyclic voltammograms of **5Zn** (a) and **11Zn** (b) in pyridine (10 mV s^{-1}, 0.1 M tetrabutylammonium tetrafluoroborate, 22 °C).

a ground state bleaching that mirrors the absorption spectrum by the major peak centred at 657 nm and two minor bands located at 630 and 600 nm. Comparison with the ground state absorption (Fig. 5a) shows that the strong negative band at 657 nm is broadened towards longer wavelengths, signalling a contribution of stimulated emission from the S_1 state. The weak positive signal is due to the excited-state absorption (ESA) originating from the S_1 state. The ESA band extends over the visible spectral region and appears within the first 150 fs *via* ultrafast internal conversion from the second excited singlet state (S_2) produced by excitation to the Soret band. Since the lifetime of the S_1 state of **5Zn** is 2.61 ns, the 0.4 ps transient spectrum does not exhibit any significant changes within the time window of the experiment.

The transient spectrum of **6Zn** at 0.4 ps is essentially identical to that of **5Zn** confirming that the initial relaxation dynamics within the TPyzPz moiety is unaffected by the addition of electron-donating peripheral substituents (Fig. 5b). The same is valid for **11Zn**, although the transient absorption spectrum at 0.4 ps differs by an additional broad bleaching around 540 nm, attributed to a charge-transfer absorption band (Fig. 5c). However, the time evolution of transient absorption spectra of **6Zn** and **11Zn** reveals significant differences when compared with **5Zn**. While no time dynamics is observed in **5Zn**, new bands at 560 and 700 nm appear in the transient absorption spectra of **6Zn** and **11Zn**, whose formation is accompanied by the decrease of S_1-state absorption and stimulated emission. The positions of the new bands are similar to those obtained after one-electron reduction of structurally similar zinc(II) TPyzPz[4] indicating that a new transient can be attributed to an ICT state.

Dynamics of the ICT state formation is shown in Fig. 6. Kinetic curves taken at 705 nm (ICT state) for **6Zn** exhibit a clear rise component characterized by a time constant of 10 ps, and the same time component appears as a decay at 510 nm (S_1 ESA) and 675 nm (S_1 stimulated emission), clearly showing that the S_1 state undergoes ultrafast ICT between the TPyzPz core and electron-donating peripheral *N*,*N*-diethylamino substituent (Fig. 6a). The same situation occurs for **11Zn** (Fig. 6b), but ICT is faster with a time constant of 7 ps. The lifetime of the ICT state is also different in the two molecules. Fig. 7 shows the kinetics of the recovery of the ground state (650 nm) and the ICT state decay (695 or 705 nm). While **5Zn** does not show any recovery of the ground state within a 450 ps window, because its lifetime is 2.61 ns, the ground state of **6Zn** recovers very fast with a time constant of 115 ps. Since the ground state recovery occurs with the same time constant as the decay of the ICT absorption, it is obvious that the ground state recovers *via* relaxation of the ICT state. The same is valid for **11Zn**, but the decay of the ICT state is significantly faster (time constant of 20 ps).

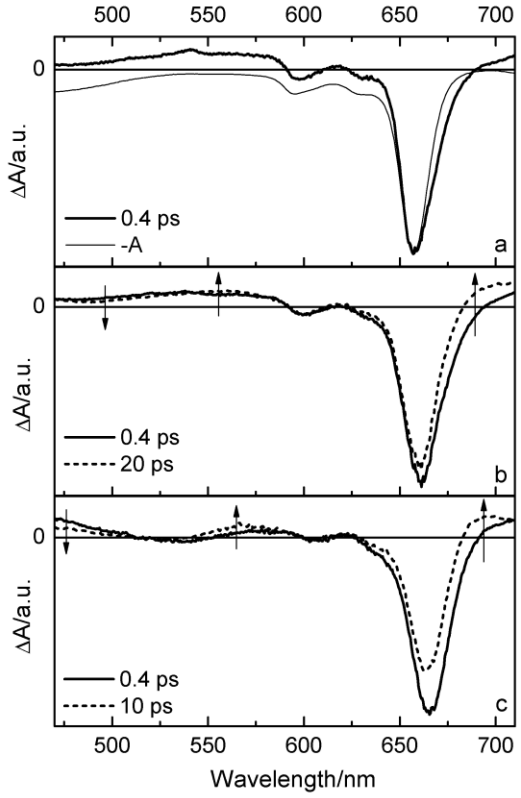

Fig. 5 Transient absorption spectra after excitation at 395 nm. (a) **5Zn** at 0.4 ps, thin solid line shows absorption spectrum multiplied by (−1), (b) **6Zn** at 0.4 ps (solid line) and 20 ps (dashed line), (c) **11Zn** at 0.4 ps (solid line) and 10 ps (dashed line). Arrows denote time evolution of the signal in different parts of the spectrum.

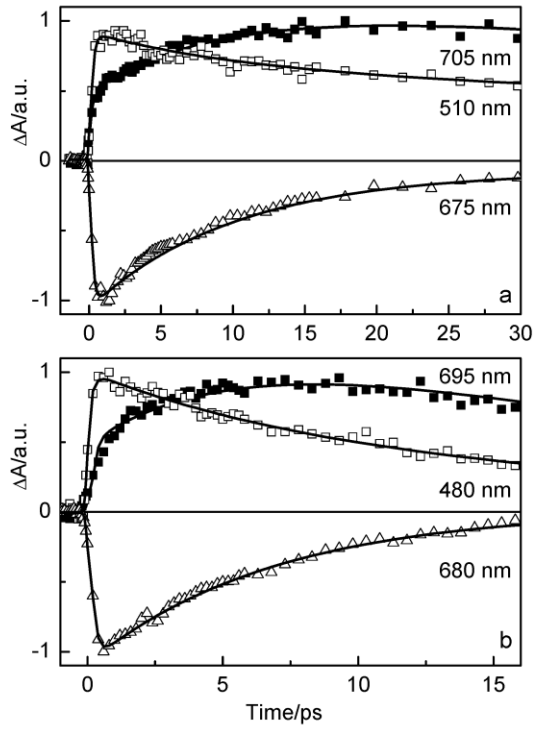

Fig. 6 Kinetics of ICT (■), S_1-state decay (□), and stimulated emission decay (△) for (a) **6Zn** and (b) **11Zn**. All kinetics are normalized, solid lines are fits obtained from the global fitting analysis.

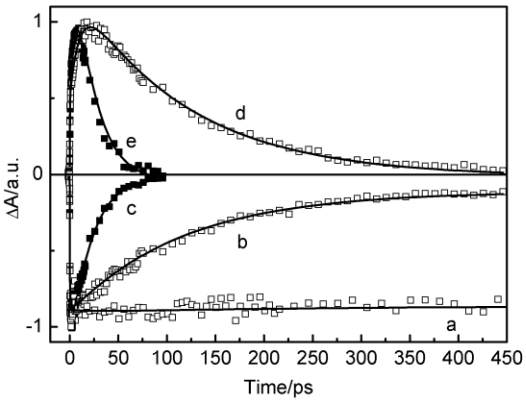

Fig. 7 Kinetics of the ground state recovery recorded at 650 nm (a, b and c stands for **5Zn**, **6Zn** and **11Zn**, respectively) and the decay of the ICT state at 695 nm (e, **11Zn**) and 705 nm (d, **6Zn**). All kinetics are normalized, solid lines are fits obtained from the global fitting analysis.

In order to obtain further insight into the excited state dynamics, all datasets were fitted globally. The resulting evolution-associated difference spectra (EADS, see the ESI† for more information) are depicted in Fig. 8. The first EADS, depicted by a solid line, is formed within the first 150 fs from the S_2 state, and corresponds to the lowest excited singlet state of TPyzPz, (S_1 state). This EADS is replaced by the second EADS (dashed line) within 10 ps (**6Zn**) and 7 ps (**11Zn**). The transformation to the second EADS is characterized by the loss of the excited state absorption in the 470–530 nm region and stimulated emission (660–680 nm) accompanied with the appearance of new absorption bands attributed to the ICT states around 565 and 700 nm. Thus, the 7 and 10 ps processes can be unequivocally attributed to ICT from electron-donating peripheral substituents to the S_1 state of **11Zn** and **6Zn**, respectively. The second EADS decays in 115 ps (**6Zn**) and 20 ps (**11Zn**) due to the fast relaxation of the ICT states. While **11Zn** has no residual signal within the time window of the experiment (*i.e.*, the quantum yield of electron transfer is 1), a weak non-decaying EADS (dotted line in Fig. 8a) is identified in **6Zn**. This EADS has the shape identical to that of the S_1 state, indicating that some fraction (<10%) of **6Zn** molecules does not form the ICT state.

These experiments confirm that the *N*,*N*-diethylamino substituents on the TPyzPz periphery induce a very fast quenching of the singlet excited states and are responsible for the nonradiative release of absorbed energy.

Number of donor centres

Following the previous experiments indicating the effect of the number of the donor centres on fluorescence properties, we evaluated the impact of the peripheral substituents on photophysical and photochemical properties in the complete series **5Zn–11Zn**. Besides Φ_F, the quantum yields of singlet oxygen formation (Φ_Δ) were also complemented. As described above, the solvent polarity and coordinating ability

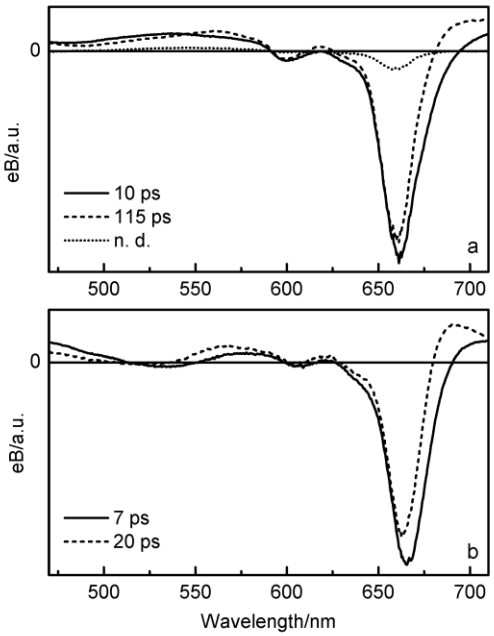

Fig. 8 Evolution associated difference spectra (EADS) of **6Zn** (a) and **11Zn** (b) extracted from global fitting of the whole datasets to a sequential model; n.d. stands for a non-decaying spectrum within the measured time window. See text for details.

significantly influence the ICT feasibility and the aggregation state of studied derivatives. Three solvent systems were employed: (i) pyridine, a polar solvent (ε_r = 12.3) which ensures a high efficiency of ICT and, due to good coordinating properties, prevents aggregation and dimer formation; (ii) non-polar toluene (ε_r = 2.4) which restricts ICT and, as a non-coordinating solvent, allows the formation of J-dimers in which ICT is partially inhibited;[28] and (iii) toluene with 1% v/v pyridine, which is sufficient for the complete monomerization, while keeping the low polarity of the solvent. All results are summarized in Table 1, Fig. 9 and S11 (see ESI†).

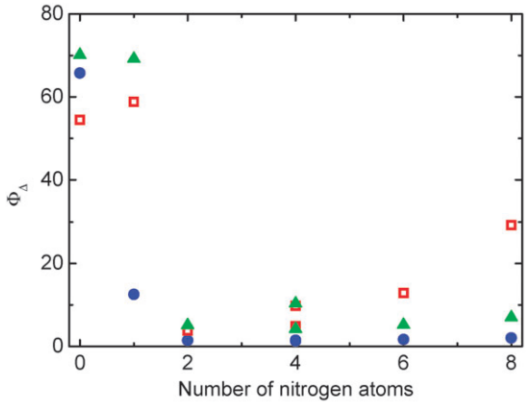

Fig. 9 Quantum yields of singlet oxygen formation (Φ_Δ) in relation to the number of peripheral *N*,*N*-diethylamino substituents in pyridine (●), toluene (□) and toluene/1% (v/v) of pyridine (▲).

In pyridine, compound **5Zn**, is a very efficient singlet oxygen producer with Φ_Δ of 0.66, while the addition of one donor centre in **6Zn** significantly decreases Φ_Δ. In agreement with the ICT concept, two or more *N*,*N*-diethylamino substituents (**7Zn–11Zn**) reduce Φ_Δ to a residual value of about 0.01.

A different relationship is observed in toluene. Compound **5Zn** has a lower Φ_Δ than in pyridine probably due to a minor contribution of stacked aggregates. In contrast to pyridine, **6Zn** has a Φ_Δ comparable to **5Zn** because ICT is blocked. The presence of two donor centres in **7Zn** leads to the effective quenching of excited states and the formation of singlet oxygen is nearly suppressed. Both **8Zn** and **9Zn** with four donor centres document the importance of the spatial arrangement of the donor centres in the molecule on the ICT efficiency because the Φ_Δ values differ almost twice (for comparison, Φ_F nearly five times). Compounds **9Zn–11Zn** form fluorescent J-dimers and, from this series, **11Zn** the most effectively. As mentioned above, the formation of J-dimers partially inhibits ICT.[28] Thus, the Φ_Δ values increase in the series from **9Zn** to **11Zn** reaching the considerable high value of 0.29 for **11Zn**.

The aggregation in toluene is eliminated by the addition of 1% v/v pyridine, so ICT is affected only by the low solvent polarity. As a result, the course of the Φ_Δ values copies that obtained in pyridine, but the Φ_Δ values are higher due to the lower feasibility of ICT.

For completion, the Φ_F values exhibited the same tendencies as described for Φ_Δ (see ESI, Fig. S11†).

Conclusions

The fluorescence behaviour of studied derivatives is consistent with efficient ICT in the locally excited TPyzPz chromophore. Further supports for this argument come from femtosecond transient absorption spectroscopy clearly documenting the ultrafast ICT state formation followed by non-fluorescent relaxation due to strong coupling with the polar solvent. The energy of the ICT states in **11Zn** can be roughly calculated from the electrochemical HOMO–LUMO energy gap, that is, the difference between the first oxidation potential of the donor and the first reduction potential of the acceptor, *i.e.*, the TPyzPz moiety. This energy lies at about 1.6 eV above the ground state in pyridine, however, the actual energy is lower than 1.6 eV because the Coulombic correction factor, which is not taken into account, will further stabilize the energy level. This accounts for the energy gap associated with charge separation $\Delta G^\circ_{cs} < -0.3$ eV using the energy corresponding to the 0–0 transition E_{00} (1.85 eV) and the estimated ΔG°_{cs} value confirms the thermodynamic feasibility of charge separation. The trends can be rationalized in terms of the three-state model where the excited singlet state S_1 associated with the TPyzPz moiety is quenched on the introduction of an electron donor substituent in the TPyzPz periphery to form the ICT state. Protonation of the *N*,*N*-diethylamino donor substituent led to a strong hindrance of ICT indicated by the increase of fluorescence intensity. It documents a key role of the free electron pair on nitrogen atom in the formation of the ICT state and consequently in the quenching process. The efficiency of the quenching process depends on the number of donor centres. The main difference is between **6Zn** and **7Zn** upon the introduction of the second amino substituent in the *ortho* position that can be attributed to better electron-donating properties of *ortho* derivatives over monosubstituted one. The introduction of another *N*,*N*-diethylamino substituent on the periphery of TPyzPz (**8Zn–11Zn**) has a minor additional quenching effect.

In the view of the presented results, we may also interpret some previously published observations. Lo *et al.* investigated photodynamic properties of silicon(IV) phthalocyanines (SiPc) with centrally bound aliphatic chains ended with tertiary amino groups.[11] Although these SiPc derivatives showed lower Φ_Δ in DMF than corresponding quaternized compounds, biological tests showed a reverse activity. Aliphatic tertiary amino groups are usually fully protonated at physiological pH 7.4 (pK_a in the range 8.5–10), therefore the photophysical properties of derivatives can strongly differ in biological environment from those in organic solvents. The promising results with these compounds in biological tests can be attributed to a combined effect of higher uptake and increased Φ_Δ due to protonation. In another paper, Montalban *et al.* described that bis(dimethylamino) zinc porphyrazine does not form singlet oxygen.[55] This is in good agreement with our results showing that two tertiary amino groups nearly completely quench excited singlet states. Recently, we have demonstrated that both Φ_F and Φ_Δ values continually decrease with increasing number of diethylaminoethylsulfanyl substituents (up to 8) in zinc(II) TPyzPz.[10] Due to a longer distance between the macrocycle and donor tertiary amino group (3 atoms) when compared with the presented series, the decrease in quantum yields was not so dramatic. In addition, protonation of diethylaminoethylsulfanyl substituents led to the restoration of quantum yields reaching values comparable with the compound without the donor centre. The quenching of phthalocyanine excited states by amino substituents within octa(phenoxy)SiPc was also referenced by Nyokong *et al.* as the presence of amino group on an axial or peripheral substituent considerably decreases the Φ_F and Φ_Δ values when compared with other substituents.[56,57]

Our results imply that the presence of tertiary (and the most likely secondary and primary) amino substituents in TPyzPz, phthalocyanines and related macrocycles (*e.g.*, porphyrins) is crucial for the applications based on fluorescence or production of singlet oxygen. The corresponding quantum yields are usually determined in neutral organic solvents. When the amino group is not blocked by protonation or quaternization, the observed quantum yields will be very low due to competitive relaxation processes within the compound.

Acknowledgements

This work has been supported by the Grant Agency of the Academy of Sciences of the Czech Republic (KJB401100801), by the Czech Science Foundation (203/07/1424), and by the Ministry of Education, Youth and Sports of the Czech Republic (MSM6007665808). The authors would like to thank to Marcel Fuciman (University of South Bohemia, Nové Hrady) for technical help with femtosecond experiments.

Notes and references

1 P. A. Stuzhin and C. Ercolani, in *The Porphyrin Handbook*, ed. K. M. Kadish, K. M. Smith and R. Guilard, Academic Press, New York, 2003, vol. 15, pp. 263–364.
2 S. Makhseed, F. Ibrahim, C. G. Bezzu and N. B. McKeown, *Tetrahedron Lett.*, 2007, **48**, 7358–7361.
3 D. Dini, M. J. F. Calvete, M. Hanack, W. Z. Chen and W. Ji, *ARKIVOC*, 2006, 77–96.
4 M. P. Donzello, Z. Ou, D. Dini, M. Meneghetti, C. Ercolani and K. M. Kadish, *Inorg. Chem.*, 2004, **43**, 8637–8648.
5 A. B. Korzhenevskii, S. V. Efimova, A. A. Zelenov and O. I. Koifman, *Russ. J. Gen. Chem.*, 2006, **76**, 822–825.
6 V. N. Shishkin, E. V. Kudrik, S. V. Makarov and G. P. Shaposhnikov, *Kinet. Catal.*, 2007, **48**, 660–663.
7 A. D. Quartarolo, I. Lanzo, E. Sicilia and N. Russo, *Phys. Chem. Chem. Phys.*, 2009, **11**, 4586–4592.
8 K. Lang, J. Mosinger and D. M. Wágnerová, *Coord. Chem. Rev.*, 2004, **248**, 321–350.
9 P. Zimcik, M. Miletin, M. Kostka, J. Schwarz, Z. Musil and K. Kopecky, *J. Photochem. Photobiol., A*, 2004, **163**, 21–28.
10 P. Zimcik, M. Miletin, Z. Musil, K. Kopecky, L. Kubza and D. Brault, *J. Photochem. Photobiol., A*, 2006, **183**, 59–69.
11 P. C. Lo, J. D. Huang, D. Y. Cheng, E. Y. Chan, W. P. Fong, W. H. Ko and D. K. Ng, *Chem.–Eur. J.*, 2004, **10**, 4831–4838.
12 M. Quintilani, A. Kahnt, T. Wölfle, W. Hieringer, P. Vázquez, A. Görling, D. M. Guldi and T. Torres, *Chem.–Eur. J.*, 2008, **14**, 3765–3775.
13 D. M. Guldi, J. Ramey, M. V. Martinez-Diaz, A. d. l. Escosura, T. Torres, T. Da Ros and M. Prato, *Chem. Commun.*, 2002, 2774–2775.
14 A. de la Escosura, M. V. Martinez-Diaz, D. M. Guldi and T. Torres, *J. Am. Chem. Soc.*, 2006, **128**, 4112–4118.
15 M. Niemi, N. V. Tkachenko, A. Efimov, H. Lehtivuori, K. Ohkubo, S. Fukuzumi and H. Lemmetyinen, *J. Phys. Chem. A*, 2008, **112**, 6884–6892.
16 C. G. Claessens, U. Hahn and T. Torres, *Chem. Rec.*, 2008, **8**, 75–97.
17 S. Fukuzumi, T. Honda, K. Ohkubo and T. Kojima, *Dalton Trans.*, 2009, 3880–3889.
18 M. S. Rodriguez-Morgade, T. Torres, C. Atienza-Castellanos and D. M. Guldi, *J. Am. Chem. Soc.*, 2006, **128**, 15145–15154.
19 S. Fukuzumi, K. Ohkubo, J. Ortiz, A. M. Gutierrez, F. Fernandez-Lazaro and A. Sastre-Santos, *Chem. Commun.*, 2005, 3814–3816.
20 A. Gouloumis, G. M. A. Rahman, J. Abel, G. de la Torre, P. Vázquez, L. Echegoyen, D. M. Guldi and T. Torres, *Aust. J. Chem.*, 2008, **61**, 256–261.
21 T. Kojima, T. Honda, K. Ohkubo, M. Shiro, T. Kusukawa, T. Fukuda, N. Kobayashi and S. Fukuzumi, *Angew. Chem., Int. Ed.*, 2008, **47**, 6712–6716.
22 S. Tannert, E. A. Ermilov, J. O. Vogel, M. T. M. Choi, D. K. P. Ng and B. Röder, *J. Phys. Chem. B*, 2007, **111**, 8053–8062.
23 F. Ito, Y. Ishibashi, S. R. Khan, H. Miyasaka, K. Kameyama, M. Morisue, A. Satake, K. Ogawa and Y. Kobuke, *J. Phys. Chem. A*, 2006, **110**, 12734–12742.
24 Y. Z. Bian, X. H. Chen, D. Y. Wang, C. F. Choi, Y. Zhou, P. H. Zhu, D. K. P. Ng, J. Z. Jiang, Y. X. Weng and X. Y. Li, *Chem.–Eur. J.*, 2007, **13**, 4169–4177.
25 E. A. Ermilov, J.-Y. Liu, D. K. P. Ng and B. Röder, *Phys. Chem. Chem. Phys.*, 2009, **11**, 6430–6440.
26 M. E. Daraio, A. Völker, P. F. Aramendía and E. San Román, *Langmuir*, 1996, **12**, 2932–2938.
27 M. E. Daraio, P. F. Aramendía and E. San Román, *Chem. Phys. Lett.*, 1996, **250**, 203–208.
28 V. Novakova, P. Zimcik, K. Kopecky, M. Miletin, J. Kuneš and K. Lang, *Eur. J. Org. Chem.*, 2008, 3260–3263.
29 T. Nyokong, *Coord. Chem. Rev.*, 2007, **251**, 1707–1722.
30 I. Rosenthal, *Photochem. Photobiol.*, 1991, **53**, 859–870.
31 K. Kopecky, P. Zimcik, V. Novakova, M. Miletin, Z. Musil and J. Stribna, *Dyes Pigm.*, 2008, **78**, 231–238.
32 M. Kostka, P. Zimcik, M. Miletin, P. Klemera, K. Kopecky and Z. Musil, *J. Photochem. Photobiol., A*, 2006, **178**, 16–25.
33 W. Ried and G. Tsiotis, *Liebigs Ann. Chem.*, 1988, 1197–1199.
34 G. De La Torre, C. G. Claessens and T. Torres, *Eur. J. Org. Chem.*, 2000, 2821–2830.
35 Z. Musil, P. Zimcik, M. Miletin, K. Kopecky, P. Petrik and J. Lenco, *J. Photochem. Photobiol., A*, 2007, **186**, 316–322.
36 S. Jin, G. Z. Cheng, G. Z. Chen and Z. P. Ji, *J. Porphyrins Phthalocyanines*, 2005, **9**, 32–39.
37 G. J. Clarkson, N. B. McKeown and K. E. Treacher, *J. Chem. Soc., Perkin Trans. 1*, 1995, 1817–1823.
38 F. Giuntini, D. Nistri, G. Chiti, L. Fantetti, G. Jori and G. Roncucci, *Tetrahedron Lett.*, 2003, **44**, 515–517.
39 Z. Musil, P. Zimcik, M. Miletin, K. Kopecky and J. Lenco, *Eur. J. Org. Chem.*, 2007, 4535–4542.
40 T. G. Linssen and M. Hanack, *Chem. Ber.*, 1994, **127**, 2051–2057.
41 V. E. Maizlish, V. P. Kulinich and G. P. Shaposhnikov, *Russ. J. Gen. Chem.*, 2004, **74**, 1801–1817.
42 P. Zimcik, M. Miletin, V. Novakova, K. Kopecky and Z. Dvorakova, *Dyes Pigm.*, 2009, **81**, 35–39.
43 N. Kobayashi, T. Ashida and T. Osa, *Chem. Lett.*, 1992, 2031–2034.
44 N. Kobayashi, H. Miwa and V. N. Nemykin, *J. Am. Chem. Soc.*, 2002, **124**, 8007–8020.
45 L. Fajari, P. Fors, K. Lang, S. Nonell and F. R. Trull, *J. Photochem. Photobiol., A*, 1996, **93**, 119–128.
46 M. Isosomppi, N. V. Tkachenko, A. Efimov and H. Lemmetyinen, *J. Phys. Chem. A*, 2005, **109**, 4881–4890.
47 I. Bruseghini, L. Fabbrizzi, M. Licchelli and A. Taglietti, *Chem. Commun.*, 2002, 1348–1349.
48 L. Fabbrizzi, M. Licchelli, A. Perotti, A. Poggi, G. Rabaioli, D. Sacchi and A. Taglietti, *J. Chem. Soc., Perkin Trans. 2*, 2001, 2108–2113.
49 A. P. Desilva and R. Rupasinghe, *J. Chem. Soc., Chem. Commun.*, 1985, 1669–1670.
50 P. Petrik, P. Zimcik, K. Kopecky, Z. Musil, M. Miletin and V. Loukotova, *J. Porphyrins Phthalocyanines*, 2007, **11**, 487–495.
51 A. Beeby, S. FitzGerald and C. F. Stanley, *J. Chem. Soc., Perkin Trans. 2*, 2001, 1978–1982.
52 K. Kasuga, K. Yashiki, T. Sugimori and M. Handa, *J. Porphyrins Phthalocyanines*, 2005, **9**, 646–650.
53 A. Beeby, S. FitzGerald and C. F. Stanley, *Photochem. Photobiol.*, 2001, **74**, 566–569.
54 D. G. Nocera and H. B. Gray, *J. Am. Chem. Soc.*, 1981, **103**, 7349–7350.
55 A. G. Montalban, H. G. Meunier, R. B. Ostler, A. G. M. Barrett, B. M. Hoffman and G. Rumbles, *J. Phys. Chem. A*, 1999, **103**, 4352–4358.
56 M. D. Maree, N. Kuznetsova and T. Nyokong, *J. Photochem. Photobiol., A*, 2001, **140**, 117–125.
57 M. D. Maree, T. Nyokong, K. Suhling and D. Phillips, *J. Porphyrins Phthalocyanines*, 2002, **6**, 373–376.

1.2. **P2**

VACHOVA L., Novakova V, Kopecky K, Miletin M., Zimcik P.: Effect of intramolecular charge transfer on fluorescence and singlet oxygen production of phthalocyanine analogues. *Dalton Trans.*, **2012**, 41, 11651–11656. IF_{2016} 4,029.

Podíl autorky: Příprava prekurzorů a cílových molekul, jejich izolace a charakterizace, fotofyzikální měření a analýza dat. Spoluautor textu.

Dalton Transactions

Cite this: *Dalton Trans.*, 2012, **41**, 11651

www.rsc.org/dalton

PAPER

Effect of intramolecular charge transfer on fluorescence and singlet oxygen production of phthalocyanine analogues†

Lenka Vachova,[a] Veronika Novakova,[b] Kamil Kopecky,[a] Miroslav Miletin[a] and Petr Zimcik*[a]

Received 28th June 2012, Accepted 12th July 2012
DOI: 10.1039/c2dt31403g

Intramolecular charge transfer (ICT) was studied on a series of magnesium, metal-free and zinc complexes of unsymmetrical tetrapyrazinoporphyrazines and tribenzopyrazinoporphyrazines bearing two dialkylamino substituents (donors) and six alkylsulfanyl or aryloxy substituents (non-donors). The dialkylamino substituents were responsible for ICT that deactivated excited states and led to considerable decrease of fluorescence and singlet oxygen quantum yields. Photophysical and photochemical properties were compared to corresponding macrocycles that do not bear any donor centers. The data showed high feasibility of ICT in the tetrapyrazinoporphyrazine macrocycle and significantly lower efficiency of this deactivation process in the tribenzopyrazinoporphyrazine type molecules. Considerable effect of non-donor peripheral substituents on ICT was also described. The results imply that tetrapyrazinoporphyrazines may be more suitable for development of new molecules investigated in applications based on ICT.

Introduction

Phthalocyanines (Pcs) and their aza-analogues azaphthalocyanines are synthetic dyes that have been extensively studied due to their unique optical, physical, electronic, spectral and structural properties.[1] Recently, they attracted also great attention in the field of dye-sensitized solar cells,[2] fluorescent probes[3,4] and photodynamic therapy.[5] A long-lived excited state and high quantum yield of fluorescence or singlet oxygen are, in general, advantageous in these applications. On the other hand, an interesting phenomenon of ultrafast intramolecular charge transfer (ICT) was recently shown to be responsible for quenching of the excited states in tetrapyrazinoporphyrazines (TPyzPz), a type of azaphthalocyanines.[6] This discovery opened a door for new applications of these macrocyclic dyes in quenching of fluorescence in DNA-hybridization probes[7] or as molecular sensors (*e.g.* pH-sensitive[8]). The effect of ICT was studied in detail for TPyzPz but similar processes were recently described also for Pc.[9,10]

Presented work is focused on synthesis and investigation of photophysical and photochemical properties of compounds bearing donor centers for ICT and containing different macrocycle ring and peripheral substituents. The aim is to compare the efficiency of ICT in these compounds and to discuss their potential to be further investigated as efficient quenchers of fluorescence or sensors.

Results and discussion

Design of the compounds

The structures of the compounds (Scheme 1) were designed to contain two donor centers (aminosubstituents) in order to allow high feasibility of ICT. ICT in compounds with only one donor center is highly sensitive to properties of environment[6] (*e.g.* polarity, acidity) that may interfere with proper interpretation of the results. The substituents on the studied derivatives were chosen to be bulky to limit aggregation of planar molecules that could lead to misinterpretation of the data. One carboxy group was introduced to the molecule in order to allow simple binding of prospective derivatives to biomolecules or other suitable modifiers in future.[7]

The porphyrazine ring was fused with three benzene and one pyrazine rings (**5** and **6**) or contains only pyrazine rings (*i.e.* TPyzPz) in the case of **7**. Compounds **6** and **7** contained the same substituents and differed only in the macrocyclic core. This series allows comparison between macrocycle types without the influence of peripheral substitution (compounds **6** and **7**) and between peripheral substituents without influence of the macrocycle ring (**5** and **6**). Symmetrical compounds **8–10** without any

[a]*Department of Pharmaceutical Chemistry and Drug Control, Faculty of Pharmacy in Hradec Kralove, Charles University in Prague, Heyrovskeho 1203, 50005, Hradec Kralove, Czech Republic. E-mail: petr.zimcik@faf.cuni.cz; Fax: +420 495067167; Tel: +420 495067257*
[b]*Department of Biophysics and Physical Chemistry, Faculty of Pharmacy in Hradec Kralove, Charles University in Prague, Heyrovskeho 1203, 50005 Hradec Kralove, Czech Republic*

†Electronic supplementary information (ESI) available: NMR spectra, MS (MALDI-TOF) spectra, absorption, emission and excitation spectra. See DOI: 10.1039/c2dt31403g

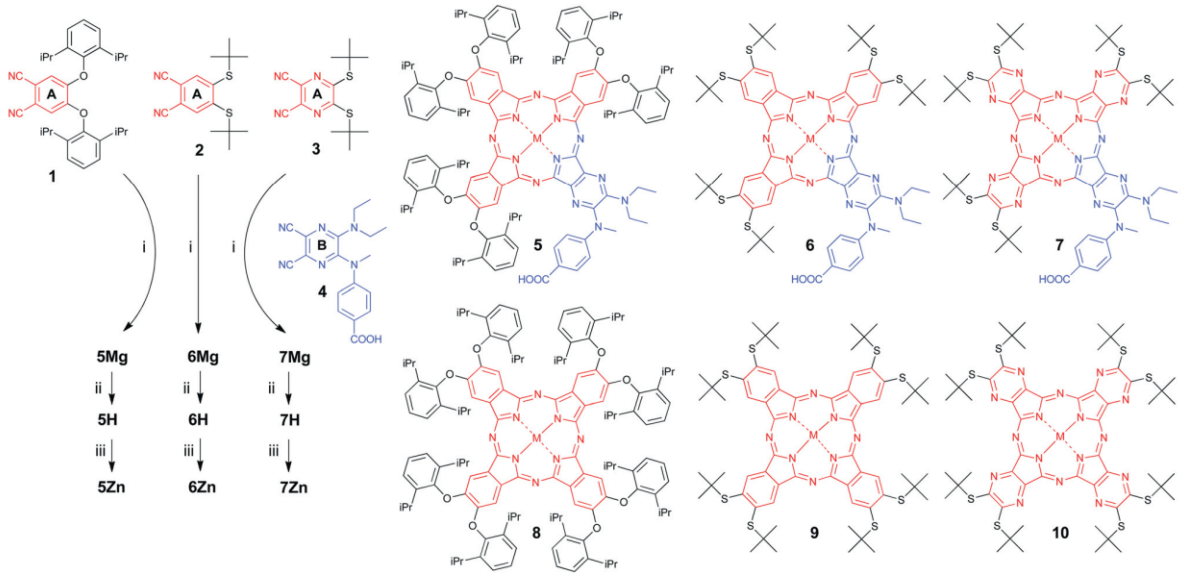

Scheme 1 Synthesis of the investigated compounds. Reaction conditions: (i) Mg, I_2, butanol, reflux, (ii) TFA or *p*TSA, chloroform, rt, (iii) $Zn(CH_3COO)_2$, pyridine, reflux.

donor center were used as negative controls where no ICT can occur.

Synthesis

Mixed cyclotetramerization (also known as statistical condensation[11]) is the simplest method for the synthesis and isolation of unsymmetrical Pc and TPyzPz of the AAAB type despite the fact that several selective approaches were developed.[12] Thus, treatment of a mixture of precursors A (**1**, **2**, or **3**) and B (compound **4**) with magnesium butoxide in butanol gave a mixture of six congeners, from which congeners of ABBB type were separated on silica to afford **5Mg–7Mg** in reasonable yields of 7–15% (Scheme 1). In order to increase the amount of the AAAB congener in the statistical mixture, the ratio of starting material was set to 3 : 1 (A : B) and the precursor A was added in three portions due to the lower reactivity of compound **4**. The isolation was facilitated by the presence of a polar substituent (carboxy group) that led to a good separation of the congeners on TLC with distinct retention factors. Despite this, purification on the silica column had to be repeated several times to obtain pure product. Magnesium complexes were demetalated using strong organic acid and the metal free derivatives **5H–7H** were converted to zinc complexes using zinc acetate in pyridine to afford **5Zn–7Zn**. The synthesis of metal complexes of compounds **8–10** was described elsewhere.[4] All analyses confirmed unequivocally the structure of the isolated congeners (see ESI, Fig. S1–S15†). Interestingly, compounds **5Mg**, **5H** and **5Zn** were extremely light sensitive and decomposed rapidly in solution or on TLC. For this reason, the solutions and silica columns were strictly protected from light by aluminum foil. In agreement with this observation, extensive photodecomposition was recently found for structurally similar **8Mg** and **8Zn** with high photobleaching quantum yields.[4]

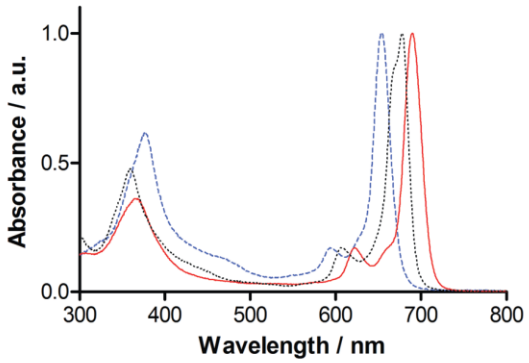

Fig. 1 Normalized absorption spectra of **5Zn** (black, dotted), **6Zn** (red, full) and **7Zn** (blue, dashed) in THF.

Absorption spectra

Absorption spectra in THF were consistent with the structures and contained high energy B-band (in area 350–390 nm) and low energy Q-band (in area 650–695 nm) with clearly marked vibrational bands (Fig. 1). The shape of the spectra was typical for monomeric species in solution, no aggregates were detected during all photophysical and photochemical measurements. In general, unsymmetrical composition of the macrocycle is indicated by splitting of the Q-band. The metal-free derivatives **5H**, **6H** and **7H** were characterized by strong splitting between the Q_x- and Q_y-bands due to lowered symmetry because of the presence of central hydrogens (see ESI, Fig. S16†). The symmetry of the porphyrazine ring was lowered also in metal complexes **5Mg–7Mg** and **5Zn–7Zn** due to the presence of different isoindole units. However, only the absorption spectra of compounds **5Mg** and **5Zn** showed hardly-noticeable splitting of the Q-band

Table 1 Photophysical and photochemical data for studied compounds in THF

	Designation[a]	Q-band λ_{max} (nm)	λ_{em} (nm)	Stokes shift (cm^{-1})	Φ_F [b]	Φ_Δ [b]	$\Phi_{F(N)}/\Phi_{F(D)}$ [c]	$\Phi_{\Delta(N)}/\Phi_{\Delta(D)}$ [c]
5Zn	D	678	682	87	0.15	0.37	1.9	1.7
5Mg	D	680	684	86	0.35	0.23	1.5	1.1
6Zn	D	689	696	146	0.071	0.10	2.3	6.6
6Mg	D	690	698	166	0.062	0.043	3.7	5.4
7Zn	D	654	662	185	0.0045	0.030	78	19
7Mg	D	655	660	116	0.0087	0.013	61	22
8Zn[d]	N	675	680	109	0.29	0.61	—	—
8Mg[d]	N	677	681	87	0.52	0.26	—	—
9Zn[d]	N	697	707	203	0.16	0.68	—	—
9Mg[d]	N	699	709	202	0.23	0.23	—	—
10Zn[d]	N	649	656	164	0.35	0.55	—	—
10Mg[d]	N	651	658	163	0.53	0.30	—	—

[a] D = compound contains donor centers, N = compound does not contain a donor center. [b] Mean of three independent measurements, estimated error ±15%. [c] Calculated by dividing the quantum yield of a compound without a donor center (N) by the quantum yield of the corresponding compound with donor centers (D), corresponding pairs: **5** and **8**, **6** and **9**, **7** and **10**. [d] Data from ref. 4.

(Fig. 1 and ESI, Fig. S17†), the metal complexes of **6** and **7** remained unsplit.

The positions of the Q-band maxima were also influenced by the composition of the macrocycle and peripheral substituents (Table 1). Considering the central metal, a very small red-shift of the maximum (approximately 1–2 nm) can be observed for magnesium complexes if compared with zinc derivatives. On the other hand, an almost 35 nm red shift was detected when three pyrazine rings in the macrocycle were exchanged for benzene rings (compare compounds **6** and **7**). Pc in general are always red-shifted for about 48 nm if compared with TPyzPz (compare the corresponding metal complexes of **9** and **10** (Table 1)).[4,13] In the case of compounds **6** and **7**, only three pyrazines were exchanged for benzene rings in the macrocycle core when going from **7** to **6**, which corresponds to a 36 nm calculated red shift. This observation is in agreement with previously published data and indicates that the position of the Q-band can be considered as an additive parameter that depends on the composition of the macrocycle.[14] Focusing on the influence of peripheral substitution (comparison between **5** and **6**), an important red-shift (about 10 nm) was observed for the alkylsulfanyl derivative.

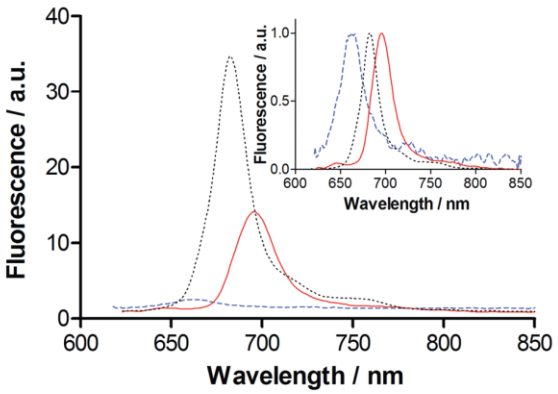

Fig. 2 Emission spectra of **5Zn** (black, dotted), **6Zn** (red, full) and **7Zn** (blue, dashed) in THF. Absorbance at the excitation wavelength (λ_{exc} = 612 nm) was the same for all compounds. Inset: normalized emission spectra.

Fluorescence and singlet oxygen production

The fluorescence was measured in THF after excitation at Q-band. Fluorescence emission spectra mirrored the absorption spectra with only small Stokes shift (Table 1). The shape of the spectra were typical for TPyzPz, Pc and related compounds (Fig. 2). The signal was very weak for **7Zn** and **7Mg**. The excitation spectra (see ESI, Fig. S17†) superimposed the absorption spectra confirming the origin of the signal and presence of only monomeric species. Thus, the observed low Φ_F values of compounds containing donor centers (see below) cannot be attributed to aggregation. The fluorescence quantum yields were determined in THF with unsubstituted ZnPc in 1-chloronaphthalene[15] (Φ_F = 0.30) as a reference. The data were collected only for the metal complexes. Metal-free TPyzPz are, in general, characterized by low fluorescence and singlet oxygen quantum yields.[4] An apparent reason may be enhanced vibrational and rotational motion that may deactivate the excited states. For this reason, these derivatives are not suitable for investigation of the influence of structure on ICT due to another relaxation channel and therefore were not included in the photophysical and photochemical study. Data obtained for compounds **5Mg–7Mg**, **5Zn–7Zn** and corresponding symmetrical derivatives without the donor center (**8Mg–10Mg** and **8Zn–10Zn**) are mentioned in Table 1. As anticipated, very low Φ_F values below 0.01 were obtained for compounds **7Mg** and **7Zn** due to efficient ICT. The values are almost two orders of magnitude lower than for corresponding compounds without the donor centers (**10Mg** and **10Zn**). This confirmed previous observations that ICT is a highly efficient relaxation pathway of excited states in this type of macrocycle.[6] Φ_F values of compounds that are structurally closer to Pc (**5** and **6**) were much higher than for compounds **7**, however; still several times lower than for the corresponding derivatives without any donor center. The moderate (for complexes **6**) or only minimal (for complexes **5**) decrease of fluorescence after the introduction of donor centers indicates that ICT

is a far less efficient deactivation process in this type of macrocycle. The results are in agreement with observations of ICT in Pc where only a moderate decrease of Φ_F values was observed after the introduction of one to four donor centers.[10]

Singlet oxygen quantum yields were determined in THF with ZnPc in THF[16] ($\Phi_\Delta = 0.53$) as a reference. The results summarized in Table 1 indicated similar dependencies as outlined above for fluorescence. The largest decrease in singlet oxygen production after the incorporation of two donor centers into the molecule was observed for compounds **7**, followed by complexes **6** and only minimal influence of ICT was detected in derivatives **5**.

The obtained results indicated that high feasibility of ICT may be closely connected with TPyzPz macrocycles. The macrocycle that is structurally closer to Pc seems to be less suitable for this deactivation process (compare **6** and **7**). Also, peripheral substituents not involved in ICT may play an important role as shown on metal complexes of **5** and **6**. The explanation for all the observed results may be related to strong electron-deficient properties of TPyzPz macrocycles if compared with Pc as shown by Donzello *et al.*[17] TPyzPz are easier to reduce as documented by literature data: the first reduction potential for $(SC_6H_{13})_8$ZnPc (analogue to **9Zn**) in CH_2Cl_2 is reported −0.79 V,[18] for TPyzPz **10Zn** in pyridine −0.58 V[6] and for octa(2-pyridyl)ZnTPyzPz even −0.34 V (in pyridine[17]). In the case of the observed deactivation process, the macrocycle ring is the acceptor while a peripheral amino substituent is the donor of the electrons. The more electron-deficient the macrocycle is the more feasibly ICT can be anticipated. This may explain the differences between compounds **6** and **7**. Moreover, strongly electron-donating peripheral substituents (*e.g.* 2,5-diisopropylphenoxy substituents in compounds **5**) may further decrease the electron-accepting properties of the ring and as a consequence also the feasibility of ICT. The photophysical and photochemical parameters of such compounds will therefore remain close to similar derivatives without the donor centers.

Conclusions

In conclusion, magnesium, metal-free and zinc complexes of three unsymmetrical derivatives of porphyrazine were synthesized from two different precursors using a statistical condensation approach. The compounds contained two peripheral amino substituents, the donors in ICT. Ultrafast ICT was responsible for the considerable decrease of both fluorescence and singlet oxygen quantum yields of these macrocycles if compared with corresponding compounds without any donor center. The strong influence of both macrocycle character and peripheral substituents on ICT was confirmed. The more efficient ICT proceeds in TPyzPz macrocycles and therefore they are more suitable for future development of different molecular sensors and quenchers of fluorescence based on ICT. High efficiency of the ICT is required in these applications in order to obtain a sufficiently quenched "OFF" state. Macrocycles that are structurally closer to Pc seem to be less suitable for these applications unless substituted by electron withdrawing substituents that may enhance the electron accepting properties of the whole macrocycle.

Experimental

General

All organic solvents used were of analytical grade. All chemicals for the synthesis were obtained from established suppliers (Aldrich, Acros, Merck, TCI Europe) and used as received. Zinc phthalocyanine (ZnPc) was purchased from Aldrich. TLC was performed on Merck aluminum sheets with silica gel 60 F254. Merck Kieselgel 60 (0.040–0.063 mm) was used for column chromatography. ^{1}H and ^{13}C NMR spectra were recorded on Varian Mercury Vx BB 300 spectrometer or VNMR S500 NMR spectrometer. Chemical shifts reported are relative to Me_4Si and were locked to the signal of a solvent. The UV-vis spectra were recorded using a Shimadzu UV-2401PC spectrophotometer. The fluorescence spectra were obtained by an AMINCO-Bowman Series 2 luminescence spectrometer. MALDI-TOF mass spectra were recorded in a positive reflectron mode on a Voyager-DE STR mass spectrometer (Applied Biosystems, Framingham, MA, USA) in *trans*-2-[3-(4-*tert*-butylphenyl)-2-methyl-2-propenylidene]malononitrile as the matrix. The instrument was calibrated externally with a five-point calibration using Peptide Calibration Mix1 (Laser-Bio Labs, Sophia-Antipolis, France). Synthesis of precursors **1**,[19] **2**,[20] **3**[20] and **4**[7] and metal complexes **8–10**[4] was performed according to the literature.

General procedure for synthesis of 5Mg–7Mg

Magnesium (28 eq.), and a small crystal of iodine were refluxed in anhydrous butanol for 3 h. After that time, compound **4** (1 eq.) was added. The second precursor (**1**, **2** or **3**, 3 eq.) was added in three equal portions during next hour and a half and heating was continued for the next 20 h. The mixture was cooled down in the air, the solvent was evaporated under reduced pressure, aqueous acetic acid (50% (v/v)) was added and the suspension was stirred for 30 min. The dark solid was filtered, washed with aqueous acetic acid and water and air-dried. The mixture of the congeners was separated by column chromatography on silica (eluents are mentioned below) to obtain magnesium complexes **5Mg–7Mg** as green solids.

Compound 5Mg. Starting amounts: **1** (1440 mg, 3 mmol), **4** (350 mg, 1 mmol), eluent: chloroform–acetone–methanol (20 : 1 : 1), yield: 200 mg (11%). λ_{max} (THF, 1 μM)/nm 680 (ε/dm^3 mol^{-1} cm^{-1} 148 300), 608 (24 600), 363 (80 950). δ_H (300 MHz, pyridine-d_5) 9.05 (s, 1H, ArH-Pc), 8.98 (s, 1H, ArH-Pc), 8.75–8.65 (m, 4H, ArH-Pc), 8.47 (d, J = 8.4 Hz, 2H, ArH-phenylamino), 7.97–7.85 (m, 4H, ArH-phenoxy), 7.77–7.40 (m, 14H, ArH-phenoxy), 7.08 (d, J = 8.4 Hz, 2H, ArH-phenylamino), 3.90–3.41 (m, 19H, CH, N–CH_2, N–CH_3), 1.58–1.00 (m, 78H, CH_3). δ_C (75 MHz, pyridine-d_5) 169.15, 155.26, 155.15, 155.00, 154.70, 153.20, 152.01, 151.26, 151.23, 151.19, 151.13, 142.25, 142.10, 141.81, 140.86, 134.24, 134.17, 133.76, 133.70, 133.66, 133.57, 131.22, 127.43, 127.30, 125.73, 125.58, 116.88, 108.15, 108.10, 107.89, 44.24, 37.89, 28.00, 24.31, 22.81, 13.27, some aromatic signals were not detected. *m/z* (MALDI TOF) 1814.81 $[M]^+$, 1837.80 $[M + Na]^+$, 1853.77 $[M + K]^+$.

Compound 6Mg. Starting amounts: **2** (730 mg, 2.4 mmol), **4** (280 mg, 0.8 mmol), eluent: chloroform–acetone–methanol (20 : 1 : 1), yield: 75 mg (7%). λ_{max} (THF, 1 μM)/nm 690 (ε/dm^3 mol^{-1} cm^{-1} 229 800), 623 (38 800), 373 (86 900). δ_H (300 MHz, pyridine-d$_5$) 10.21 (s, 1H, ArH-Pc), 10.19–10.15 (m, 4H, ArH-Pc), 10.14 (s, 1H, ArH-Pc), 8.45 (d, J = 8.2 Hz, 2H, ArH-phenylamino), 7.21–7.17 (m, 2H, ArH-phenylamino), 3.91 (s, 3H, N–CH$_3$), 3.79 (q, J = 7.1 Hz, 4H, N–CH$_2$), 1.64 (s, 18H, CH$_3$), 1.63–1.60 (m, 18H, CH$_3$), 1.58 (s, 9H, CH$_3$), 1.50 (s, 9H, CH$_3$), 1.15 (t, J = 7.1 Hz, 6H, NCH$_2$C*H*$_3$). δ_C (75 MHz, pyridine-d$_5$) 168.99, 155.25, 155.17, 154.96, 154.68, 154.42, 153.81, 152.84, 151.01, 146.85, 146.39, 142.85, 142.21, 142.13, 141.80, 141.70, 141.39, 139.08, 138.98, 138.95, 138.80, 132.84, 132.18, 131.60, 131.50, 131.44, 131.36, 131.16, 124.75, 117.20, 48.78, 48.73, 48.69, 48.63, 44.03, 39.03, 31.39, 13.28, some aromatic signals were not detected. *m/z* (MALDI TOF) 1286.39 [M]$^+$, 1309.38 [M + Na]$^+$, 1325.35 [M + K]$^+$.

Compound 7Mg. Starting amounts: **3** (460 mg, 1.5 mmol), **4** (175 mg, 0.5 mmol), eluent: chloroform–acetone–methanol (40 : 2 : 1), yield: 96 mg (15%). λ_{max} (THF, 1 μM)/nm 655 (ε/dm^3 mol^{-1} cm^{-1} 189 500), 595 (30 700), 382 (119 900). δ_H (300 MHz, pyridine-d$_5$) 8.51 (d, J = 8.2 Hz, 2H, ArH), 7.24 (d, J = 8.2 Hz, 2H, ArH), 3.99 (s, 3H, N–CH$_3$), 3.85–3.74 (m, 4H, N–CH$_2$), 2.31–2.16 (m, 45H, CH$_3$), 2.12 (s, 9H, CH$_3$), 1.30–1.20 (m, 6H, NCH$_2$C*H*$_3$). δ_C (75 MHz, pyridine-d$_5$) 158.13, 145.47, 131.22, 117.88, 51.31, 51.27, 51.21, 51.17, 44.42, 38.45, 30.76, 13.40, some aromatic signals were not detected. *m/z* (MALDI TOF) 1292.40 [M]$^+$, 1315.38 [M + Na]$^+$, 1331.36 [M + K]$^+$.

General procedure for synthesis of 5H–7H

The magnesium complex (**5Mg**, **6Mg** or **7Mg**, 1 eq.) was dissolved in chloroform and stirred at rt for 1 h with acid (*p*-toluenesulfonic acid in THF for **5Mg**, trifluoroacetic acid for **6Mg** and **7Mg**, 15 eq.). Thereafter, the solvents were evaporated under reduced pressure, the crude product was washed with water and purified by column chromatography (eluents are mentioned below) to obtain a green solid.

Compound 5H. Starting amount: **5Mg** (154 mg, 0.084 mmol), eluent: chloroform–acetone–methanol (80 : 2 : 1), yield: 103 mg (68%). λ_{max} (THF, 1 μM)/nm 700 (ε/dm^3 mol^{-1} cm^{-1} 59 800), 662 (50 600), 637 (24 600), 606(13 700), 506 (7200), 353 (42 700). δ_H (300 MHz, pyridine-d$_5$) 9.01 (s, 1H, ArH-Pc), 8.94 (s, 1H, ArH-Pc), 8.68–8.63 (m, 4H, ArH-Pc), 8.52 (d, J = 8.8 Hz, 2H, ArH-phenylamino), 7.94 (t, J = 7.8 Hz, 4H, ArH-phenoxy), 7.75 (d, J = 7.8 Hz, 8H, ArH-phenoxy), 7.70–7.52 (m, 6H, ArH-phenoxy), 7.21–7.15 (m, 2H, ArH-phenylamino), 3.91–3.67 (m, 10H, CH), 3.66–3.56 (m, 7H, N–CH$_2$, N–CH$_3$), 3.45–3.30 (m, 2H, CH), 1.58–1.20 (m, 72H, CHCH$_3$), 1.20–1.11 (m, 6H, NCH$_2$C*H*$_3$), −0.71 (s, 2H, NH). δ_C (75 MHz, pyridine-d$_5$) 169.06, 152.53, 152.09, 152.04, 151.92, 151.84, 149.23, 142.17, 142.07, 142.04, 142.00, 141.77, 141.32, 134.80, 132.37, 131.73, 131.23, 127.62, 127.51, 127.34, 125.86, 125.83, 125.73, 125.43, 125.13, 117.72, 108.13, 107.93, 44.26, 38.20, 28.03, 27.82, 27.78, 24.31, 23.04, 13.19, some aromatic signals were not detected. *m/z* (MALDI TOF) 1792.76 [M]$^+$, 1815.72 [M + Na]$^+$, 1831.70 [M + K]$^+$.

Compound 6H. Starting amount: **6Mg** (42 mg, 0.033 mmol), eluent: chloroform–acetone–methanol (20 : 1 : 1), yield: 40 mg (97%). λ_{max} (THF, 1 μM)/nm 715 (ε/dm^3 mol^{-1} cm^{-1} 143 800), 684 (130 500), 655 (46 000), 624 (33 900), 549 (21 000), 352 (79 700). δ_H (500 MHz, pyridine-d$_5$) 10.00 (s, 1H, ArH-Pc), 9.98 (s, 1H, ArH-Pc), 9.91 (s, 1H, ArH-Pc), 9.90 (s, 1H, ArH-Pc), 9.88 (s, 1H, ArH-Pc), 9.81 (s, 1H, ArH-Pc), 8.61 (d, J = 8.4 Hz, 2H, ArH-phenylamino), 7.49 (d, J = 8.4 Hz, 2H, ArH-phenylamino), 4.04 (s, 3H, N–CH$_3$), 3.89–3.78 (m, 4H, N–CH$_2$), 1.76 (s, 9H, CH$_3$), 1.75 (s, 9H, CH$_3$), 1.74 (s, 9H, CH$_3$), 1.72 (s, 9H, CH$_3$), 1.66 (s, 9H, CH$_3$), 1.59 (s, 9H, CH$_3$), 1.21–1.14 (m, 3H, NCH$_2$C*H*$_3$), −0.65 (s, 2H, NH). δ_C (125 MHz, pyridine-d$_5$) 168.90, 153.35, 144.14, 143.82, 143.47, 143.04, 142.12, 131.39, 119.04, 49.13, 49.06, 48.99, 48.90, 48.78, 48.66, 43.84, 39.74, 31.48, 31.47, 31.43, 31.42, 13.13, some aromatic signals were not detected. *m/z* (MALDI TOF) 1264.40 [M]$^+$.

Compound 7H. Starting amount: **7Mg** (60 mg, 0.05 mmol), eluent: toluene–chloroform–pyridine (8 : 10 : 1), yield: 56 mg (94%). λ_{max} (THF, 1 μM)/nm 674 (ε/dm^3 mol^{-1} cm^{-1} 106 300), 648 (90 900), 618sh, 593 (31 000), 551 (27 800), 474 (40 800), 366 (101 700). δ_H (300 MHz, pyridine-d$_5$) 12.60 (s, 2H, NH), 8.62 (d, J = 8.6 Hz, 2H, ArH), 7.54 (d, J = 8.6 Hz, 2H, ArH), 4.27 (s, 3H, N–CH$_3$), 3.99 (q, J = 7.2 Hz, 4H, N–CH$_2$), 2.30 (s, 9H, CH$_3$), 2.26 (s, 18H, CH$_3$), 2.23 (s, 27H, CH$_3$), 1.45–1.36 (m, 6H, NCH$_2$C*H*$_3$). δ_C (75 MHz, pyridine-d$_5$) 168.92, 159.64, 159.56, 159.39, 159.14, 158.48, 158.44, 152.75, 147.61, 145.07, 144.83, 131.25, 126.23, 119.24, 51.93, 51.91, 51.43, 51.38, 51.30, 44.69, 39.18, 30.82, 30.72, 13.56, some aromatic signals were not detected. *m/z* (MALDI TOF) 1270.42 [M]$^+$, 1293.41 [M + Na]$^+$, 1309.38 [M + K]$^+$.

General procedure for synthesis of 5Zn–7Zn

Metal-free derivatives **5H–7H** (1 eq.) were dissolved in pyridine and anhydrous zinc acetate (15–20 eq.) was added. The mixture was put into a preheated oil bath to 130 °C and stirred at this temperature for 2.5 h. After this time, solvent was removed under reduced pressure and the dark solid washed thoroughly with water. Finally, the product was purified by column chromatography on silica (eluents are mentioned below) to obtain a green solid.

Compound 5Zn. Starting amount: **5H** (88.2 mg, 0.05 mmol), eluent: chloroform–acetone–methanol (20 : 1 : 1), yield: 42 mg (46%). λ_{max} (THF, 1 μM)/nm 678 (ε/dm^3 mol^{-1} cm^{-1} 201 900), 607 (34 200), 359 (96 100). δ_H (500 MHz, pyridine-d$_5$) 9.04 (s, 1H, ArH-Pc), 8.97 (s, 1H, ArH-Pc), 8.74–8.64 (m, 4H, ArH-Pc), 8.49 (d, J = 8.4 Hz, 2H, ArH-phenylamino), 7.95–7.88 (m, 4H, ArH-phenoxy), 7.77–7.46 (m, 14H, ArH-phenoxy), 7.10 (d, J = 8.4 Hz, 2H, ArH-phenylamino), 3.85–3.66 (m, 12H, CH), 3.62 (q, J = 7.0 Hz, 4H, N–CH$_2$), 3.55 (s, 3H, N–CH$_3$), 1.57–1.06 (m, 78H, CH$_3$). δ_C (125 MHz, pyridine-d$_5$) 169.15, 155.15, 155.03, 154.90, 154.58, 153.89, 153.16, 152.07, 151.39, 151.36, 151.33, 151.29, 151.24, 149.35, 148.88, 145.82, 145.63, 142.26, 142.15, 142.12, 142.11, 141.82, 140.53, 135.99, 133.85, 133.77,

133.33, 133.29, 133.23, 133.15, 131.22, 127.50, 127.45, 127.34, 127.28, 125.77, 125.74, 125.66, 125.60, 124.38, 117.03, 108.28, 108.05, 108.00, 107.76, 44.31, 37.92, 28.02, 24.62, 22.90, 13.29, some aromatic signals were not detected. *m/z* (MALDI TOF) 1854.63 $[M]^+$, 1877.61 $[M + Na]^+$, 1893.59 $[M + K]^+$.

Compound 6Zn. Starting amount: **6H** (31.3 mg, 0.025 mmol), eluent: chloroform–acetone–methanol (20 : 1 : 1), yield: 21 mg (62%). λ_{max} (THF, 1 μM)/nm 689 (ε/dm^3 mol^{-1} cm^{-1} 267 800), 622 (45 300), 365 (97 100). δ_H (300 MHz, pyridine-d_5) 10.21 (s, 1H, ArH-Pc), 10.17 (s, 2H, ArH-Pc), 10.16 (s, 2H, ArH-Pc), 10.14 (s, 1H, ArH-Pc), 8.47 (d, J = 8.7 Hz, 2H, ArH-phenylamino), 7.22 (d, J = 8.7 Hz, 2H, ArH-phenylamino), 3.94 (s, 3H, N–CH_3), 3.81 (q, J = 7.1 Hz, 4H, N–CH_2), 1.66 (s, 18H, CH_3), 1.64 (s, 9H, CH_3), 1.63 (s, 9H, CH_3), 1.60 (s, 9H, CH_3), 1.51 (s, 9H, CH_3), 1.21–1.14 (m, 6H, NCH_2CH_3). δ_C (75 MHz, pyridine-d_5) 168.95, 155.41, 155.31, 155.13, 154.81, 154.59, 153.97, 152.94, 151.26, 146.64, 146.41, 143.13, 142.41, 142.33, 142.31, 141.90, 141.52, 141.35, 138.49, 138.38, 138.33, 138.19, 132.64, 131.90, 131.36, 130.82, 117.40, 48.85, 48.83, 48.78, 48.74, 48.67, 44.06, 39.09, 31.38, 31.35, 13.26, some aromatic signals were not detected. *m/z* (MALDI TOF) 1326.28 $[M]^+$, 1349.25 $[M + Na]^+$.

Compound 7Zn. Starting amount: **7H** (40 mg, 0.03 mmol), eluent: chloroform–acetone–methanol (40 : 2 : 1), yield: 37 mg (88%). λ_{max} (THF, 1 μM)/nm 654 (ε/dm^3 mol^{-1} cm^{-1} 177 100), 594 (29 500), 377 (108 500). δ_H (300 MHz, pyridine-d_5) 8.53 (d, J = 8.7 Hz, 2H, ArH), 7.29 (d, J = 8.7 Hz, 2H, ArH), 4.03 (s, 3H, N–CH_3), 3.84 (q, J = 7.1 Hz, 4H, N–CH_2), 2.29–2.22 (m, 45H, CH_3), 2.14 (s, 9H, CH_3), 1.34–1.21 (m, 6H, NCH_2CH_3). δ_C (75 MHz, pyridine-d_5) 168.89, 159.20, 158.90, 158.44, 158.40, 158.16, 158.05, 153.01, 152.41, 152.22, 151.91, 151.35, 151.11, 150.99, 150.72, 150.70, 147.03, 146.25, 145.34, 145.12, 145.00, 144.77, 144.75, 144.69, 141.58, 131.25, 125.22, 118.02, 51.35, 51.28, 44.51, 38.50, 30.74, 29.98, 13.40. *m/z* (MALDI TOF) 1332.33 $[M]^+$, 1355.32 $[M + Na]^+$, 1371.29 $[M + K]^+$.

Singlet oxygen and fluorescence quantum yields

Quantum yields of singlet oxygen formation (Φ_Δ) and fluorescence (Φ_F) were measured in THF using the comparative methods with zinc phthalocyanine (ZnPc) as a reference (Φ_Δ = 0.53 in THF,[16] Φ_F = 0.30 in chloronaphthalene[15]). Excitation wavelength for Φ_F determination was set to 612 nm. Details on the methods can be found elsewhere.[4] No changes in the shape or intensity of the absorption bands of tested dyes were observed within the course of the experiments. All the samples used for quantum yields determinations were further purified on silica TLC plates to ensure their high purity. The eluents used are given above for each compound. Corresponding parts of the plates were scraped off, the sample was extracted from the silica with THF, filtered and the solvent was evaporated.

Acknowledgements

The work was supported by Charles University in Prague (projects GAUK 68110/2010 and SVV 265 001). Authors are grateful to Jiří Kuneš for NMR measurements and to Vojtěch Tambor for measurements of MS spectra.

Notes and references

1 *Handbook of Porphyrin Science*, ed. K. M. Kadish, K. M. Smith and R. Guilard, World Scientific Publishing, Singapore, 2010.
2 (*a*) M. V. Martinez-Diaz, G. de la Torrea and T. Torres, *Chem. Commun.*, 2010, **46**, 7090–7108; (*b*) L. Giribabu, V. K. Singh, C. V. Kumar, Y. Soujanya, P. Y. Reddy and M. L. Kantam, *Sol. Energy*, 2011, **85**, 1204–1212.
3 I. V. Nesterova, C. A. Bennett, S. S. Erdem, R. P. Hammer, P. L. Deininger and S. A. Soper, *Analyst*, 2011, **136**, 1103–1105.
4 P. Zimcik, V. Novakova, K. Kopecky, M. Miletin, R. Z. Uslu Kobak, E. Svandrlikova, L. Váchová and K. Lang, *Inorg. Chem.*, 2012, **51**, 4215–4223.
5 (*a*) P. Zimcik, M. Miletin, H. Radilova, V. Novakova, K. Kopecky, J. Svec and E. Rudolf, *Photochem. Photobiol.*, 2010, **86**, 168–175; (*b*) J. T. F. Lau, P.-C. Lo, W.-P. Fong and D. K. P. Ng, *Chem.–Eur. J.*, 2011, **17**, 7569–7577.
6 V. Novakova, P. Zimcik, M. Miletin, L. Vachova, K. Kopecky, K. Lang, P. Chábera and T. Polívka, *Phys. Chem. Chem. Phys.*, 2010, **12**, 2555–2563.
7 K. Kopecky, V. Novakova, M. Miletin, R. Kucera and P. Zimcik, *Bioconjugate Chem.*, 2010, **21**, 1872–1879.
8 (*a*) V. Novakova, E. H. Mørkved, M. Miletin and P. Zimcik, *J. Porphyrins Phthalocyanines*, 2010, **14**, 582–591; (*b*) V. Novakova, M. Miletin, K. Kopecky and P. Zimcik, *Chem.–Eur. J.*, 2011, **17**, 14273–14282.
9 (*a*) X. F. Zhang, *J. Fluoresc.*, 2011, **21**, 1559–1564; (*b*) X. J. Jiang, P. C. Lo, S. L. Yeung, W. P. Fong and D. K. P. Ng, *Chem. Commun.*, 2010, **46**, 3188–3190.
10 (*a*) X. F. Zhang, H. W. Zheng, S. M. Jin and R. Y. Wang, *Dyes Pigm.*, 2010, **87**, 139–143; (*b*) X. F. Zhang and W. F. Guo, *J. Photochem. Photobiol., A*, 2011, **225**, 117–124.
11 G. De La Torre, C. G. Claessens and T. Torres, *Eur. J. Org. Chem.*, 2000, 2821–2830.
12 (*a*) J. Mack and N. Kobayashi, *Chem. Rev.*, 2011, **111**, 281–321; (*b*) A. J. Wang, L. L. Long and C. Zhang, *Tetrahedron*, 2012, **68**, 2433–2451.
13 M. Kostka, P. Zimcik, M. Miletin, P. Klemera, K. Kopecky and Z. Musil, *J. Photochem. Photobiol., A*, 2006, **178**, 16–25.
14 Z. Musil, P. Zimcik, M. Miletin, K. Kopecky and J. Lenco, *Eur. J. Org. Chem.*, 2007, 4535–4542.
15 P. G. Seybold and M. Gouterman, *J. Mol. Spectrosc.*, 1969, **31**, 1–13.
16 L. Kaestner, M. Cesson, K. Kassab, T. Christensen, P. D. Edminson, M. J. Cook, I. Chambrier and G. Jori, *Photochem. Photobiol. Sci.*, 2003, **2**, 660–667.
17 M. P. Donzello, Z. Ou, D. Dini, M. Meneghetti, C. Ercolani and K. M. Kadish, *Inorg. Chem.*, 2004, **43**, 8637–8648.
18 A. R. Özkaya, A. G. Gurek, A. Gül and O. Bekaroğlu, *Polyhedron*, 1997, **16**, 1877–1883.
19 N. B. McKeown, S. Makhseed, K. J. Msayib, L. L. Ooi, M. Helliwell and J. E. Warren, *Angew. Chem., Int. Ed.*, 2005, **44**, 7546–7549.
20 P. Zimcik, M. Miletin, V. Novakova, K. Kopecky, M. Nejedla, V. Stara and K. Sedlackova, *Aust. J. Chem.*, 2009, **62**, 425–433.

Dalton Transactions

Electronic Supplementary Information

Effect of intramolecular charge transfer on fluorescence and singlet oxygen production of phthalocyanine analogues

Lenka Vachova,[a] Veronika Novakova,[b] Kamil Kopecky,[a] Miroslav Miletin[a] and Petr Zimcik*[a]

[a]Department of Pharmaceutical Chemistry and Drug Control, Faculty of Pharmacy in Hradec Kralove, Charles University in Prague, Heyrovskeho 1203, 50005, Hradec Kralove, Czech Republic. Fax: +420 495067167; Tel: +420 495067257, E-mail: petr.zimcik@faf.cuni.cz,

[b]Department of Biophysics and Physical Chemistry, Faculty of Pharmacy in Hradec Kralove, Charles University in Prague, Heyrovskeho 1203, 50005, Hradec Kralove, Czech Republic.

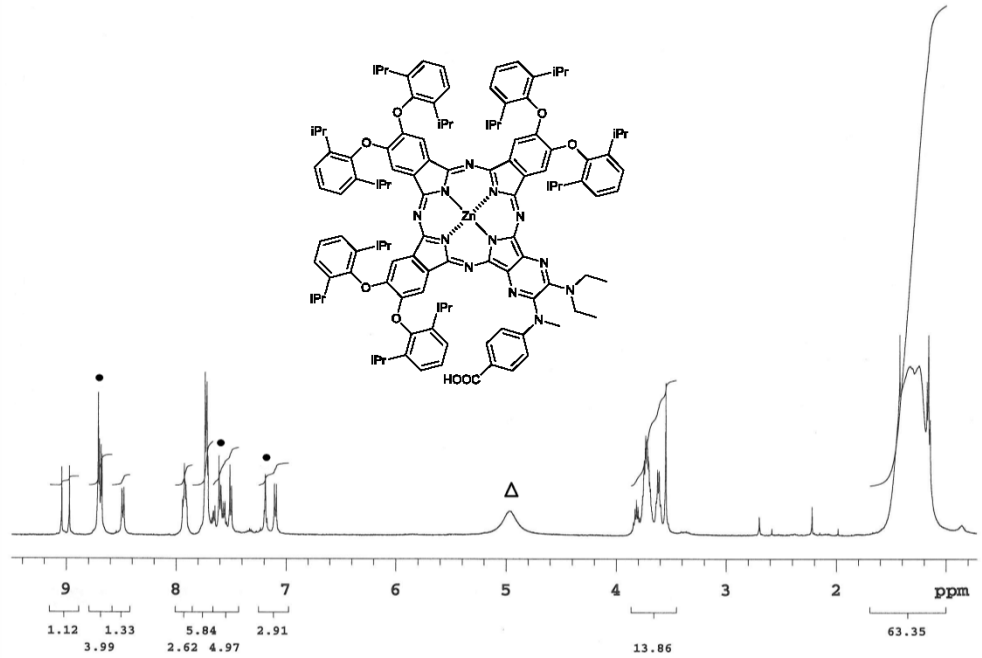

Figure S1. ^{1}H NMR spectrum of compound **5Zn** in pyridine-d_5. Dots indicate residual signal of non-deuterated solvent, triangle indicates signal of water.

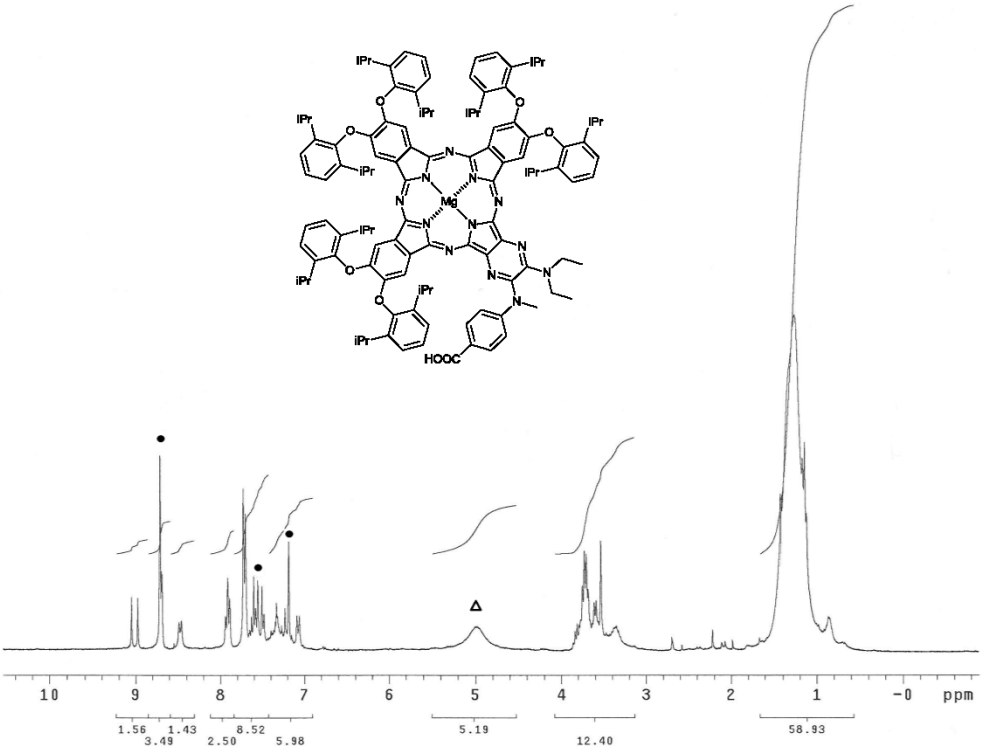

Figure S2. ^{1}H NMR spectrum of compound **5Mg** in pyridine-d_5. Dots indicate residual signal of non-deuterated solvent, triangle indicates signal of water.

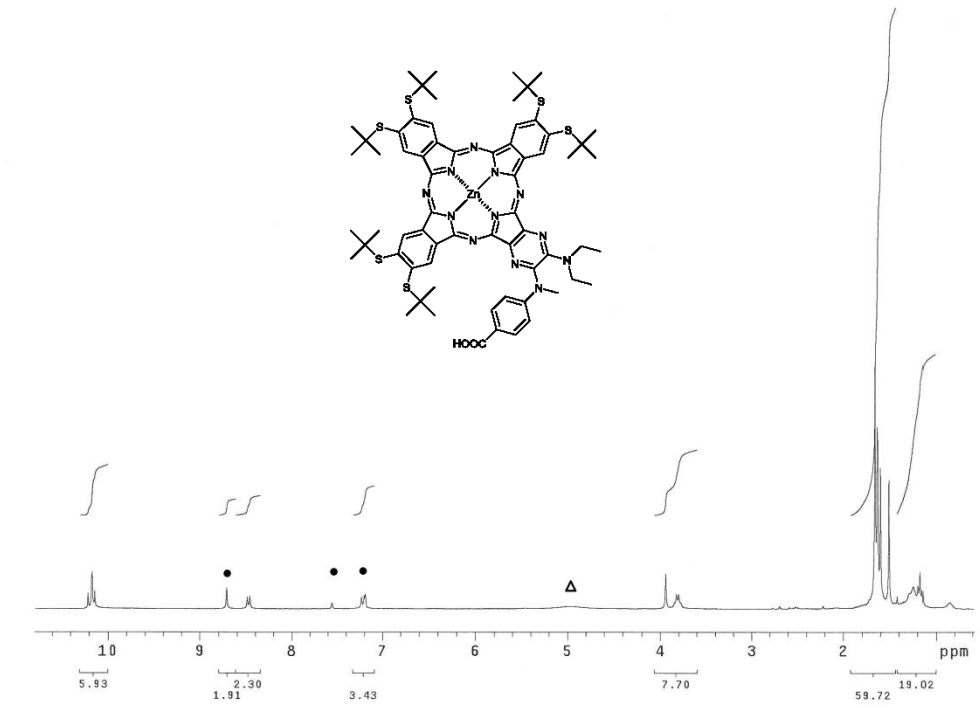

Figure S3. ^{1}H NMR spectrum of compound **6Zn** in pyridine-d_5. Dots indicate residual signal of non-deuterated solvent, triangle indicates signal of water.

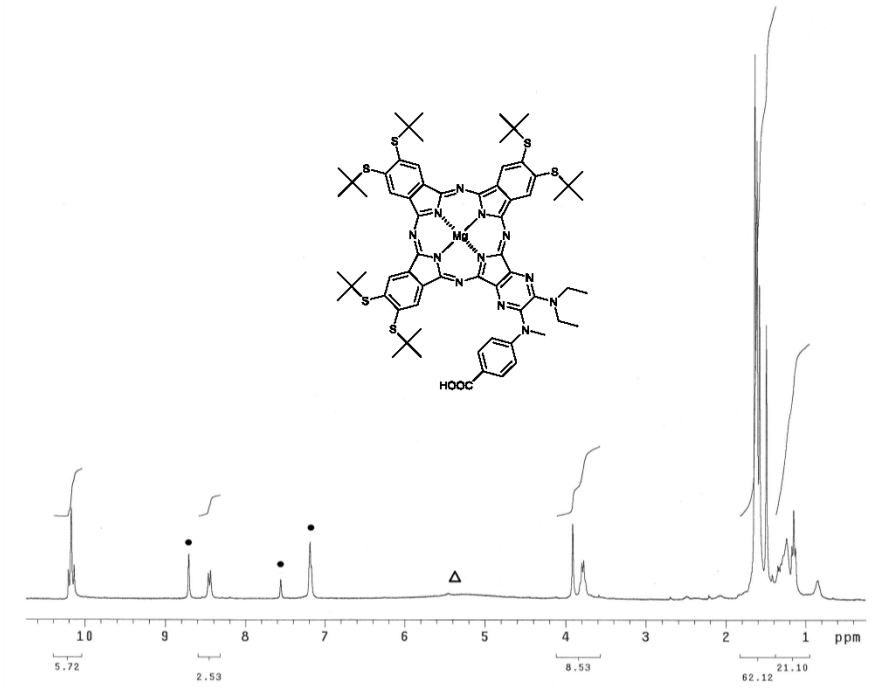

Figure S4. ^{1}H NMR spectrum of compound **6Mg** in pyridine-d_5. Dots indicate residual signal of non-deuterated solvent, triangle indicates signal of water.

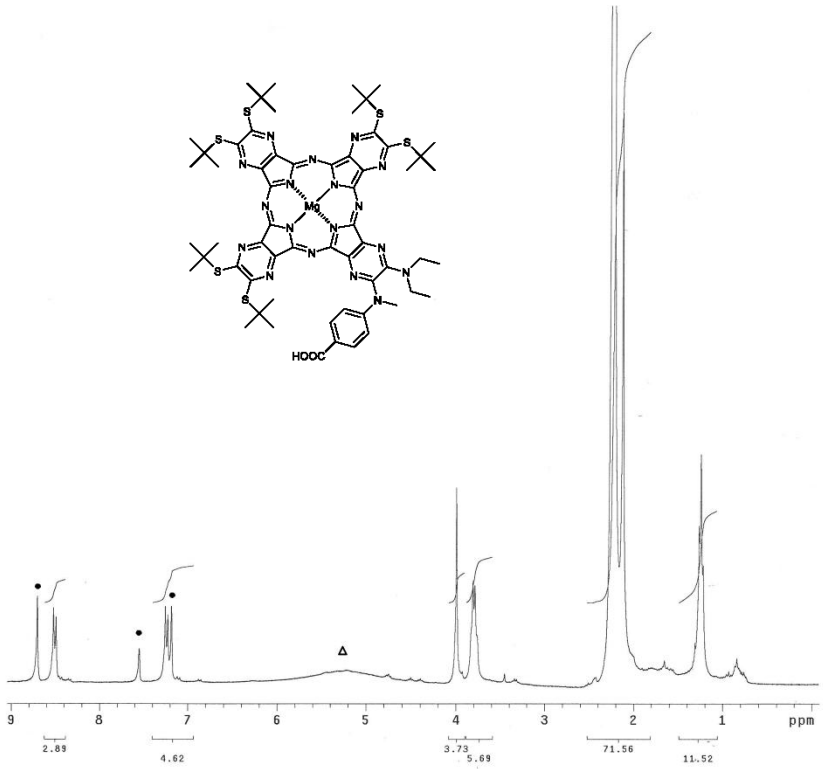

Figure S5. ^{1}H NMR spectrum of compound **7Mg** in pyridine-d_5. Dots indicate residual signal of non-deuterated solvent, triangle indicates signal of water.

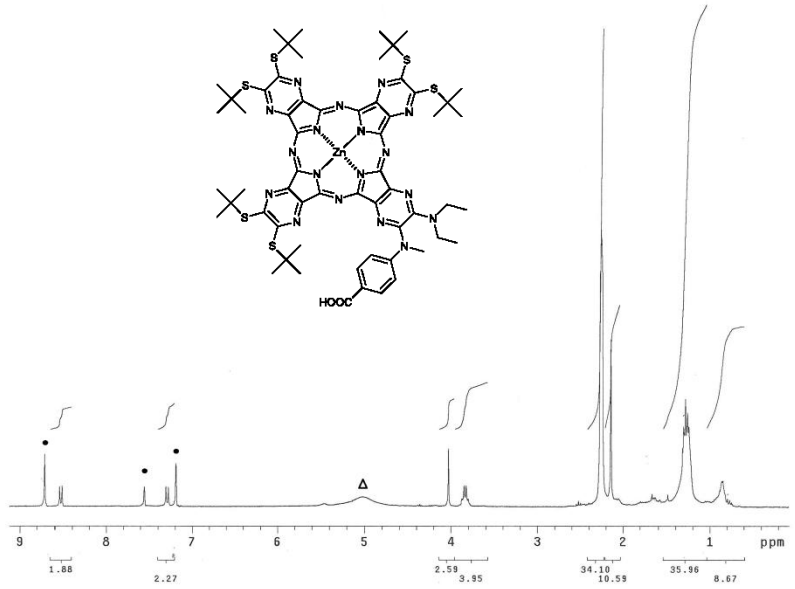

Figure S6. ^{1}H NMR spectrum of compound **7Zn** in pyridine-d_5. Dots indicate residual signal of non-deuterated solvent, triangle indicates signal of water.

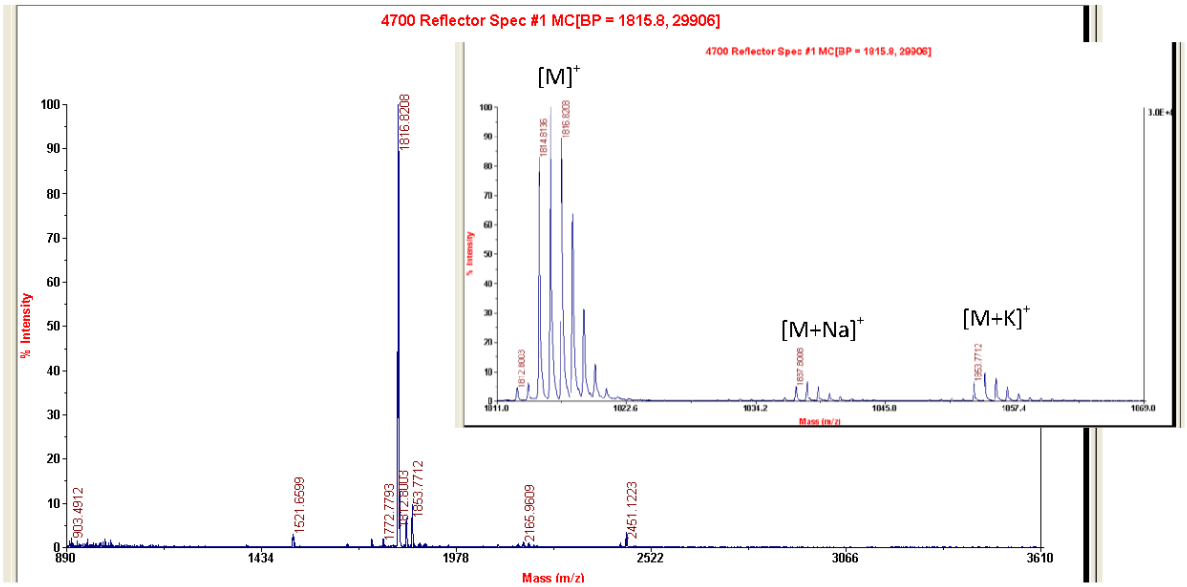

Figure S7. MALDI-TOF mass spectra of compound **5Mg**.

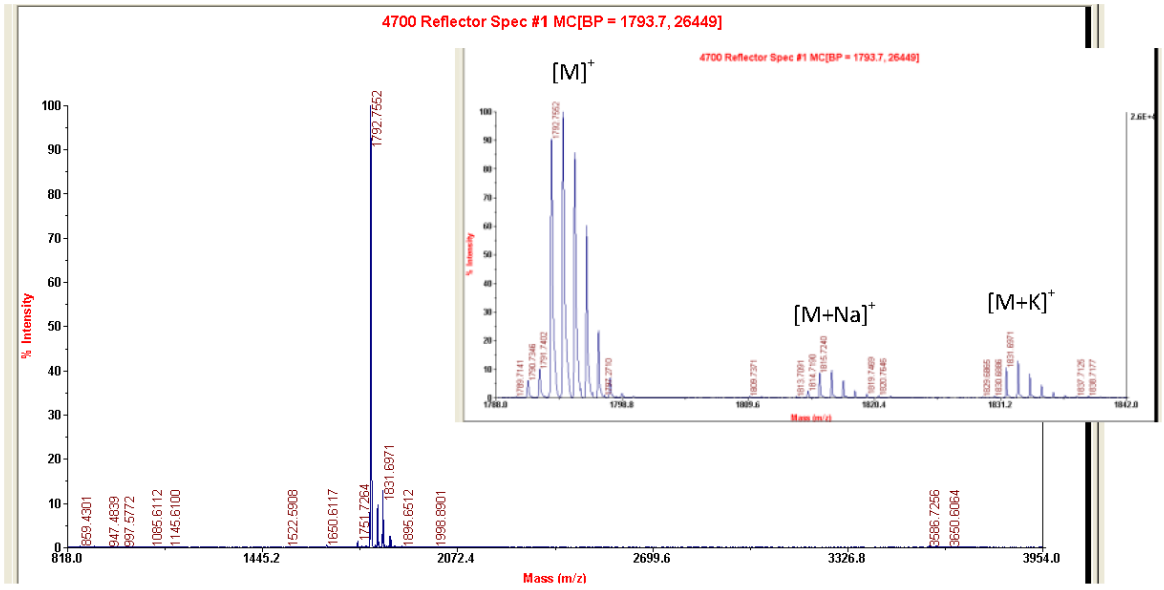

Figure S8. MALDI-TOF mass spectra of compound **5H**.

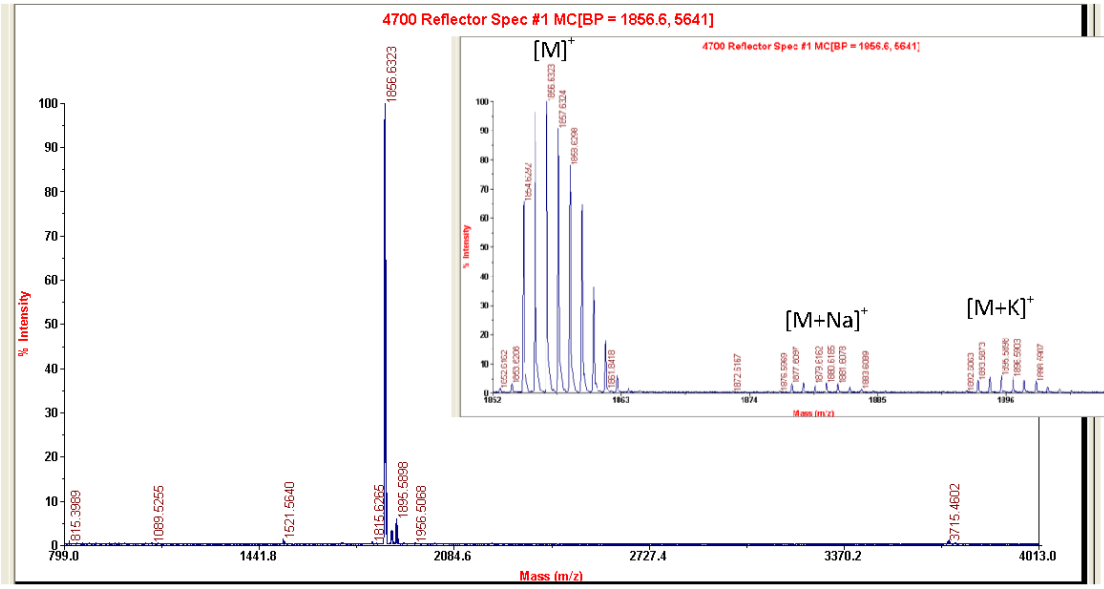

Figure S9. MALDI-TOF mass spectra of compound **5Zn**.

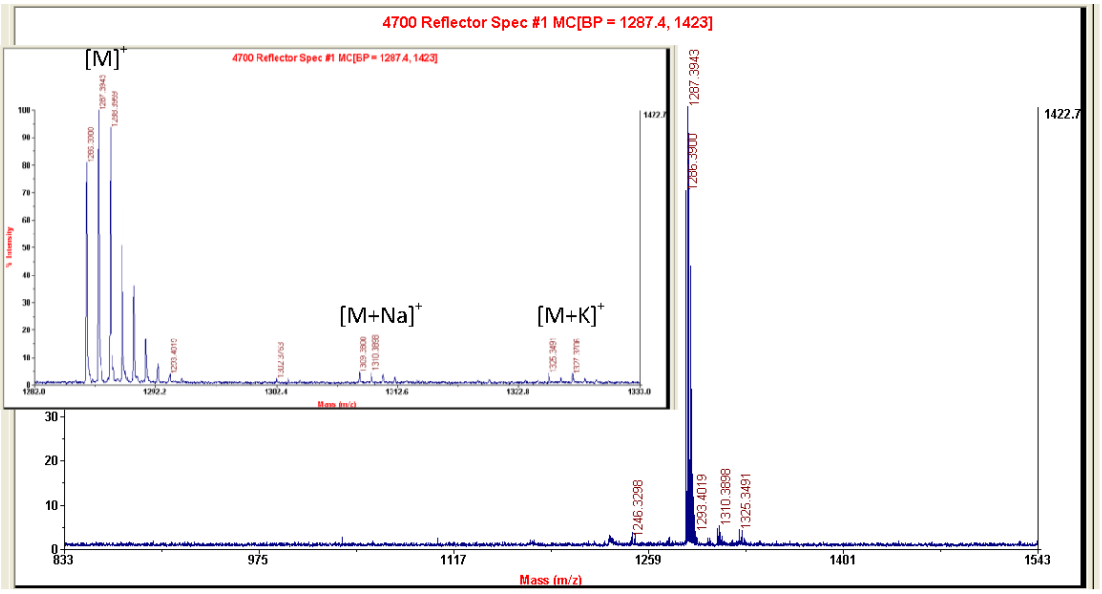

Figure S10. MALDI-TOF mass spectra of compound **6Mg**.

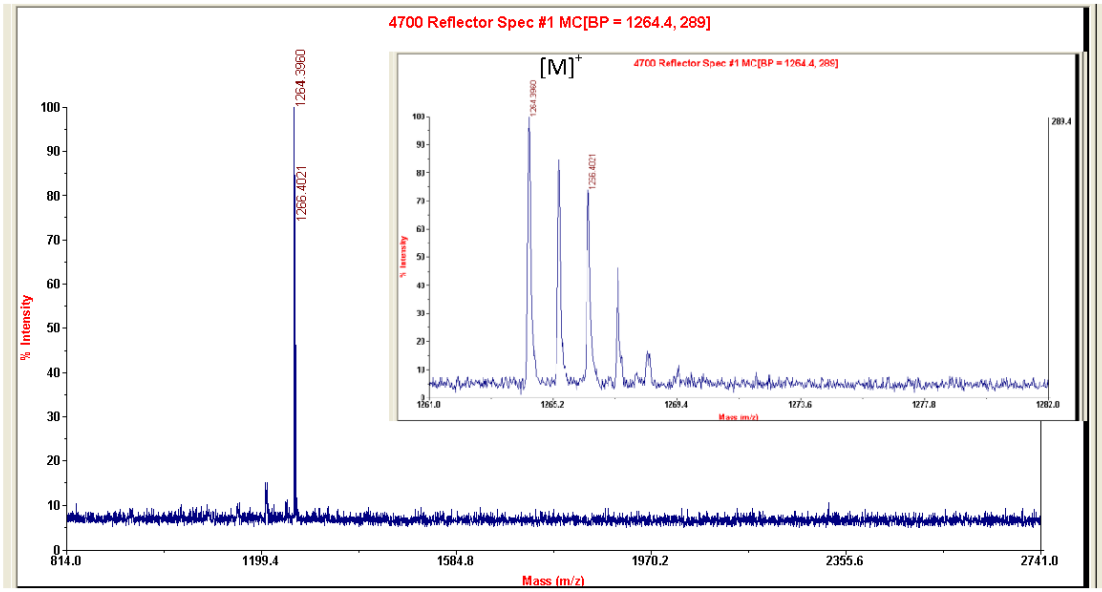

Figure S11. MALDI-TOF mass spectra of compound **6H**.

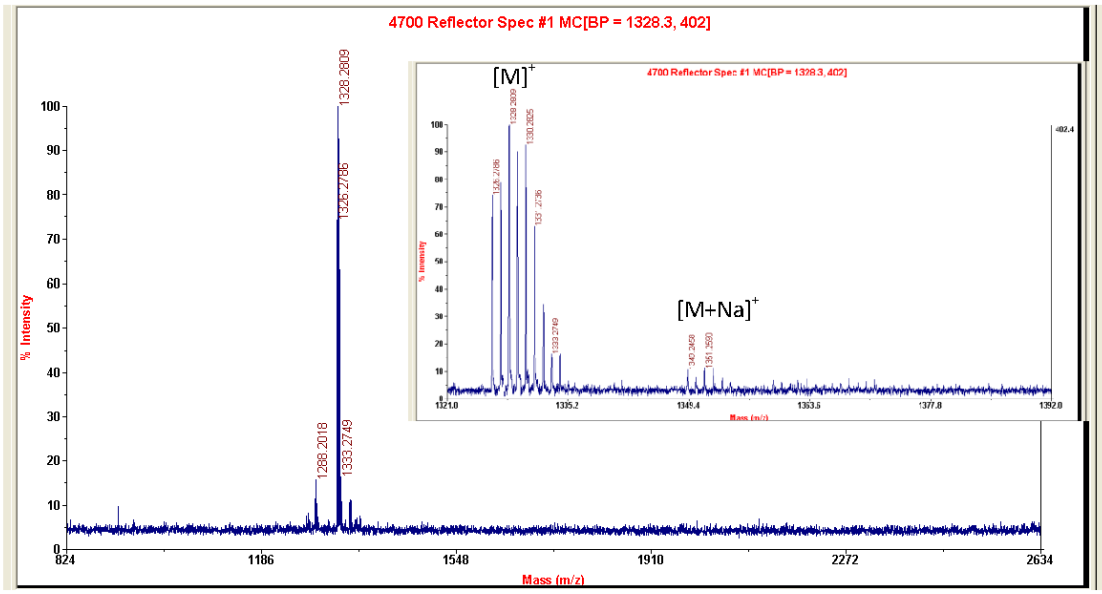

Figure S12. MALDI-TOF mass spectra of compound **6Zn**.

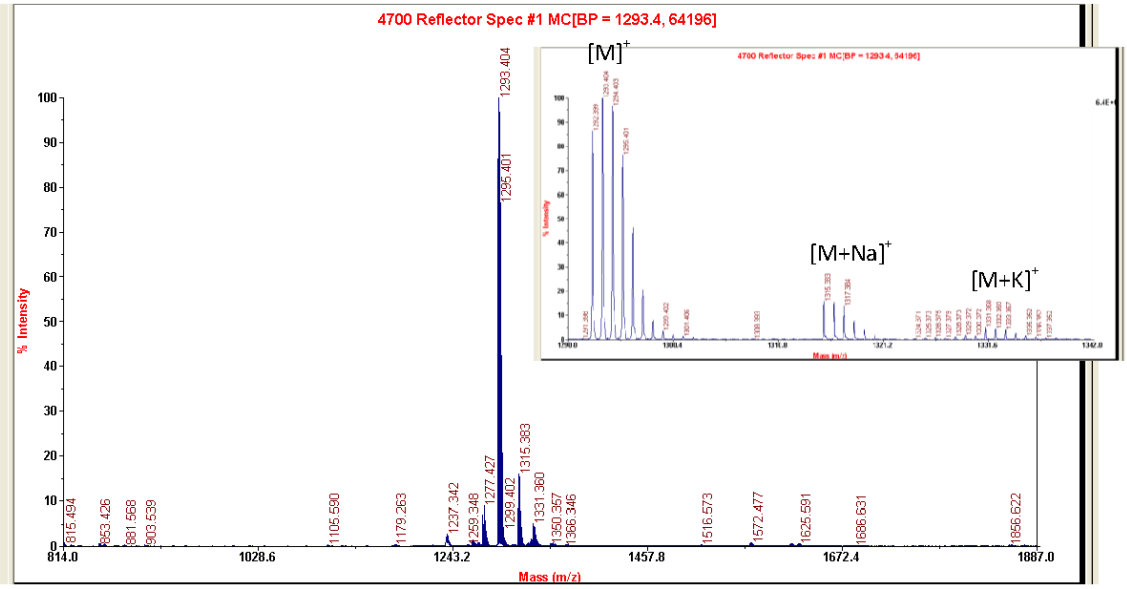

Figure S13. MALDI-TOF mass spectra of compound **7Mg**.

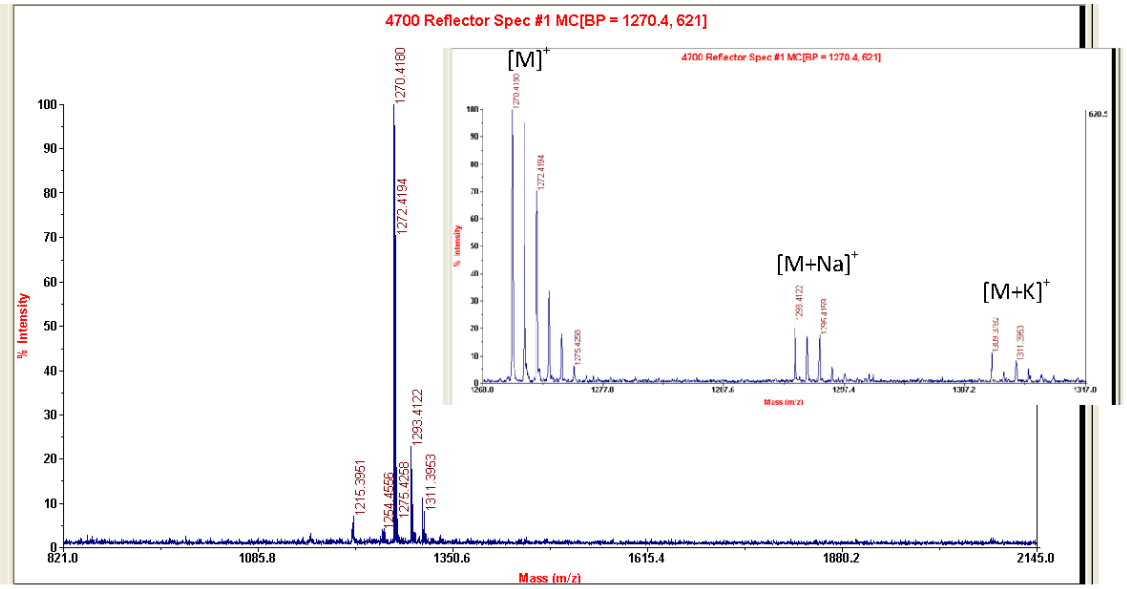

Figure S14. MALDI-TOF mass spectra of compound **7H**.

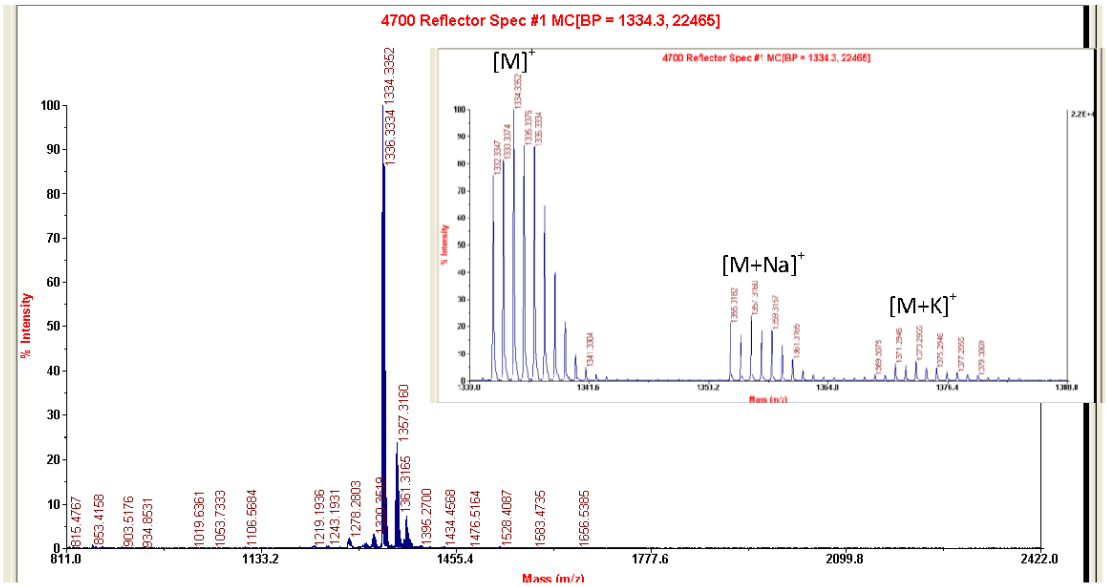

Figure S15. MALDI-TOF mass spectra of compound **7Zn**.

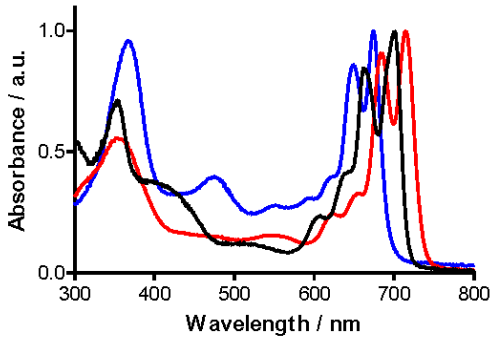

Figure S16. Absorption spectra of **5H** (black), **6H** (red) and **7H** (blue) in THF. Spectra were normalized to the same absorption in Q-band maximum.

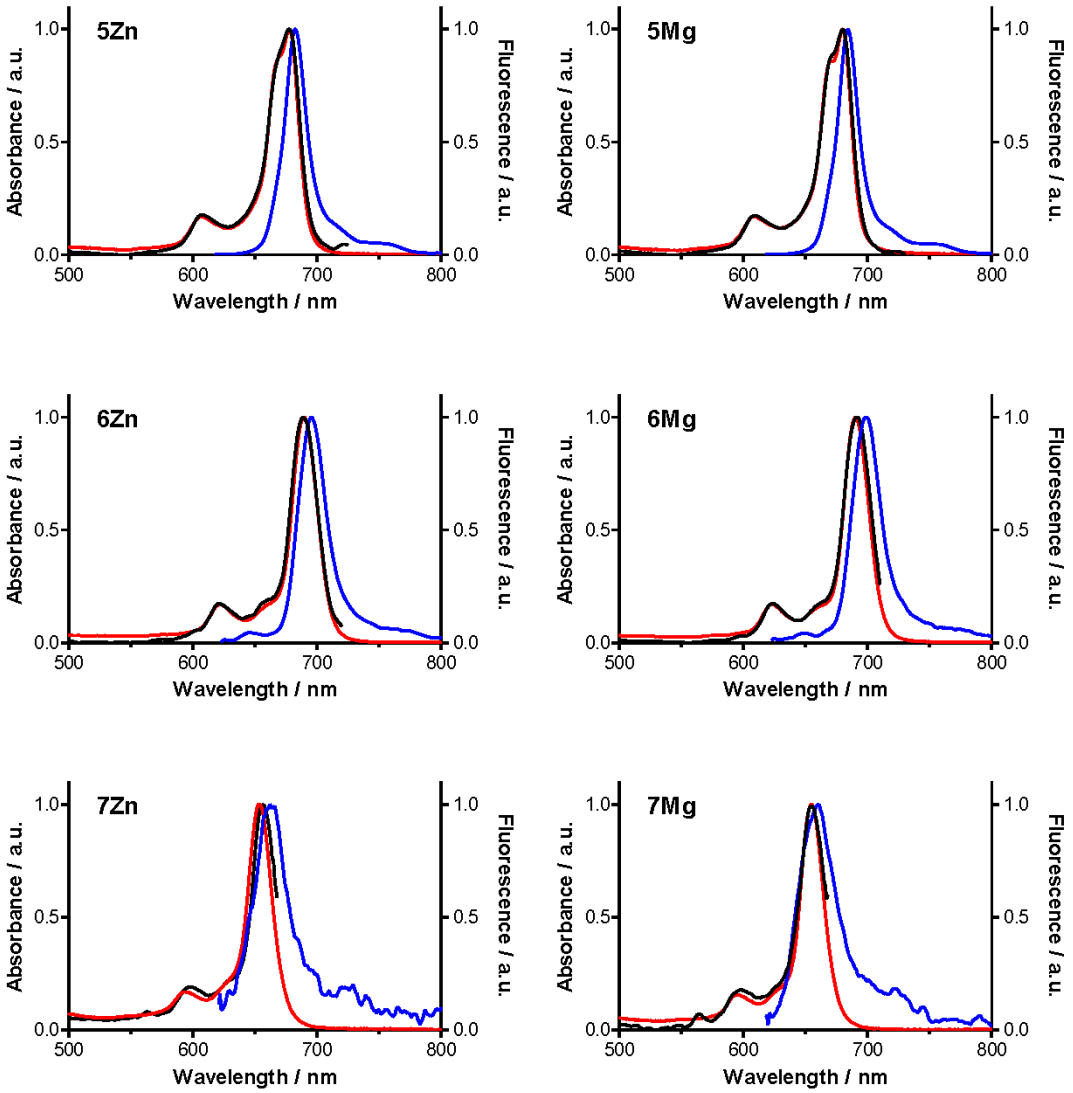

Figure S17. Absorption (red), emission (blue) and excitation (black) spectra of compounds **5Mg**-**7Mg** and **5Zn**-**7Zn** in THF. λ_{exc} = 612 nm. Emission wavelength that was observed during collecting excitation spectra was 675 nm (**7Zn**, **7Mg**), 720 nm (**6Mg**), 730 nm (**6Zn**) and 740 nm (**5Mg**, **5Zn**).

1.3. **P3**

VACHOVA L., Machacek M., Kučera R., Demuth J., Cermak P., Kopecky K., Miletin M., Jedlickova A., Simunek T., Novakova V., Zimcik P.: Heteroatom-substituted tetra(3,4-pyrido)-porphyrazines: a stride toward near-infrared absorbing macrocycles. *Org. Biomol. Chem*., **2015**, 13, 5608-5612. IF_{2016} 3,564.

Podíl autorky: Syntéza většiny prekurzorů a cílových molekul, jejich izolace a charakterizace, fotofyzikální měření, příprava vzorků na HPLC chromatografii, analýza dat. Spoluautor textu.

Organic & Biomolecular Chemistry

COMMUNICATION

Heteroatom-substituted tetra(3,4-pyrido)-porphyrazines: a stride toward near-infrared-absorbing macrocycles†

Lenka Vachova,[a] Miloslav Machacek,[b] Radim Kučera,[a] Jiri Demuth,[c] Pavel Cermak,[c] Kamil Kopecky,[a] Miroslav Miletin,[a] Adela Jedlickova,[b] Tomas Simunek,[b] Veronika Novakova*[c] and Petr Zimcik*[a]

Cite this: *Org. Biomol. Chem.*, 2015, **13**, 5608

Received 1st April 2015,
Accepted 8th April 2015

DOI: 10.1039/c5ob00651a

www.rsc.org/obc

A synthesis procedure for heteroatom-substituted tetra(3,4-pyrido)-porphyrazines that absorb light near 800 nm was developed. Based on the observed relationships between the structure and photophysical parameters, a novel highly photodynamically active (IC_{50} = 0.26 μM) compound was synthesized and biologically characterized.

Tetrapyridoporphyrazines (TPyPzs) are a class of phthalocyanine (Pc) aza analogs in which all four benzene rings are replaced by pyridines. In general, the two types of TPyPz derivatives, namely tetrapyrido[3,4-*b*:3′,4′-*g*:3″,4″-*l*:3‴,4‴-*q*]-porphyrazines (tetra(3,4-pyrido)porphyrazines) and tetrapyrido-[2,3-*b*:2′,3′-*g*:2″,3″-*l*:2‴,3‴-*q*]porphyrazines (tetra(2,3-pyrido)-porphyrazines), are distinguished by the nitrogen position in the pyridine ring. The main Q-band absorption peak of the 2,3-isomer undergoes an undesirable blue shift relative to that of the parent Pc.[1,2] On the other hand, the absorption properties of the former remain unchanged after isosteric replacement of CH for nitrogen in the Pc benzene ring.[1,2] Recently, 3,4-isomers have received much attention for use in many applications because of their intriguing electrocatalytical,[1,3] photosensitizing,[4] and surface-binding properties.[5] Surprisingly, although TPyPzs were among the first Pc analogs described by Linstead in 1937,[6] their structural modifications have been limited to central cation exchange and quaternization of the pyridine nitrogen till now.[7] Very few reports on alkyl-substituted derivatives have appeared in the literature.[8]

It is well known that heteroatoms, such as O, S and N, substantially influence both the spectral and photophysical properties of Pc-type macrocycles when they are attached directly to the core,[9] particularly in non-peripheral (α) positions.[10,11] This work therefore focuses on developing the first heteroatom-substituted TPyPzs and investigating their properties to determine their potential for use in photodynamic therapy (PDT). The substituents in this study were chosen not only to study the effects of different connecting heteroatoms (O, S, N) but also to ensure that their bulkiness prevented aggregation of the TPyPzs in solution. Thus, precursors **2**, **3** and **4** (Scheme 1) were selected for this study. Zinc(II) and Mg(II) were used as the central cations in the target TPyPzs due to their suitable photophysical properties.

TPyPzs are typically synthesized by cyclotetramerization of pyridine-3,4-dicarbonitrile. The synthesis of the precursors **2–4** was achieved by high-yielding nucleophilic substitutions with thiolate, phenolate or amine in **1** (**1** was synthesized according to the literature method[12]) due to the strongly electron-deficient character of its $C_{(2)}$ (Scheme 1). The precursor **1** was smoothly converted to *tert*-butylsulfanyl derivative **2** by the

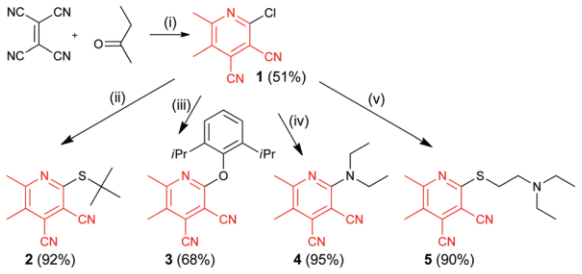

Scheme 1 Reaction conditions: (i) HCl, dioxane, 65 °C. (ii) *t*BuSH, aq. NaOH, THF, rt. (iii) 2,6-Di(isopropyl)phenol, CsF, anhydr. DMF, Ar, rt. (iv) Diethylamine, THF, reflux. (v) Diethylaminoethanethiol, K_2CO_3, DMSO, rt.

[a]*Department of Pharmaceutical Chemistry and Drug Control, Faculty of Pharmacy in Hradec Kralove, Charles University in Prague, Heyrovskeho 1203, 500 05 Hradec Kralove, Czech Republic. E-mail: petr.zimcik@faf.cuni.cz; Fax: +420 495067167; Tel: +420 495067257*

[b]*Department of Biochemical Sciences, Faculty of Pharmacy in Hradec Kralove, Charles University in Prague, Heyrovskeho 1203, 500 05 Hradec Kralove, Czech Republic*

[c]*Department of Biophysics and Physical Chemistry, Faculty of Pharmacy in Hradec Kralove, Charles University in Prague, Heyrovskeho 1203, 500 05 Hradec Kralove, Czech Republic. E-mail: veronika.novakova@faf.cuni.cz; Fax: +420 495067167; Tel: +420 495067380*

† Electronic supplementary information (ESI) available: Experimental procedures and NMR, MS, absorption and fluorescence spectra. See DOI: 10.1039/c5ob00651a

reaction with 2-methylpropane-2-thiol in THF in the presence of aqueous NaOH with a yield of 92% (other bases can be used as well, *e.g.* K_2CO_3). The aryloxy derivative **3** can be synthesized using only CsF in anhydrous DMF. Attempts to apply other bases (NaOH, triethylamine, pyridine, K_2CO_3) did not lead to **3** at all. Compound **4** was received almost quantitatively by the reaction of **1** with excess of diethylamine.‡

None of the tested template methods for the cyclotetramerization of precursors to yield TPyPz (with zinc acetate in DMF, pyridine, or quinoline or with $Zn(quinoline)_2Cl_2$ in a melt) gave the desired product. The TPyPz ring was only formed when alkoxides were used as initiators (*i.e.* original Linstead conditions, Scheme 2). A milder initiator, magnesium butoxide, was employed for the cyclotetramerizations of **2** and **3** to avoid possible exchange reactions with the peripheral substituents in the aryloxy and alkylsulfanyl derivatives, which was reported for some Pc aza-analogs synthesized using a lithium alkoxide initiator.[13] In contrast, a lithium alkoxide initiator was necessary for the cyclotetramerization of **4** because the strongly electron-donating diethylamino substituent hindered the reaction and no product was detected with magnesium butoxide. The reaction with lithium butoxide gave the metal-free derivative **8H**. The magnesium complexes **6Mg** and **7Mg** (obtained from reaction with magnesium butoxide) were subsequently demetallated with a strong organic acid, and the metal-free derivatives **6H–8H** were converted into zinc or magnesium complexes using the corresponding acetates in pyridine to afford **5Zn–8Zn** and **8Mg**.

Each TPyPz **6–8** could potentially exist as four positional isomers (Fig. S34†) due to the unsymmetrical structures of the starting dicarbonitriles. The isomer distribution is theoretically predicted to be 12.5% of the D_{2h} and C_{4h} isomers, 25% of the C_{2v} isomer, and 50% of the C_s isomer.[14] Several isomers were detected using HPLC (Table S1†), but only the **7Mg** isomers could be identified based on their absorption spectra. Four peaks denoted A (C_{2v}), B (D_{2h}), C (C_{4h}) and D (C_s) with the distribution 1%, 1.5%, 30.5% and 67%, respectively, were detected in the **7Mg** HPLC chromatogram (Fig. 1). The peaks were assigned to the different isomers based on the Q-band splitting, which varies substantially for isomers with different symmetries as recently predicted by TD-DFT theoretical calculations.[15] The obvious deviations from the theoretical isomer distribution can be explained by the significant steric hindrance of the bulky 2,6-diisopropylphenoxy substituents in **7Mg**. Thus, the percent of the least sterically hindered C_{4h} isomer increased by almost 2.5 times, while only 1.5% of the most sterically hindered D_{2h} isomer was detected. In addition to the steric effects, electronic effects might play a role in the observed isomer distribution because the steric hindrance does not explain the marked difference in the amounts of the similarly sterically hindered C_s and C_{2v} isomers, similarly as

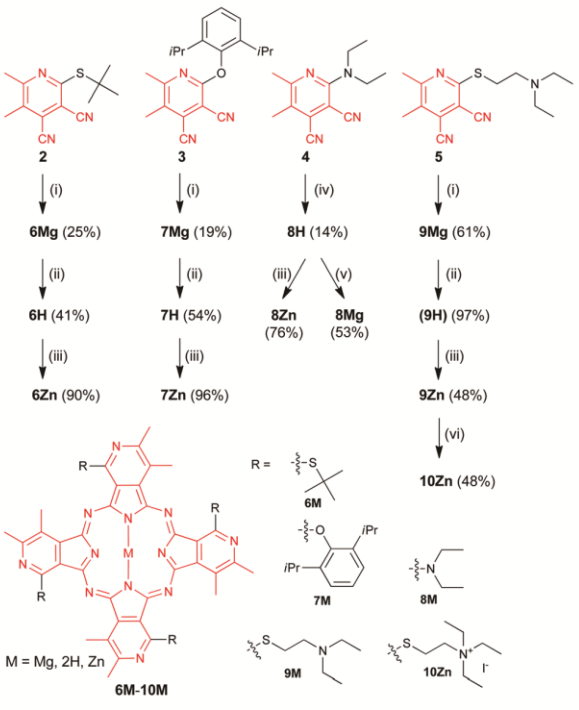

Scheme 2 (i) Mg, anhydr. BuOH, reflux. (ii) TsOH, $CHCl_3$ or THF/MeOH, rt. (iii) $Zn(CH_3COO)_2$, pyridine, reflux. (iv) Li, anhydr. BuOH, reflux. (v) $Mg(CH_3COO)_2$, pyridine, reflux. (vi) CH_3CH_2I, NMP, rt.

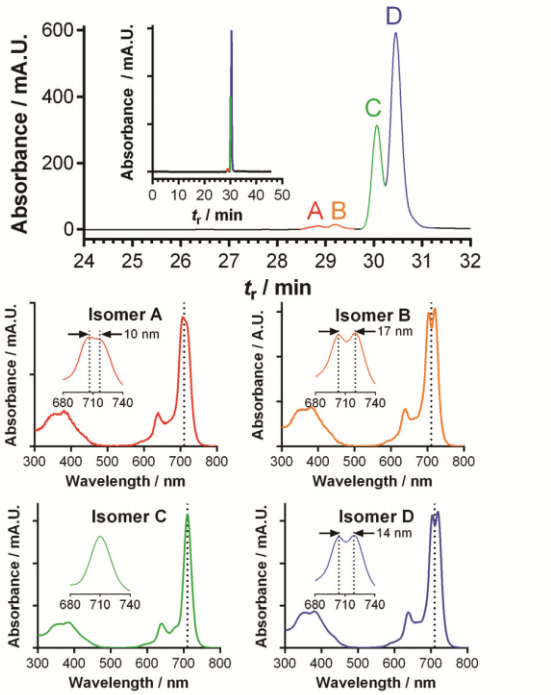

Fig. 1 HPLC chromatogram (λ = 710 nm) of **7Mg** regioisomers (inset: full chromatogram) with the absorption spectra collected at the HPLC peak maxima of isomers A–D. The detailed Q-bands are presented in the insets.

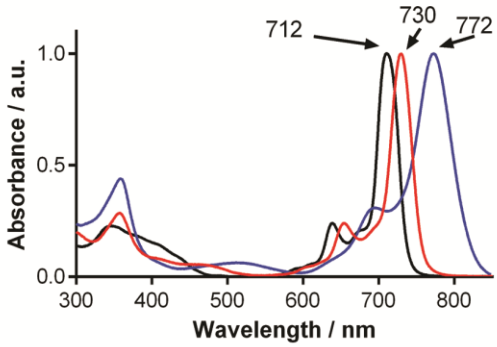

Fig. 2 Normalized absorption spectra of **6Zn** (red), **7Zn** (black) and **8Zn** (blue) in THF.

Table 1 Photophysical data of the studied TPyPzs in THF[a]

Cpd	X	λ_{max} [nm] (ε [dm^3 mol^{-1} cm^{-1}])	λ_F [nm]	$\Delta\lambda$ [cm^{-1}]	Φ_Δ [b]	Φ_F [b]
6Mg	S	728 (225 000)	739	204	0.36	0.38
6H[c]	S	743	771	489	0.10	0.11
6Zn	S	730 (154 000)	742	222	0.69	0.14
7Mg	O	712 (193 000)	721	175	0.29	0.46
7H	O	741 (89 000)	748	126	0.14	0.26
7Zn	O	712 (126 000)	724	233	0.58	0.23
8Mg	N	771 (95 000)	802	501	0.18	0.10[d]
8H	N	806 (86 000)	825	286	0.01	0.02[d]
8Zn	N	772 (94 000)	802	485	0.41	0.06[d]
10Zn[e]	S	722 (207 500)	735	245	0.61	0.10

[a] Connecting heteroatom (X), Q-band absorption maximum (λ_{max}), extinction coefficient (ε), emission maximum (λ_F), Stokes shift ($\Delta\lambda$), singlet oxygen quantum yield (Φ_Δ), fluorescence quantum yield (Φ_F). [b] Determined using ZnPc as a reference ($\Phi_{F(THF)}$ = 0.32, $\Phi_{\Delta(THF)}$ = 0.53, $\Phi_{\Delta(DMF)}$ = 0.56), three independent experiments, estimated error ± 15%. [c] Poor solubility, partially aggregated. [d] Estimated error ± 50%. [e] In DMF.

reported.[16] The isomers could not be isolated due to strongly overlapping TLC spots. Thus, all the samples were isomer mixtures, and the NMR spectra were very complex (Fig. S11–S19†). Despite this complexity, the **7Mg** ^{1}H NMR results (Fig. S14†) indicated that the C_s isomer was the predominant species, which is consistent with the HPLC data.

The absorption spectral shapes for the TPyPzs **6–8** (regioisomer mixtures) in THF (Fig. 2 and S35†) were similar to those for the Pcs and their aza analogs, and a high-energy B-band and low-energy Q-band were observed in the ranges of 315–390 nm and 710–806 nm, respectively (Table 1). As expected, the positions of the Q-band maxima were affected considerably by the nature of the heteroatom. Unsubstituted zinc tetra(3,4-pyrido)porphyrazine in pyridine was reported to absorb at 676 nm.[17] The presence of an aryloxy substituent induced a significant red shift of 36 nm in the Q-band position (λ_{max} (**7Zn**) = 712 nm). Larger bathochromic shifts were observed for the alkylsulfanyl-substituted (λ_{max} (**6Zn**) = 730 nm) and dialkylamino-substituted (λ_{max} (**8Zn**) = 772 nm) complexes. Importantly, the absorption band of the metal-free dialkylamino-substituted TPyPz was observed at an even longer wavelength (λ_{max} (**8H**) = 806 nm) and is comparable to those of recently synthesized near-infrared-absorbing metal-free Pcs that have non-peripheral chalcogen substituents.[11] However, the ability of an amine to induce a red shift is apparently stronger than that of a chalcogen as demonstrated by the fact that the four amino substituents in **8H** induced the same red shift in the Q-band as the eight chalcogen substituents. This result indicated that amino substituents in non-peripheral positions on the macrocycle are highly promising for the development of near-infrared-absorbing Pcs and their analogs. However, the synthesis of Pcs with amino substituents in non-peripheral positions has been challenging due to the limited number of synthesis procedures for suitably substituted phthalonitriles; very few reports can be found in the literature.[8,18] Amino-substituted TPyPzs are therefore a suitable alternative because their synthesis procedures are simple and their precursors are easily prepared in high yields.‡

The shapes of the fluorescence emission spectra and the small Stokes shifts observed in this study were typical of those of Pc and its analogs (Fig. S35,† Table 1). Excitation spectra were collected and they corresponded well to the absorption spectra. It indicated that the compounds did not aggregate during the measurements (only **6H** formed aggregates) (Fig. S35†). The photophysical data (Φ_Δ and Φ_F, Table 1) can be interpreted in several ways. The sum of Φ_Δ and Φ_F, the two most important relaxation pathways for the excited state, was low for all the metal-free TPyPzs regardless of the type of substituent. These results are consistent with those for metal-free Pcs and tetrapyrazinoporphyrazines, which were attributed to other relaxation pathways that have not yet been completely elucidated.[9] For the dialkylamino derivatives (**8**), another excited state deactivation process, namely intramolecular charge transfer (ICT), must also be considered due to the presence of donor amino substituents. The $\Phi_\Delta + \Phi_F$ values for the amino TPyPz metal complexes (**8Zn**, **8Mg**) were lower than those for the corresponding alkylsulfanyl (**6Mg**, **6Zn**) and aryloxy (**7Zn**, **7Mg**) TPyPzs, indicating that ICT influenced the photophysical properties of **8**. However, its effect was rather limited compared to that observed for (di)alkylamino tetrapyrazinoporphyrazines, for which ICT is a major relaxation pathway.[19] The aryloxy and alkylsulfanyl TPyPz metal complexes had $\Phi_\Delta + \Phi_F$ values of up to 0.80, suggesting that other relaxation pathways were not significant. The compounds differed only in the ratio of the fluorescence to singlet oxygen production. Strong fluorescence was observed for the aryloxy derivatives and magnesium complexes, while the singlet oxygen production of the alkylsulfanyl derivatives and zinc complexes was high. This can be interpreted to result from a two-dimensional heavy atom effect due to the central metal (first dimension) and the substituents (second dimension), which is consistent with a recently published study.[20]

Based on the photophysical data, the most promising compounds for PDT are the zinc complexes of alkylsulfanyl TPyPzs. They had the highest production of singlet oxygen, the

most important cytotoxic species in PDT, and exhibit an important red shift in the Q-band maximum to $\lambda_{max} \sim 730$ nm. Thus, water-soluble compound **10Zn** was designed, synthesized (Scheme 2) and photophysically characterized (Table 1). Both the fluorescence and singlet oxygen quantum yields were similar to those of the model compound **6Zn**, confirming the observed relationships between the structure and photophysical properties. The photodynamic activity of compound **10Zn** was subsequently evaluated using the HeLa human cervix carcinoma cell line to demonstrate the potential of TPyPzs in PDT. The dark toxicity (without light activation) was low (TC_{50} = 105 ± 9.5 μM). Activating the compound with light (λ > 570 nm, 12.4 mW cm^{-2}, 11.2 J cm^{-2}) resulted in a lethal photodynamic effect on the HeLa cells with IC_{50} = 0.26 ± 0.089 μM (Fig. S37†), which is comparable to the IC_{50} value obtained when HeLa cells were treated with octacationic Pcs under the same conditions.[21] The high ratio of the toxic concentration to the active concentration ($TC_{50}/IC_{50} \sim 400$) suggested that this compound is a promising photosensitizer. To gain deeper insight into its mechanism of action, the subcellular localization of **10Zn** was studied by fluorescence microscopy (Fig. 3). The punctate red fluorescence of TPyPz **10Zn** in the HeLa cells colocalized exclusively with lysosomes, indicating that they are the primary singlet oxygen targets. The morphological changes observed in different organelles after irradiation (lysosome rupture, TPyPz diffusion into the cytosol followed by destruction of the mitochondria and, finally, interactions between the cationic TPyPz and nuclear DNA) were consistent with the behavior induced by octacationic Pcs,[21] suggesting a similar sequence of events leading primarily to necrotic cell death.

In summary, a versatile procedure for synthesizing heteroatom-substituted TPyPzs was developed. This paved an interesting way for further functionalization of TPyPz macrocycles, the modifications of which were strongly limited until now. The basic photophysical relationships of the series were determined and can be used to rationally design TPyPzs with specific photophysical properties. The dialkylamino and alkylsulfanyl derivatives seem to be particularly promising for further development. The dialkylamino derivatives were characterized by an unusually large red shift (almost 100 nm) in the Q-band maximum, which was induced by just four substituents. The relatively straightforward synthesis makes them promising candidates in the development of near-infrared-absorbing macrocycles. The alkylsulfanyl derivatives were characterized by high singlet oxygen production, making them suitable for use as photosensitizers for PDT. The potential of alkylsulfanyl TPyPzs in this application was demonstrated by the high photodynamic activity of cationic, water-soluble **10Zn**.

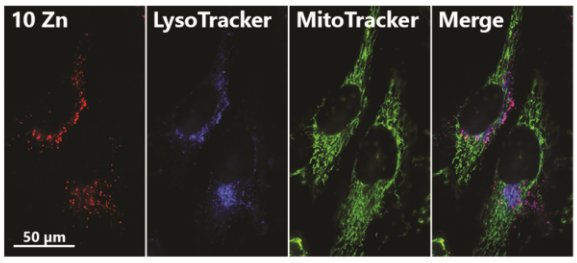

Fig. 3 Subcellular localization of **10Zn** (red) in HeLa cells visualized by fluorescence microscopy after co-incubation with the organelle-specific fluorescent probes MitoTracker (green) and LysoTracker (blue).

The work was financially supported by the Czech Science Foundation (13-27761S). Authors thank Lucie Novakova for HRMS data.

Notes and references

‡The reaction of **1** with other amines also gave high yields that were typically greater than 70% (not shown), and **1** also reacted readily with the residual traces of *N*,*N*-dimethylamine in DMF.

1 J. Shao, K. Richards, D. Rawlins, B. Han and C. A. Hansen, *J. Porphyrins Phthalocyanines*, 2013, **17**, 317–330.
2 Y. Rio, M. S. Rodriguez-Morgade and T. Torres, *Org. Biomol. Chem.*, 2008, **6**, 1877–1894; P. A. Stuzhin and C. Ercolani, in *The Porphyrin Handbook*, ed. K. M. Kadish, K. M. Smith and R. Guilard, Academic Press, New York, 2003, vol. 15, pp. 263–364; E. G. Galpern, E. A. Lukyanets and M. G. Galpern, *Izv. Akad. Nauk. SSSR, Ser. Khim.*, 1973, **9**, 1976–1980.
3 J. Chen, J. Zhang, Y.-H. Tse, P. Janda, D. Christendat and A. B. P. Lever, *J. Porphyrins Phthalocyanines*, 2006, **10**, 1238–1248.
4 E. A. Dupouy, D. Lazzeri and E. N. Durantini, *Photochem. Photobiol. Sci.*, 2004, **3**, 992–998.
5 J. Tarábek, M. Klusáčková, P. Janda, H. Tarábková, L. Rulíšek and J. Plšek, *J. Phys. Chem. C*, 2014, **118**, 4198–4206; Y. Ishida, T. Shimada and S. Takagi, *J. Phys. Chem. C*, 2014, **118**, 20466–20471.
6 R. P. Linstead, E. G. Noble and J. M. Wright, *J. Chem. Soc.*, 1937, 911–921.
7 C. Marti, S. Nonell, M. Nicolau and T. Torres, *Photochem. Photobiol.*, 2000, **71**, 53–59; K. Sakamoto, S. Yoshino, M. Takemoto and N. Furuya, *J. Porphyrins Phthalocyanines*, 2013, **17**, 605–627; Y. H. Tse, P. Janda and A. B. P. Lever, *Anal. Chem.*, 1994, **66**, 384–390.
8 E. A. Lukyanets and V. N. Nemykin, *J. Porphyrins Phthalocyanines*, 2010, **14**, 1–40.
9 P. Zimcik, V. Novakova, K. Kopecky, M. Miletin, R. Z. Uslu Kobak, E. Svandrlikova, L. Váchová and K. Lang, *Inorg. Chem.*, 2012, **51**, 4215–4223.
10 N. Kobayashi, H. Ogata, N. Nonaka and E. A. Luk'yanets, *Chem. – Eur. J.*, 2003, **9**, 5123–5134.
11 T. Furuyama, K. Satoh, T. Kushiya and N. Kobayashi, *J. Am. Chem. Soc.*, 2014, **136**, 765–776.
12 K. V. Lipin, V. N. Maksimova, O. V. Ershov, A. V. Eremkin, Y. S. Kayukov and O. E. Nasakin, *Russ. J. Org. Chem.*, 2010, **46**, 617–618.
13 V. Novakova, M. Miletin, T. Filandrová, J. Lenčo, A. Růžička and P. Zimcik, *J. Org. Chem.*, 2014, **79**, 2082–2093.

14 G. De La Torre, C. G. Claessens and T. Torres, *Eur. J. Org. Chem.*, 2000, 2821–2830.
15 Y. Gao and V. N. Nemykin, *J. Mol. Graphics Modell.*, 2013, **42**, 73–80.
16 V. Novakova, J. Roh, P. Gela, J. Kuneš and P. Zimcik, *Chem. Commun.*, 2012, **48**, 4326–4328.
17 W. S. Szulbinski and J. R. Kincaid, *Inorg. Chem.*, 1998, **37**, 5014–5020.
18 S. A. Mikhalenko, V. M. Derkacheva and E. A. Lukyanets, *Zh. Obshch. Khim.*, 1981, **51**, 1650–1657; F. Peri, C. Lorenzetti, S. Cimitan and M. Grob, *WO*, 2008/83918, 2008; V. N. Nemykin and E. A. Lukyanets, in *Handbook of Prophyrin Science*, ed. K. M. Kadish, K. M. Smith and R. Guilard, World Scientific, Singapore, 2010, vol. 3, pp. 1–323.
19 V. Novakova, P. Zimcik, M. Miletin, L. Vachova, K. Kopecky, K. Lang, P. Chábera and T. Polívka, *Phys. Chem. Chem. Phys.*, 2010, **12**, 2555–2563.
20 J. Svec, P. Zimcik, L. Novakova, O. A. Rakitin, S. A. Amelichev, P. A. Stuzhin and V. Novakova, *Eur. J. Org. Chem.*, 2015, 596–604.
21 M. Machacek, A. Cidlina, V. Novakova, J. Svec, E. Rudolf, M. Miletin, R. Kucera, T. Simunek and P. Zimcik, *J. Med. Chem.*, 2015, **58**, 1736–1749.

Supporting Information

Heteroatom-substituted tetra(3,4-pyrido)porphyrazines: A stride toward near-infrared-absorbing macrocycles

Lenka Vachova,[a] Miloslav Machacek,[b] Radim Kučera,[a] Jiri Demuth,[c] Pavel Cermak,[c] Kamil Kopecky,[a] Miroslav Miletin,[a] Adela Jedlickova,[b] Tomas Simunek,[b] Veronika Novakova*[c] and Petr Zimcik*[a]

[a] Department of Pharmaceutical Chemistry and Drug Control, Faculty of Pharmacy in Hradec Kralove, Charles University in Prague, Heyrovskeho 1203, 500 05, Hradec Kralove, Czech Republic, E-mail: petr.zimcik@faf.cuni.cz; Fax: +420 495067167; Tel: +420 495067257

[b] Department of Biochemical Sciences, Faculty of Pharmacy in Hradec Kralove, Charles University in Prague, Heyrovskeho 1203, 500 05, Hradec Kralove, Czech Republic.

[c] Department of Biophysics and Physical Chemistry, Faculty of Pharmacy in Hradec Kralove, Charles University in Prague, Heyrovskeho 1203, 500 05, Hradec Kralove, Czech Republic. E-mail: veronika.novakova@faf.cuni.cz; Fax: +420 495067167; Tel: +420 495067380

Content

Experimental

General

All organic solvents used were of analytical grade. Anhydrous butanol for synthesis was stored over magnesium and distilled prior to use. Tetrahydrofuran for photophysical and photochemical measurements was distilled prior to use. All chemicals for synthesis were obtained from established suppliers (Aldrich, Acros, Merck) and used as received. Zinc phthalocyanine (ZnPc) was purchased from Sigma-Aldrich. TLC was performed on Merck aluminum sheets coated with silica gel 60 F254. Merck Kieselgel 60 (0.040−0.063 mm) was used for column chromatography. Melting points were measured on an Electrothermal IA9200-series digital melting-point apparatus (Electrothermal Engineeering, Southend-on-Sea, Essex, Great Britain). The infrared spectra were measured on a Nicolet 6700 spectrometer in ATR mode. ^{1}H and ^{13}C NMR spectra were recorded on a Varian Mercury Vx BB 300 NMR or VNMR S500 NMR spectrometer. The reported chemical shifts are given relative to $Si(CH_3)_4$ and were locked to the signal of the solvent. Elemental analyses were performed on an Automatic Microanalyser EA1110CE (Fisons Instruments, Milan, Italy). The UV−vis spectra were recorded using a Shimadzu UV-2401PC and UV-2600 spectrophotometers (Shimadzu Europa, GmbH, Duisburg, Germany). The steady-state fluorescence spectra were measured using an AMINCO-Bowman Series 2 luminescence spectrometer (SLM-Aminco, Urbana, Illinois, USA). MALDI-TOF mass spectra were recorded in a positive reflectron mode on a Voyager-DE STR mass spectrometer (Applied Biosystems, Framingham, Massachusetts, USA) in *trans*-2-[3-(4-*tert*butylphenyl)-2-methyl-2-propenylidene]-malononitrile as a matrix. The instrument was calibrated externally with a five-point calibration using a Peptide Calibration Mix1 kit (LaserBio Laboratories, Sophia- Antipolis, France). High resolution mass spectra (HR MS) were measured with the use of UHPLC system Acquity UPLC I-class (Waters, Millford, USA) coupled to high resolution mass spectrometer Synapt G2Si (Waters, Manchester, UK) based on Q-TOF. Chromatography for this HRMS measurement was performed using Acquity UPLC BEH300 C4 (2.1 x 50 mm, 1.7 um) column using isocratic elution with acetonitrile and 10 mM ammonium formate buffer pH 3 (90:10) at flow-rate 0.4 ml/min. Electrospray ionization was operated in positive mode. The ESI spectra were recorded in the range 200 - 2000 m/z using glu-fibrinopeptide B as a lock mass reference and sodium iodide for calibration.

Synthesis of 2-chloro-5,6-dimethylpyridine-3,4-dicarbonitrile (1).

Tetracyanoethylene (1 g, 7.8 mmol) was added to a solution of butan-2-one (675 mg, 9.36 mmol) in 1,4-dioxane (20 mL). Concentrated hydrochloric acid (8 mL) was slowly dropped

into the mixture and the reaction was heated at 65 °C for 2 hours. (Caution! Highly toxic HCN is an elimination product from the reaction!) Subsequently, the mixture was diluted with water (150 mL), the precipitate was collected and the liquid residue was extracted three times with ethyl acetate. The organic layer was dried over anhydrous Na_2SO_4 and the solvent was evaporated. The combined crude product (the precipitate and organic layer from extraction) was purified over the silica with toluene/acetone 20:1 as an eluent (alternatively also chloroform can be used as eluent) and recrystallized from propan-2-ol to yield white needles (763 mg, 51 %). R_f (toluene/acetone 20:1) = 0.49, R_f (hexane/ethyl acetate 5:1) = 0.18, R_f (chloroform) = 0.56, mp 75.7-76.6 °C ; IR (ATR, cm^{-1}): 2236 (CN), 1562, 1540, 1387, 1275, 992, 889 and 806; elemental analysis found (%): C, 56.4; H, 3.3; N, 21.7; $C_9H_6N_3Cl$ requires (%): C, 56.4; H, 3.2; N, 21.9; δ_H ($CDCl_3$, 300 MHz): 2.56 (3H, s, CH_3), 2.66 (3H, s, CH_3); δ_C ($CDCl_3$, 75 MHz): 17.3, 23.7, 109.2, 112.4, 112.7, 125.9, 134.3, 150.1, 164.4. Analytical data corresponded well with those published for this compound.[1]

Synthesis of 2-(*tert*-butylsulfanyl)-5,6-dimethylpyridine-3,4-dicarbonitrile (2)

A solution of 1.77 mL (15.7 mmol) of 2-methylpropane-2-thiol in tetrahydrofurane (30 mL) was stirred at room temperature with 9.12 mL of aq. NaOH (1.0 mol/dm^3) for 30 min. Thereafter, a solution of 600 mg (3.13 mmol) of **1** in 15mL of tetrahydrofurane was added dropwise. The reaction was stirred for another 30 min, evaporated and the solid was washed several times with water. Crude product was purified over the silica with toluene/acetone 20:1 to give **2** as a white solid (707 mg, 92%). R_f (toluene/acetone 20:1) = 0.70, mp 130.1-130.8 °C; IR (ATR, cm^{-1}): 2966, 2929, 2222 (CN), 1552, 1457, 1390, 1362, 1263, 1232, 1163, 1007, 884 and 806; elemental analysis found (%): C, 63.6; H, 6.1; N, 16.9; for $C_{13}H_{15}N_3S$ requires (%): C, 63.6; H, 6.2; N, 17.1; δ_H ($CDCl_3$, 500 MHz): 1.62 (9H, s, *t*Bu), 2.47 (3H, s, CH_3), 2.62 (3H, s, CH_3); δ_C ($CDCl_3$, 125 MHz): 17.0, 23.8, 30.3, 50.4, 106.9, 113.4, 113.5, 124,4, 129.5, 161.9, 162.1.

Synthesis of 2-(2,6-diisopropylphenoxy)-5,6-dimethylpyridine-3,4-dicarbonitrile (3)

Cesium fluoride (2.38 g, 15.7 mmol) was dried at 300 °C under vacuum. After cooling to the room temperature, the flask was filled with argon, and 2,6-diisopropylphenol (1.12 g, 6.26 mmol) in anhydrous DMF (20 mL) was added by a syringe through a septum. Compound **1** (1.00 g, 5.2 mmol) was dissolved in anhydrous DMF (20 mL) under argon atmosphere and added dropwise through the septum to the suspension of cesium fluoride with 2,6-diisoprolyphenol in DMF using a syringe. The solution turned immediately deep purple. The reaction mixture was stirred next 2 hours at room temperature. Then, water (200 mL) was

poured into the mixture, purple precipitate was collected by filtration and washed thoroughly with water. Crude product was purified by column chromatography on silica with hexane/ethyl acetate 5:1 as an eluent and recrystallized from hexane. Yield 1.19 g (68 %) of shiny white crystals. R_f (hexane/ethyl acetate 5:1) = 0.44, mp 152.7-153.8 °C; IR (ATR, cm^{-1}): 2968, 2869, 2232 (CN), 1568, 1408, 1332, 1244, 1169, 1120 and 765; elemental analysis found (%): C, 75.8; H, 7.4; N, 12.7; for $C_{21}H_{23}N_3O$ requires (%): C, 75.7; H, 7.0; N, 12.6; δ_H ($CDCl_3$, 300 MHz): 1.15 (12H, br s, CHC$\underline{H}_3$), 2.38 (3H, s, CH_3), 2.47 (3H, s, CH_3), 2.82 (2H, sep, J= 6.9 Hz, CH), 7.18 (1H, d, J=1.9 Hz, ArH), 7.24-7.31 (2H, m, ArH); δ_C ($CDCl_3$, 75 MHz): 16.8, 22.7, 23.4, 23.7, 27.6, 94.8, 112.6, 113.5, 124.1, 126.3, 126.7, 128.6, 140.8, 146.8, 161.7, 163.1.

Synthesis of 2-(diethylamino)-5,6-dimethylpyridine-3,4-dicarbonitrile (4)

Diethylamine (2.3 g, 31 mmol) was added dropwise to solution of **1** (850 mg, 4.4 mmol) in tetrahydrofuran (30 mL) and the mixture was refluxed for 30 h. At the end of the reaction the mixture was cooled and precipitated diethylamine hydrochloride was filtered off. The solution was evaporated under reduced pressure and purified by column chromatography on the silica with chloroform. Pure fractions were collected and finally recrystallized from MeOH to give **4** (962 mg, 95%) as yellow solid needles. R_f (hexane/ethyl acetate 5:1) = 0.42, mp 66.2-67.0 °C; IR (ATR, cm^{-1}): 2988, 2941, 2201 (CN), 1565, 1541, 1497, 1471, 1457, 1434, 1376, 1358, 1260, 1171, 810, 758 and 689; δ_H ($CDCl_3$, 500 MHz): 1.25 (6H, t, J=7.0 Hz, $CH_2C\underline{H}_3$), 2.35 (3H, s, CH_3), 2.43 (3H, s, CH_3), 3.69 (4H, q, J=7.0 Hz, CH_2); δ_C ($CDCl_3$, 125 MHz): 13.4, 16.3, 23.9, 44.2, 86.5, 114.8, 117.0, 122.3, 126.6, 155.5, 162.2.

Synthesis of 2-{[2-(diethylamino)ethyl]sulfanyl}-5,6-dimethylpyridine-3,4-dicarbonitrile (5).

Finelly ground anhydr. K_2CO_3 (4.34 g, 31.4 mmol) was added to solution of **1** (1.50 g, 7.85 mmol) and diethylaminoethanethiol hydrochloride (1.60 g, 9.42 mmol) in DMSO (50 mL) and the mixture was stirred at rt for 1 h. The deep purple solution turned slowly to brown and dark yellow within 10-15 min. The reaction was diluted with water (300 mL) and yellow precipitate was collected and thoroughly washed with water. The crude product was dissolved in water with the use of HCl (to acid pH of the solution) and washed three times with chloroform. The water phase was made basic with the use of KOH, extracted with chloroform three times and the organic phase was dried over sodium sulfate. Evaporation of the solvent gave pure **5** as orange solid (1.27 g, 56%). Another portion of slightly impure **5** can be obtained after evaporation of the first chloroform extract and conversion to free base with KOH (773 mg,

34%). mp 65.7-67.4 °C; IR (ATR, cm^{-1}): 2973, 2936, 2873, 2803, 2220 (CN), 1556, 1438, 1389, 1263; δ_H (CD_3COCD_3, 500 MHz): 1.01 (6H, t, J = 7.1 Hz, $CH_2C\underline{H}_3$), 2.50 (3H, s, CH_3), 2.57 (4H, q, J = 7.1 Hz, $NC\underline{H}_2CH_3$), 2.66 (3H, s, CH_3), 2.79-2.69 (2H, m, $NC\underline{H}_2CH_2$), 3.44-3.33 (2H, m, SCH_2); δ_C (CD_3COCD_3, 125 MHz): 12.7, 17.1, 23.9, 29.1, 47.7, 52.9, 106.1, 114.3, 114.5, 125.0, 131.2, 161.2, 164.2; HRMS *m/z*: found: $[M+H]^+$ 289.1493; $C_{15}H_{21}N_4S$ requires $[M+H]^+$ 289.1481.

General procedure for synthesis of tetra(3,4-pyrido)porphyrazines 6Mg and 7Mg

Magnesium (7 equiv) and a small crystal of iodine were heated to reflux for 2.5 h in anhydrous butanol. Precursor **2** or **3** (1 eq.) was added and reflux continued for the next 20 h. The reaction mixture was left to cool down in the air, the solvent was evaporated under reduced pressure, aqueous acetic acid (50% (v/v)) was added and the suspension was stirred for 30 min at rt. The dark solid was filtered, washed with aqueous acetic acid and water and air-dried. The reaction mixture was purified by column chromatography on the silica (eluents are mentioned below) to obtain magnesium complexes **6Mg** and **7Mg** as green solids.

1,8,15,22-Tetrakis(tert-butylsulfanyl)-3,4,10,11,17,18,24,25-octamethyltetrapyrido[3,4-b:3',4'-g:3'',4''-l:3''',4'''-q]porphyrazinato magnesium (II) (6Mg). Starting amount of **2** (500 mg, 2.0 mmol), eluent: toluene/chloroform/tetrahydrofuran 10:1:0.5, yield: 125 mg (25%) of a green solid, R_f (toluene/chloroform/tetrahydrofuran 10:1:0.5) = 0.48; HPLC (t_R, min): 21.9 (61.5 %), 22.77 (38.5 %); IR (ATR, cm^{-1}): 2957, 2913, 1547, 1264, 1182, 1106, 1018, 982, 913, 791 and 760; δ_H ($CDCl_3$/pyridine-d_5, 300 MHz): 2.09-2.25 (36H, several s, *t*Bu), 2.98-3.19 (12H, several s, CH_3), 3.58-4.20 (12H, several s, CH_3); δ_C ($CDCl_3$/pyridine-d_5, 75 MHz): 156.82, 156.76, 156.15, 155.95, 154.70, 154.63, 154.59, 154.53, 154.14, 153.97, 153.76, 153.71, 153.63, 153.33, 153.11, 152.88, 152.60, 151.98, 151.62, 143.80, 143.76, 143.66, 143.41, 142.76, 128.72, 128.65, 128.24, 128.18, 127.89, 124.15, 124.07, 48.65, 47.88, 47.81, 31.56, 31.06, 31.03, 23.26, 23.20, 23.04, 17.05, 16.86, 16.72, 16.08, 15.92; MS (MALDI-TOF) *m/z*: 1004.4 $[M]^+$, 948.3 $[M-C_4H_8]^+$, 892.3 $[M-2\times C_4H_8]^+$; HRMS *m/z*: found: $[M+H]^+$ 1005.3864; $C_{52}H_{61}MgN_{12}S_4$ requires $[M+H]^+$ 1005.3875; UV-Vis λ_{max}/THF; nm (ε/THF; $dm^3mol^{-1}cm^{-1}$): 728 (225 200), 653 (49 700), 465 (12 200), 365 (61 300).

1,8,15,22-Tetrakis(2,6-diisopropylphenoxy)-3,4,10,11,17,18,24,25-octamethyltetrapyrido[3,4-b:3',4'-g:3'',4''-l:3''',4'''-q]porphyrazinato magnesium (II) (7Mg). Starting amount of **3** (1 g, 3.0 mmol), eluent: toluene/chloroform/tetrahydrofuran 10:1:0.2, yield: 195 mg (19%) of a deep green solid, R_f (toluene/chloroform/tetrahydrofuran 10:1:0.5) = 0.48; HPLC (t_R, min): 28.8 (1 %), 29.2 (1.5 %), 30.0 (30.5 %), 30.5 (67 %); IR

(ATR, cm^{-1}): 2965, 2930, 2868, 1734, 1596, 1417, 1322, 1263, 1170, 1096, 1061, 1003, 930, 796 and 766; δ_H ($CDCl_3$/pyridine-d_5, 300 MHz): 0.90-1.62 (m, CHC<u>H</u>$_3$), 2.31-2.44 (m), 2.70 (s, CH_3), 2.76 (s, CH_3), 2.82 (s, CH_3), 2.87 (s, CH_3), 3.27-3.47 (m, CH), 3.60-3.79 (m, CH), 3.82 (s, CH_3), 3.84 (s, CH_3), 3.87 (s, CH_3), 3.89 (s, CH_3), 7.22-7.40 (m, ArH), 7.45-7.57 (m, ArH), number of protons cannot be assigned due to complex mixture of isomers, for details see graphical spectra; δ_C ($CDCl_3$/pyridine-d_5, 75 MHz): 158.50, 158.41, 157.78, 157.54, 157.29, 156.32, 154.48, 153.33, 151.83, 146.88, 146.72, 146.58, 142.11, 142.05, 141.69, 141.64, 125.83, 125.50, 124.09, 123.80, 117.66, 117.28, 29.91, 27.79, 27.71, 24.30, 23.46, 23.35, 23.23, 22.89, 22.73, 15.77, 15.71, 14.19, 14.14; MS (MALDI-TOF) *m/z*: 1356.6 $[M]^+$; HRMS *m/z*: found: $[M+H]^+$ 1357.7270; $C_{84}H_{93}MgN_{12}O_4$ requires $[M+H]^+$ 1357.7290; UV-Vis λ_{max}/THF; nm (ε/THF; $dm^3mol^{-1}cm^{-1}$): 712 (192 500), 639 (43 700), 389 (41 700), 346 (38 100). Despite the complexity of the spectra, the predominant presence of C_s isomers in the mixture is supported by appearance of four signals of roughly same intensity (besides other smaller signals) for both methyls on pyridine ring (see insets of Figure S14). C_s isomer is the only one where four signals of each of the methyls can be expected.

General procedure for synthesis of metal-free tetra(3,4-pyrido)porphyrazines 6H and 7H

The magnesium complex (**6Mg** or **7Mg**, 1 eq.) was dissolved in chloroform and stirred at rt for 1 h with *p*-toluenesulfonic acid (10 eq.). Thereafter, the solvent was evaporated, the crude product was washed with water and purified by column chromatography with hexane/ethyl acetate 20:1 as an eluent to obtain a dark green solid **6H** or **7H**.

1,8,15,22-Tetrakis(tert-butylsulfanyl)-3,4,10,11,17,18,24,25-octamethyltetrapyrido[3,4-b:3',4'-g:3'',4''-l:3''',4'''-q]porphyrazine (6H). Starting amount of **6Mg** (100 mg, 0.1 mmol), yield: 39 mg (41%), R_f (hexane/ethyl acetate 20:1) = 0.55; HPLC was not performed due to low solubility; IR (ATR, cm^{-1}): 3296 (NH), 2922, 2853, 1739, 1575, 1457, 1262, 1171, 1030, 973 and 761; δ_H ($CDCl_3$/pyridine-d_5, 300 MHz): 1.77 (9H, s, *t*Bu), 1.93-2.32 (27H, several s, *t*Bu), 2.52-4.11 (24H, several s, CH_3); δ_C ($CDCl_3$/pyridine-d_5, 75 MHz): no signals were detected; MS (MALDI-TOF) *m/z*: 982.3 $[M]^+$; UV-Vis λ_{max}/THF; nm (ε could not be properly determined due to low solubility): 743, 695, 331.

1,8,15,22-Tetrakis(2,6-diisopropylphenoxy)-3,4,10,11,17,18,24,25-octamethyltetrapyrido[3,4-b:3',4'-g:3'',4''-l:3''',4'''-q]porphyrazine (7H). Starting amount of **7Mg** (41 mg, 0.03 mmol), yield: 22 mg (54%), R_f (hexane/ethyl acetate 20:1) = 0.38; HPLC (t_R, min): 26.9, 28.0; IR (ATR, cm^{-1}): 3257 (NH), 2960, 2925, 2855, 1734, 1594, 1438, 1311, 1270, 1165, 1097. 1080, 991, 913 and 766; δ_H ($CDCl_3$/pyridine-d_5, 500 MHz): 1.82-1.55 (m,

CHC$\underline{H}_3$), 1.62-1.79 (m), 2.00-2.44 (m), 2.66 (s, CH_3), 2.73 (s, CH_3), 2.78 (s, CH_3), 2.84 (s, CH_3), 3.24-3.38 (m, CH), 3.57-3.72 (m, CH), 3.76 (s, CH_3), 3.78 (s, CH_3), 3.81 (s, CH_3), 7.20-7.32 (m, ArH), 7.42-7.52 (m, ArH), number of protons cannot be assigned due to complex mixture of isomers, for details see graphical spectra; δ_C ($CDCl_3$/pyridine-d_5, 125 MHz): 159.72, 159.49, 158.97, 158.23, 158.03, 157.77, 157.50, 157.34, 148.84, 142.04, 141.95, 141.62, 126.08, 125.55, 124.18, 124.00, 122.39, 122.27, 115.52, 115.10, 37.58, 33.90, 32.94, 32.11, 30.36, 29.90, 29.56, 27.86, 27.83, 27.72, 24.30, 23.42, 23.27, 23.17, 22.99, 22.89, 15.73, 14.40, 14.33, 14.23; MS (MALDI-TOF) *m/z*: 1334.6 $[M]^+$; HRMS *m/z*: found: $[M+H]^+$ 1335.7566; $C_{84}H_{95}N_{12}O_4$ requires $[M+H]^+$ 1335.7599; UV-Vis λ_{max}/THF; nm (ε/THF; $dm^3mol^{-1}cm^{-1}$): 741 (88 700), 714 (82 600), 674 (27 300), 646 (26 000), 325 (32 500).

General procedure for synthesis of zinc tetra(3,4-pyrido)porphyrazines 6Zn and 7Zn

A metal-free TPyPzs **6H** or **7H** (1 eq.) was dissolved in pyridine and anhydrous zinc acetate (7 eq) was added. The mixture was refluxed for 2.5 h. Pyridine was evaporated and the product was washed thoroughly with water to yield a crude TPyPzs **6Zn** or **7Zn** that were purified by column chromatography on the silica (eluents see below).

1,8,15,22-Tetrakis(tert-butylsulfanyl)-3,4,10,11,17,18,24,25-octamethyltetrapyrido[3,4-b:3',4'-g:3'',4''-l:3''',4'''-q]porphyrazinato zinc (II) (6Zn). Starting amounts: **6H** (20 mg, 0.02 mmol), eluent: toluene/chloroform/tetrahydrofuran 10:1:0.5, yield: 19 mg (90%) of a green solid, R_f (toluene/chloroform/tetrahydrofuran 10:1:0.5) = 0.58; HPLC (t_R, min): 24.6, 25.5; IR (ATR, cm^{-1}): 2914, 2853, 1544, 1472, 1456, 1265, 1185, 1104, 1007, 984 and 752; δ_H ($CDCl_3$/pyridine-d_5, 300 MHz): 1.99-2.35 (36H, several s, *t*Bu), 2.85-4.28 (24H, several s, CH_3); δ_C ($CDCl_3$/pyridine-d_5, 75 MHz): 156.73, 156.67, 156.20, 155.78, 154.59, 154.25, 153.71, 153.64, 153.55, 153.42, 153.05, 151.93, 151.13, 151.08, 150.95, 143.08, 142.54, 141.42, 128.87, 128.35, 128.31, 127.68, 126.81, 125.25, 48.90, 48.79, 48.01, 47.97, 47.82, 32.09, 31.69, 31.65, 31.14, 31.06, 23.65, 23.41, 23.37, 23.10, 22.95, 22.87, 17.49, 16.98, 16.76, 16.45, 16.13; MS (MALDI-TOF) *m/z*: 1044.2 $[M]^+$, 988.9 $[M-C_4H_8]^+$; HRMS *m/z*: found: $[M+H]^+$ 1045.3306; $C_{52}H_{61}N_{12}S_4Zn$ requires $[M+H]^+$ 1045.3316; UV-Vis λ_{max}/THF; nm (ε/THF; $dm^3mol^{-1}cm^{-1}$): 730 (154 200), 653 (37 400), 461 (9 800), 359 (45 000).

1,8,15,22-Tetrakis(2,6-diisopropylphenoxy)-3,4,10,11,17,18,24,25-octamethyltetrapyrido[3,4-b:3',4'-g:3'',4''-l:3''',4'''-q]porphyrazinato zinc (II) (7Zn). Starting amounts: **6H** (19.5 mg, 0.015 mmol), eluent: toluene/chloroform/tetrahydrofuran 10:1:0.2, yield: 19.6 mg (96%) of a green solid, R_f (toluene/chloroform/tetrahydrofuran 10:1:0.5) = 0.69; HPLC (t_R, min): 22.0, 22.2; IR (ATR, cm^{-1}): 2960, 2924, 2854, 1593, 1577, 1438, 1314, 1272, 1170, 1128, 1096, 1002, 928 and 767; δ_H ($CDCl_3$/pyridine-d_5, 300 MHz):

0.83-1.64 (m, CHC<u>H</u>$_3$), 2.00-2.26 (m), 2.72-2.50 (m), 2.67 (s, CH_3), 2.74 (s, CH_3), 2.79 (s, CH_3), 2.85 (s, CH_3), 3.27-3.45 (m, CH), 3.58-3.78 (m, CH), 3.77- 3.99 (m, CH_3), 7.20-7.37 (m, ArH), 7.40-7.57 (m, ArH), number of protons cannot be assigned due to complex mixture of isomers, for details see graphical spectra; δ_C ($CDCl_3$/pyridine-d_5, 75 MHz): 158.25, 157.83, 157.70, 157.58, 157.49, 157.39, 157.20, 157.02, 156.33, 156.27, 156.18, 155.42, 154.80, 154.65, 154.12, 154.01, 153.78, 153.38, 152.71, 151.35, 146.53, 146.24, 142.02, 141.70, 131.07, 125.83, 125.30, 124.03, 122.08, 117.53, 117.45, 117.25, 38.87, 34.10, 32.07, 29.86, 29.51, 27.72, 24.25, 23.52, 23.41, 23.34, 23.07, 22.84, 22.70, 15.71, 14.30, 14.19, 14.10; MS (MALDI-TOF) *m/z*: 1396.5 $[M]^+$; HRMS *m/z*: found: $[M+H]^+$ 1397.6729; $C_{84}H_{93}N_{12}O_4Zn$ requires $[M+H]^+$ 1397.6734; UV-Vis λ_{max}/THF; nm (ε/THF; $dm^3mol^{-1}cm^{-1}$): 712 (125 900), 639 (31 800), 314 (88 000).

1,8,15,22-Tetrakis(diethylamino)-3,4,10,11,17,18,24,25-octamethyltetrapyrido[3,4-b:3',4'-g:3'',4''-l:3''',4'''-q]porphyrazine (8H). Compound **4** (700 mg, 3.1 mmol) was heated to reflux in dry butanol (10 mL) and then lithium metal (149 mg, 21.5 mmol) was added. The mixture was refluxed for 15 h. After this time, the solution was evaporated to dryness, aqueous acetic acid (50% v/v, 50 ml) were poured in and the suspension was collected and washed with aqueous acetic acid and water. The product was purified by column chromatography on silica with toluene/chloroform/tetrahydrofuran 5:1:1 as an eluent. Yield 97 mg (14%) of a purple solid, R_f (toluene/chloroform/tetrahydrofuran 10:1:0.5) = 0.57; HPLC (t_R, min): 26.5 (16 %), 28.5 (71 %), 29.0 (13 %); IR (ATR, cm^{-1}): 3292 (NH), 2968, 2931, 2867, 1560, 1442, 1424, 1254, 1237, 1180, 1060, 1037, 986, 909 and 760; δ_H ($CDCl_3$/pyridine-d_5, 300 MHz): 1.06-1.49 (24H, m, $CH_2C\underline{H}_3$), 3.00 (12H, br s, CH_3), 3.66 (5H, br s, CH_3), 3.78 (7H, br s, CH_3), 4.24-4.52 (16H, m, CH_2, overlapped with signal of residual H_2O); δ_C ($CDCl_3$/pyridine-d_5, 75 MHz): 158.58, 158.43, 157.64, 157.53, 156.03, 155.07, 154.28, 154.02, 46.36, 45.38, 23.48, 14.25, 13.50, 13.10; MS (MALDI-TOF) *m/z*: 914.5 $[M]^+$; HRMS *m/z*: found: $[M+H]^+$ 915.5716; $C_{52}H_{67}N_{16}$ requires $[M+H]^+$ 915.5735; UV-Vis λ_{max}/THF; nm (ε/THF; $dm^3mol^{-1}cm^{-1}$): 806 (85 700), 718sh, 537 (9 600), 339 (38 500).

1,8,15,22-Tetrakis(diethylamino)-3,4,10,11,17,18,24,25-octamethyltetrapyrido[3,4-b:3',4'-g:3'',4''-l:3''',4'''-q]porphyrazinato magnesium (II) (8Mg). Metal-free **8H** (30 mg, 0.033 mmol) was dissolved in pyridine (5mL) and excess of anhydrous magnesium acetate (33 mg, 0.23 mmol) was added. Reaction mixture was heated at reflux for 24 h. After this time, pyridine was removed under reduced pressure and dark solid washed thoroughly with water. A crude product was purified by column chromatography with

toluene/chloroform/tetrahydrofuran 10:1:0.2 as an eluent. Yield 16 mg (53%) of a purplish brown solid. R_f (toluene/chloroform/tetrahydrofuran 10:1:0.5) = 0.29; HPLC (t_R, min): 18.4, 18.6, 18.8; IR (ATR, cm^{-1}): 2973, 2933, 2869, 1559, 1444, 1253, 1173, 1083, 1060, 992, 934 and 764; δ_H ($CDCl_3$/pyridine-d_5, 300 MHz): 1.10-1.68 (24H, m, $CH_2C\underline{H}_3$), 2.86-3.27 (12H, m, CH_3), 3.56-3.97 (12H, m, CH_3), 4.13-4.70 (16H, m, CH_2); δ_C ($CDCl_3$/pyridine-d_5, 75 MHz): 47.79, 45.62, 23.20, 13.18, aromatic signals were not detected; MS (MALDI-TOF) *m/z*: 936.4 $[M]^+$, 908.4 $[M\text{-}C_2H_4]^+$; HRMS *m/z*: found: $[M+H]^+$ 937.5400; $C_{52}H_{65}MgN_{16}$ requires $[M+H]^+$ 937.5429; UV-Vis λ_{max}/THF; nm (ε/THF; $dm^3mol^{-1}cm^{-1}$): 771 (94 800), 690 (32 900), 505 (10 400), 367 (48 200).

1,8,15,22-Tetrakis(diethylamino)-3,4,10,11,17,18,24,25-octamethyltetrapyrido[3,4-b:3',4'-g:3'',4''-l:3''',4'''-q]porphyrazinato zinc (II) (8Zn). Metal-free **8H** (30 mg, 0.033 mmol) was dissolved in pyridine (5 mL), anhydrous zinc acetate (42 mg, 0.23 mmol) was added and the reaction mixture was heated at reflux for 4 h. After this time, pyridine was removed under reduced pressure and dark solid washed thoroughly with water. A crude product was purified by column chromatography on silica with toluene/chloroform/tetrahydrofuran 10:1:0.5 as an eluent. Yield 24 mg (76%) of a purple solid. R_f (toluene/chloroform/tetrahydrofuran 10:1:0.5) = 0.41; HPLC (t_R, min): 17.7, 18, 20, 21; IR (ATR, cm^{-1}): 2967, 2930, 2867, 1559, 1480, 1442, 1253, 1172, 1124, 1087, 1061, 991, 937 and 755; δ_H ($CDCl_3$/pyridine-d_5, 300 MHz): 1.33 (24H, br s, $CH_2C\underline{H}_3$), 3.01 (12H, br s, CH_3), 3.78 (5H, br s, CH_3), 3.87 (7H, br s, CH_3), 4.22-4.66 (16H, m, CH_2); δ_C ($CDCl_3$/pyridine-d_5, 75 MHz): 156.50, 155.19, 153.98, 46.62, 45.28, 23.35, 15.63, 14.37, 13.47, 12.85; MS (MALDI-TOF) *m/z*:. 976.4 $[M]^+$, HRMS *m/z*: found: $[M+H]^+$ 977.4854; $C_{52}H_{64}N_{16}Zn$ requires $[M+H]^+$ 977.4870; UV-Vis λ_{max}/THF; nm (ε/THF; $dm^3mol^{-1}cm^{-1}$): 772 (94 000), 697 (29 400), 504 (54 000), 359 (37 400).

1,8,15,22-Tetrakis{[2-(diethylamino)ethyl]sulfanyl}-3,4,10,11,17,18,24,25-octamethyltetrapyrido[3,4-b:3',4'-g:3'',4''-l:3''',4'''-q]porphyrazinato magnesium (II) (9Mg).

Magnesium turnings (708 mg, 29.1 mmol) and a small crystal of iodine were refluxed in freshly distilled butanol (30 mL) for 3 h. Compound **5** (1.20 g, 4.16 mmol) was added and the reflux continued for next 4 h. Solvent was evaporated and the green product was carefully extracted from the mixture with tetrahydrofuran. The crude product was adsorbed on silica and washed with MeOH. The silica with product was dried under reduced pressure and the product was purified by column chromatography on silica with pyridine/MeOH 5:1. The pure product was further repurified by precipitation of the concentrated chloroform solution (5 mL) with hexane. Yield 743 mg (61%) of green solid. R_f (pyridine/MeOH 5:1) = 0.5-0.1; IR (ATR, cm^{-1}): 2968,

2930, 2871, 2810, 1553, 1468, 1406, 1330, 1266, 1230, 1184, 1107; δ_H ($CDCl_3$/pyridine-d_5, 300 MHz): 1.27-1.58 (24H, m, $NCH_2C\underline{H}_3$), 2.57-3.93 (56H, m, CH_2+CH_3); δ_C ($CDCl_3$/pyridine-d_5, 75 MHz): 156.70, 155.93, 152.91, 151.97, 142.85, 127.60, 124.51, 124.25, 53.17, 47.75, 47.38, 26.51, 26.28, 23.51, 23.36, 23.27, 16.86, 12.84, 12.76; MS (MALDI-TOF) *m/z*:. 1177.5 $[M+H]^+$, 1104.45 $[M-NC_4H_{10}]^+$; UV-Vis λ_{max}/THF; nm (ε/THF; $dm^3mol^{-1}cm^{-1}$): 728 (232 000), 654 (50 900), 365 (62 400).

1,8,15,22-Tetrakis{[2-(diethylamino)ethyl]sulfanyl}-3,4,10,11,17,18,24,25-octamethyltetrapyrido[3,4-b:3',4'-g:3'',4''-l:3''',4'''-q]porphyrazine (II) (9H)

Magnesium TPyPz **9Mg** (680 mg, 0.58 mmol) was dissolved in tetrahydrofuran (50 mL) and *p*-toluenesulfonic acid (1.65 g, 8.65 mmol) was added. The mixture was stirred at rt for 15 min and the green precipitate was formed. The precipitate dissolved after addition of MeOH (50 mL) and the reaction was further stirred at rt for next 30 min. The solvents were evaporated under reduced pressure, water was added and the green solution was neutralized by $NaHCO_3$. The green precipitate that was formed was collected and washed thoroughly with water. The product (green solid, 650 mg, 97%) was not further analyzed and was used directly in the next reaction to synthesize **9Zn**.

1,8,15,22-Tetrakis{[2-(diethylamino)ethyl]sulfanyl}-3,4,10,11,17,18,24,25-octamethyltetrapyrido[3,4-b:3',4'-g:3'',4''-l:3''',4'''-q]porphyrazinato zinc (II) (9Zn)

Metal-free **9H** (650 mg, 0.56 mmol) and anhydrous zinc acetate (720 mg, 3.94 mmol) were dissolved in pyridine (20 mL) and refluxed for 1 h. Pyridine was evaporated under reduced pressure, water was added and the green product was extracted three times with chloroform. Part of the product still remained in the water phase, for this reason, the water was acidified with HCl and then again neutralized with $NaHCO_3$. Very fine precipitate was formed and was extracted to chloroform three times. The chloroform extracts were combined, evaporated under reduced pressure and washed with water and acetone. The product was purified by column chromatography on silica with step gradient elution with pyridine/MeOH 20:1 changing to 5:1. The pure product was dissolved in very small amount of chloroform, precipitated by hexane, the fine precipitate was collected and dried. Yield 331 mg (48%) of green solid. R_f (pyridine/MeOH 5:1) = 0.62-0.26; IR (ATR, cm^{-1}): 2969, 2932, 2810, 1555, 1473, 1407, 1330, 1267, 1231, 1108; δ_H ($CDCl_3$/pyridine-d_5, 300 MHz): 1.27-1.59 (24H, m, $NCH_2C\underline{H}_3$), 2.73-3.99 (56H, m, CH_2+CH_3); δ_C ($CDCl_3$/pyridine-d_5, 75 MHz): 52.63, 47.30, 46.99, 26.23, 23.14, 22.99, 12.31, 12.19 (aromatic signals were not detected); MS (MALDI-TOF) *m/z*:. 1217.4

$[M+H]^+$, 1144.4 $[M-NC_4H_{10}]^+$; UV-Vis λ_{max}/THF; nm (ε/THF; $dm^3mol^{-1}cm^{-1}$): 729 (115 600), 658sh, 357 (45 200).

1,8,15,22-Tetrakis{[2-(triethylammonio)ethyl]sulfanyl}-3,4,10,11,17,18,24,25-octamethyltetrapyrido[3,4-b:3',4'-g:3'',4''-l:3''',4'''-q]porphyrazinato zinc (II) tetraiodide (10Zn)

TPyPz **9Zn** (100 mg, 82 μmol) was dissolved in ethyliodide (5 mL) and stirred at rt for 2 days. The green precipitate that was formed was dissolved after addition of *N*-methylpyrrolidinon (5 mL) and the reaction continued at rt for next 4 days. Then, the product was precipitated by addition of diethylether (100 mL), collected and washed with diethylether. The product was purified by repeated (three times) dissolution in MeOH, precipitation by diethylether and collection of the precipitate. The alkylated product **10Zn** was obtained as green solid (72 mg, 48%). Under these conditions, only the aliphatic tertiary nitrogens are alkylated (not the one in pyridine). This fact was confirmed by alkylation of **6Zn** under the same conditions where no reaction proceeded as detected on TLC. IR (ATR, cm^{-1}): 2978, 2943, 1555, 1475, 1404, 1330, 1265, 1229, 1186, 1111; δ_H (DMSO-d_6/pyridine-d_5, 500 MHz): 1.28-1.64 (36H, m, $NCH_2C\underline{H}_3$), 2.91-4.01 (64H, m,CH_2+ CH_3, overlapped with signal of water); δ_C (DMSO-d_6/pyridine-d_5, 125 MHz): 56.74, 53.11, 23.38, 21.49, 17.13, 8.13; elemental analysis found (%): C, 42.81; H, 5.47; N, 11.67; $C_{68}H_{100}I_4N_{16}S_4Zn$ + $3H_2O$ requires (%): C, 43.06; H, 5.63; N, 11.81; UV-Vis λ_{max}/DMF; nm (ε/DMF; $dm^3mol^{-1}cm^{-1}$): 722 (207 500), 649 (41 700), 365 (40 300).

NMR spectra

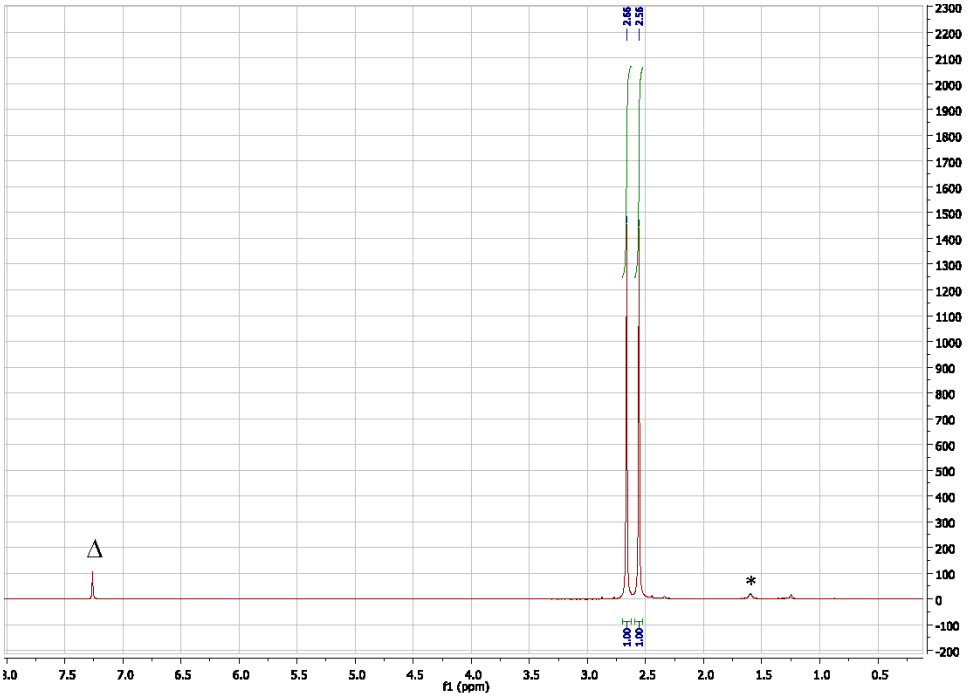

Figure S1. ^{1}H NMR spectrum of **1** in $CDCl_3$. Asterisk = signal of residual water. Triangle = residual signal of non-deuterated solvent.

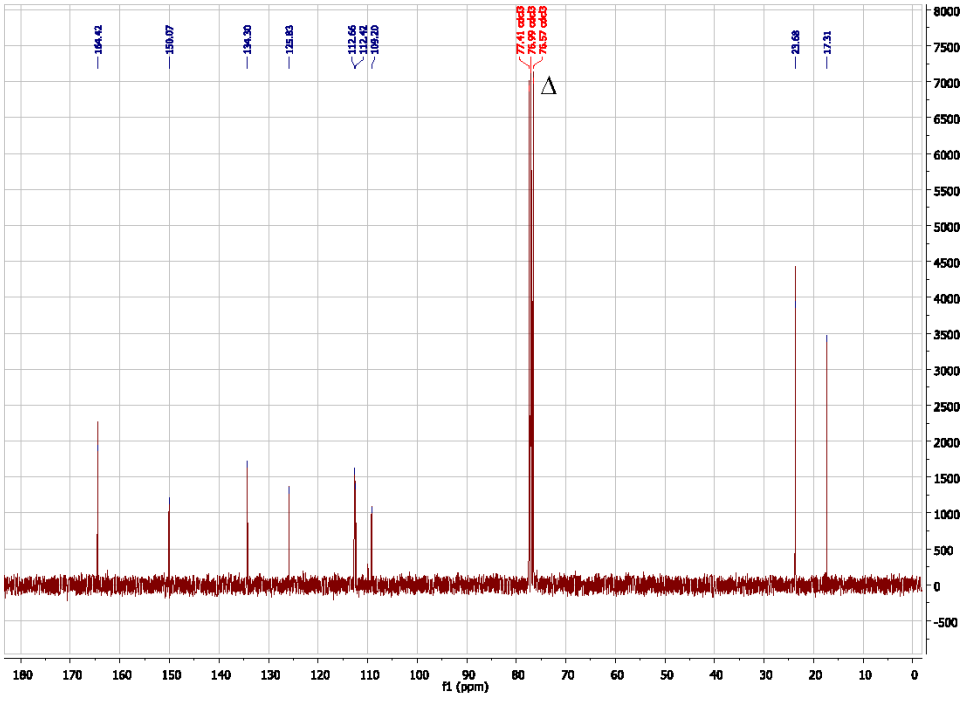

Figure S2. ^{13}C NMR spectrum of **1** in $CDCl_3$. Triangle = signal of solvent.

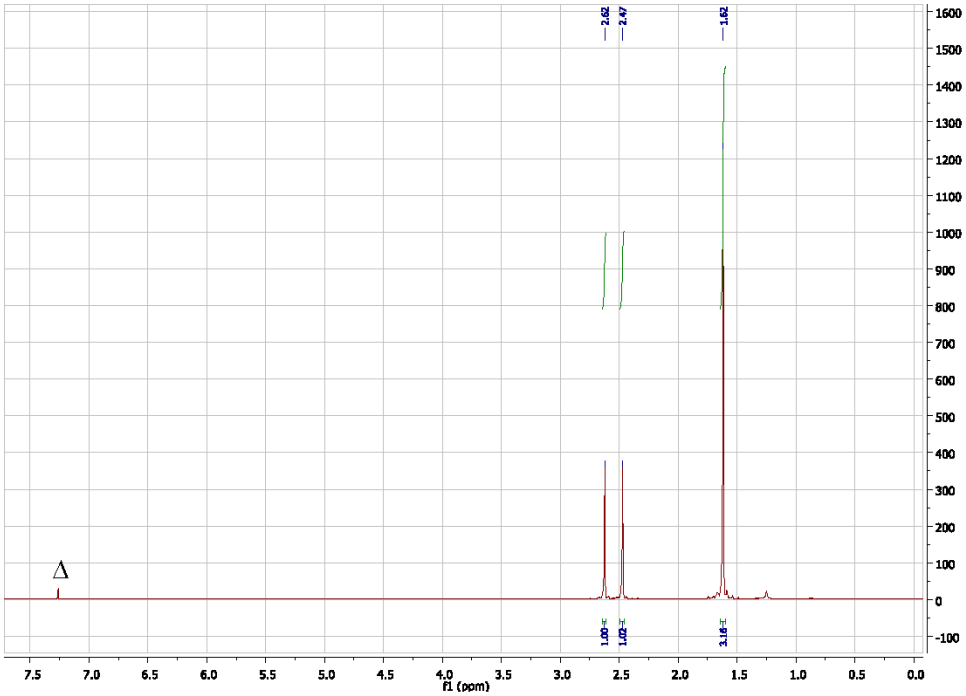

Figure S3. ^{1}H NMR spectrum of **2** in $CDCl_3$. Triangle = residual signal of non-deuterated solvent.

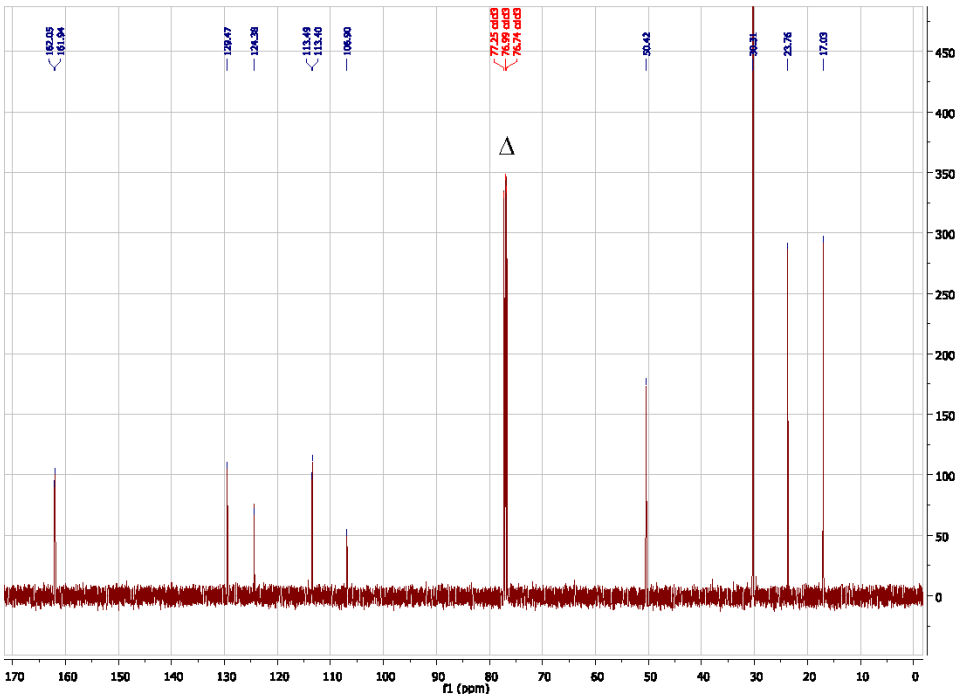

Figure S4 ^{13}C NMR spectrum of **2** in $CDCl_3$. Triangle = signal of solvent.

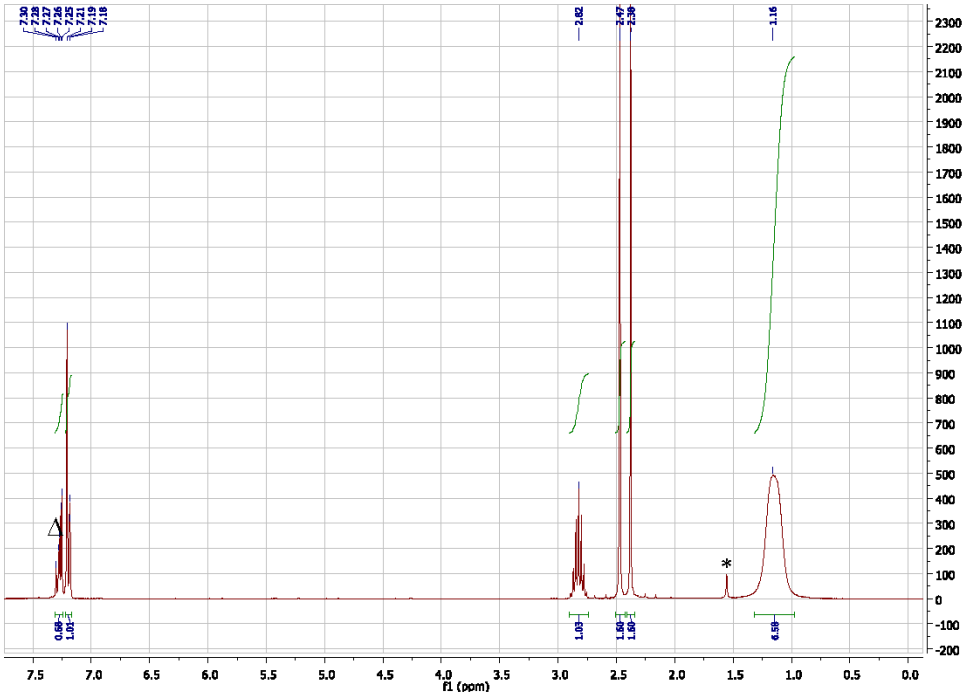

Figure S5. ^{1}H NMR spectrum of **3** in $CDCl_3$. Asterisk = signal of residual water. Triangle = residual signal of non-deuterated solvent.

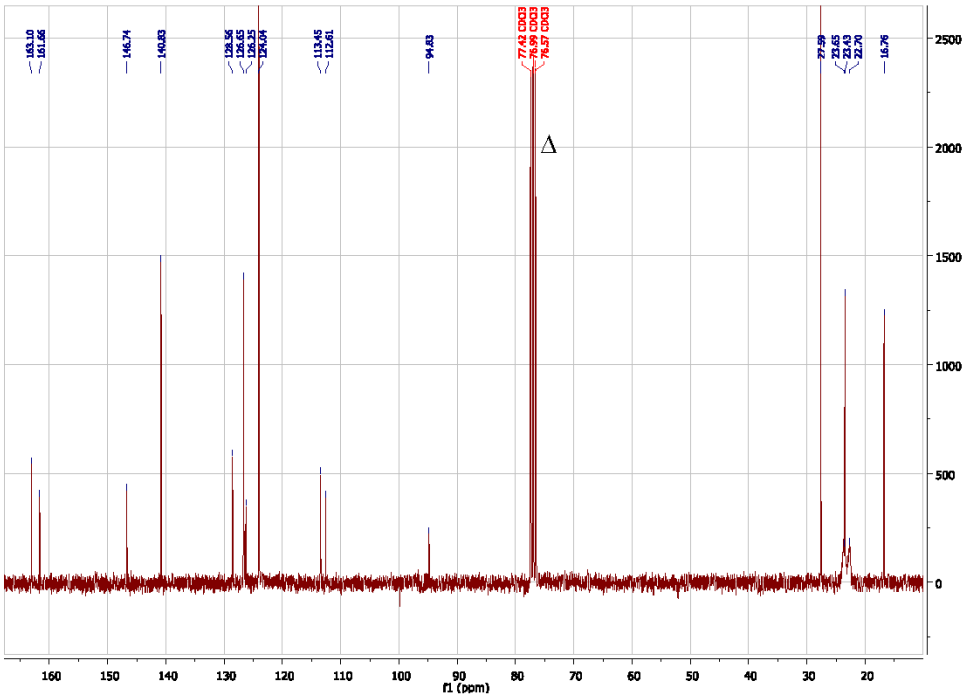

Figure S6. ^{13}C NMR spectrum of **3** in $CDCl_3$. Triangle = signal of solvent.

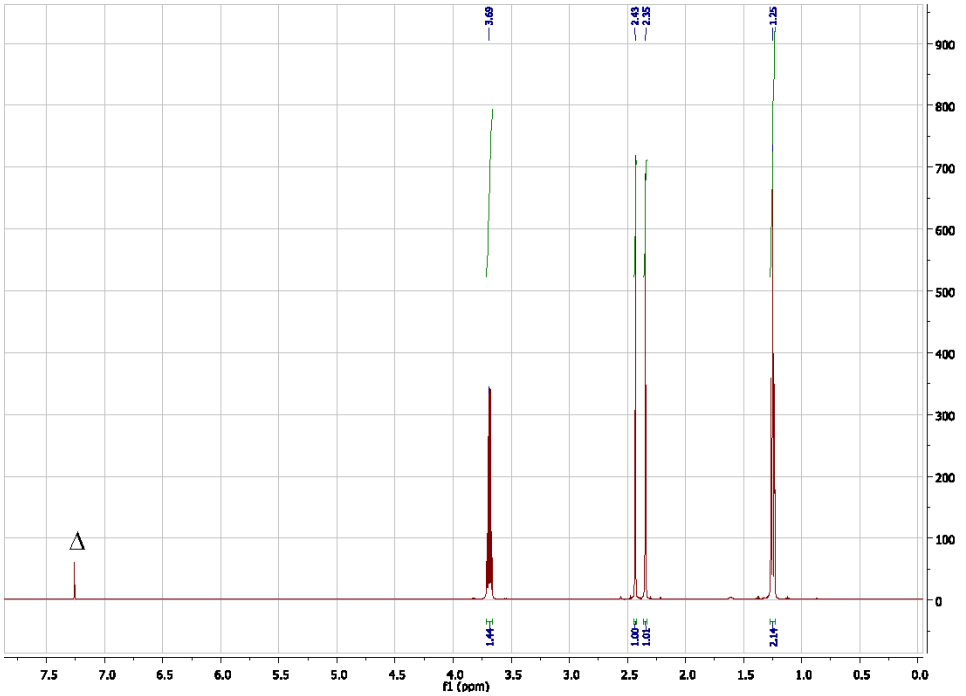

Figure S7. ^{1}H NMR spectrum of **4** in $CDCl_3$. Triangle = residual signal of non-deuterated solvent.

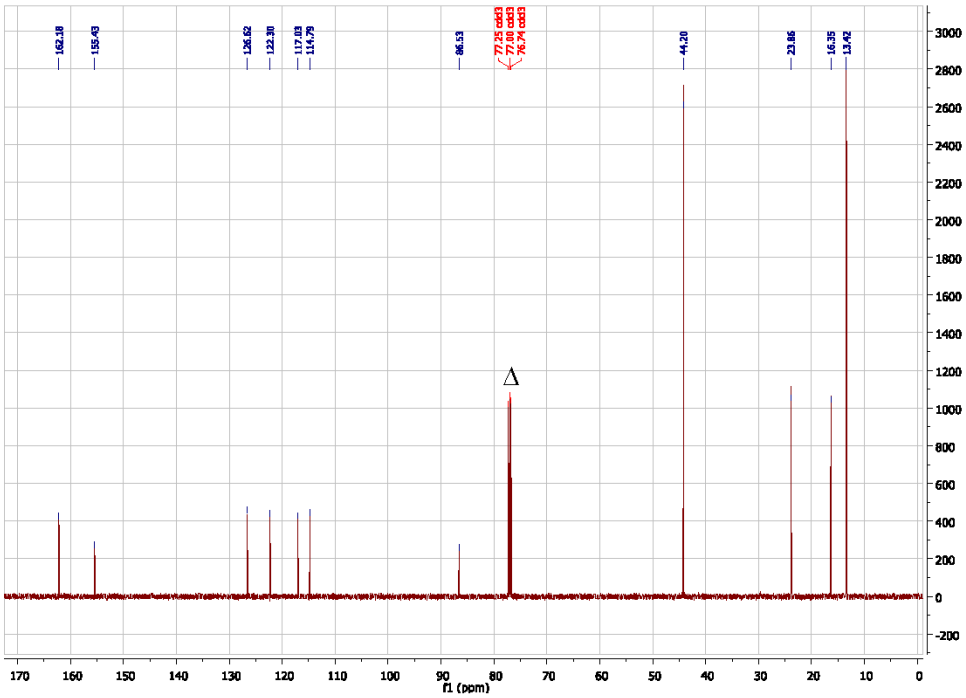

Figure S8. ^{13}C NMR spectrum of **4** in $CDCl_3$. Triangle = signal of solvent.

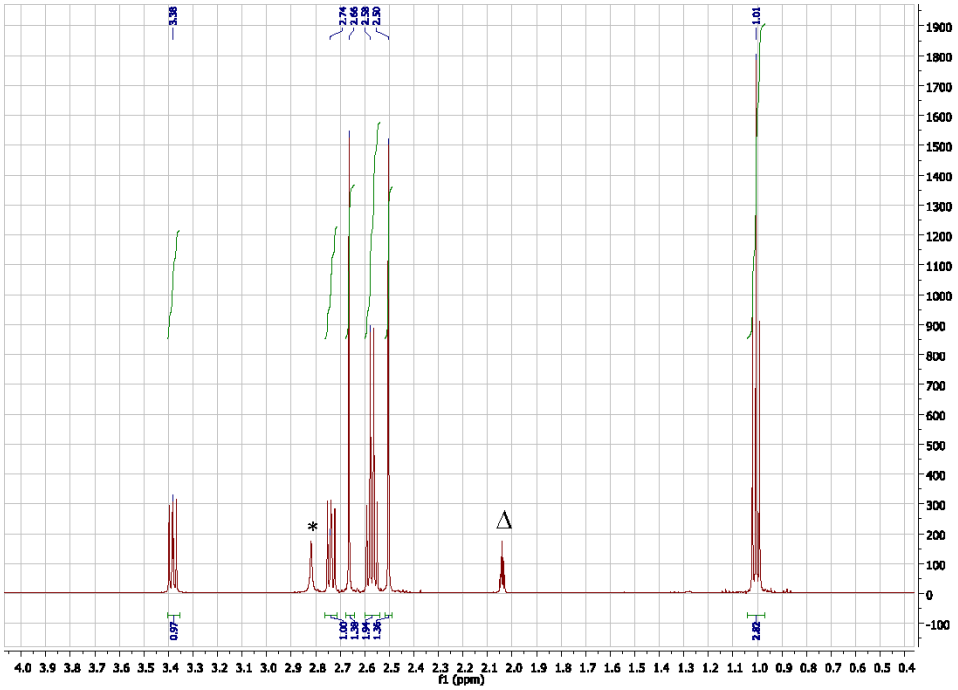

Figure S9. ^{1}H NMR spectrum of **5** in CD_3COCD_3. Asterisk = signal of residual water. Triangle = residual signal of non-deuterated solvent.

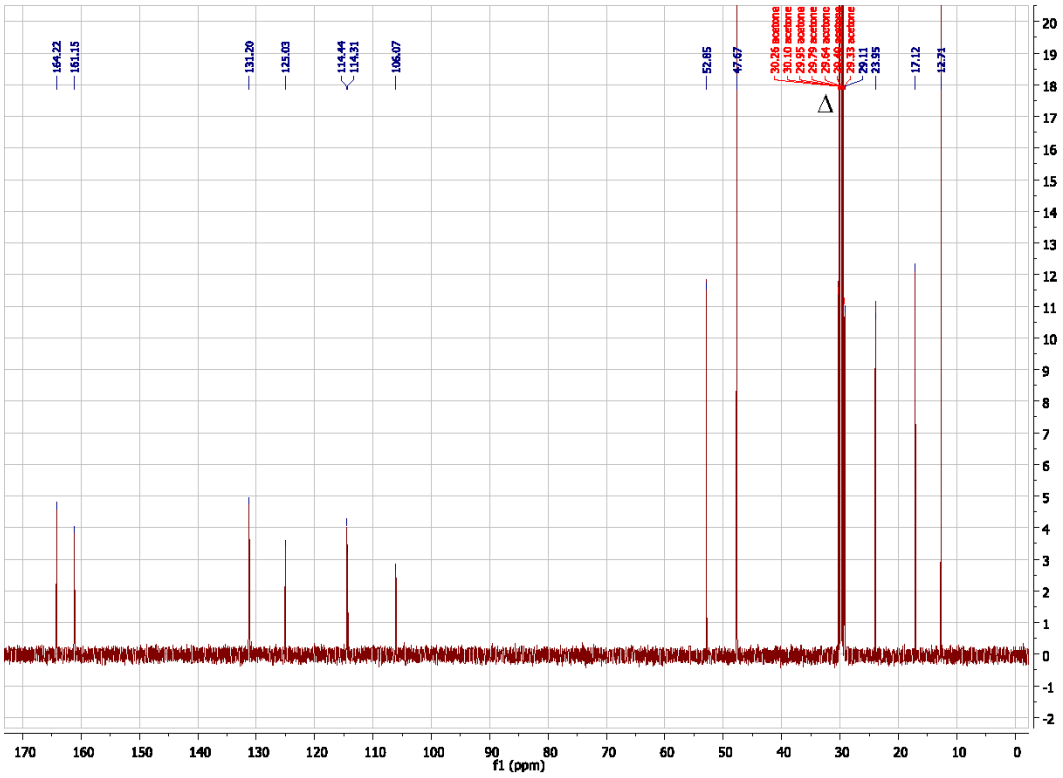

Figure S10. ^{13}C NMR spectrum of **5** in CD_3COCD_3. Triangle = signal of solvent.

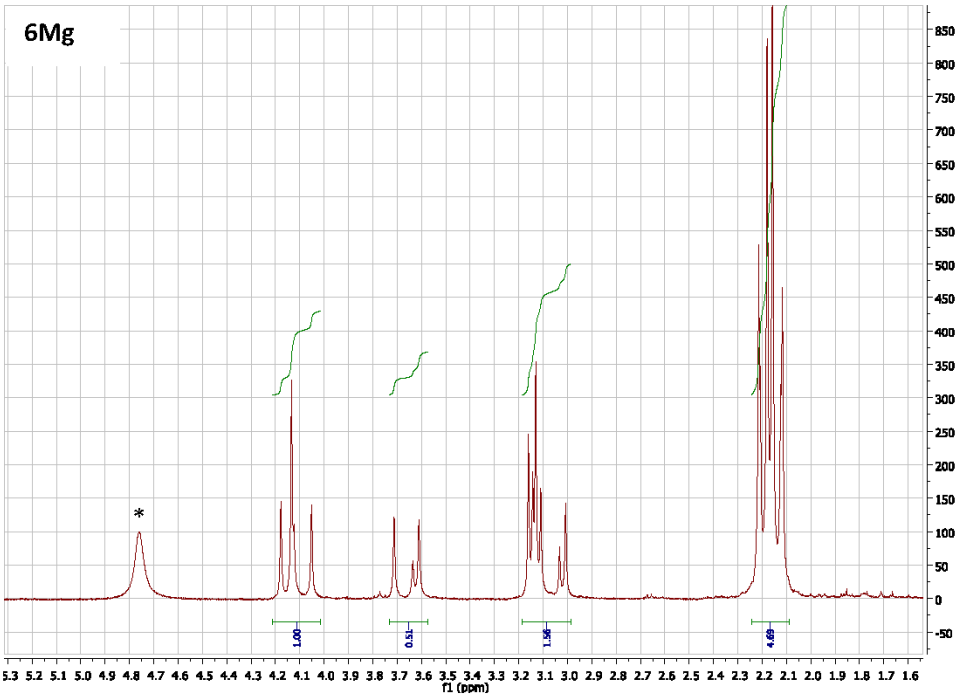

Figure S11. ^{1}H NMR spectrum of **6Mg** in $CDCl_3$/pyridine-d_5. Asterisk = signal of residual water.

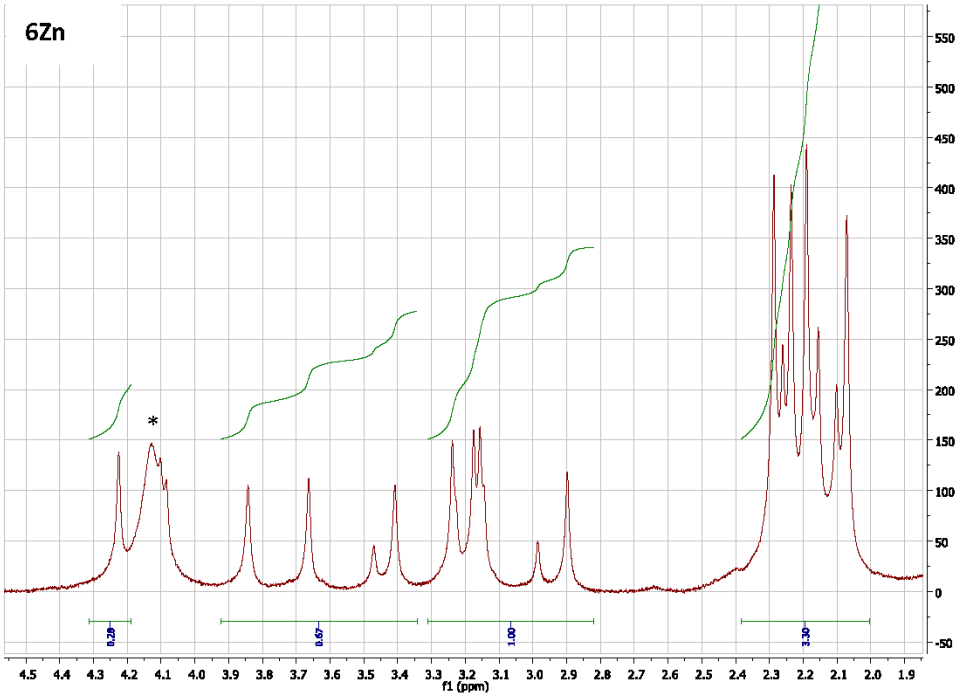

Figure S12. ^{1}H NMR spectrum of **6Zn** in $CDCl_3$/pyridine-d_5. Asterisk = signal of residual water.

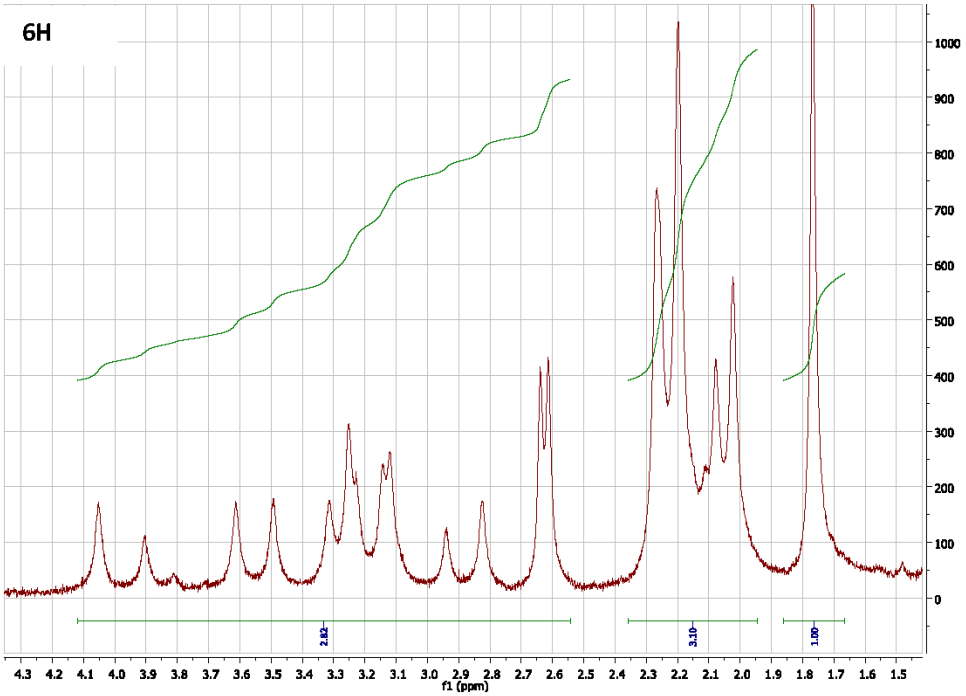

Figure S13. ^{1}H NMR spectrum of **6H** in $CDCl_3$/pyridine-d_5.

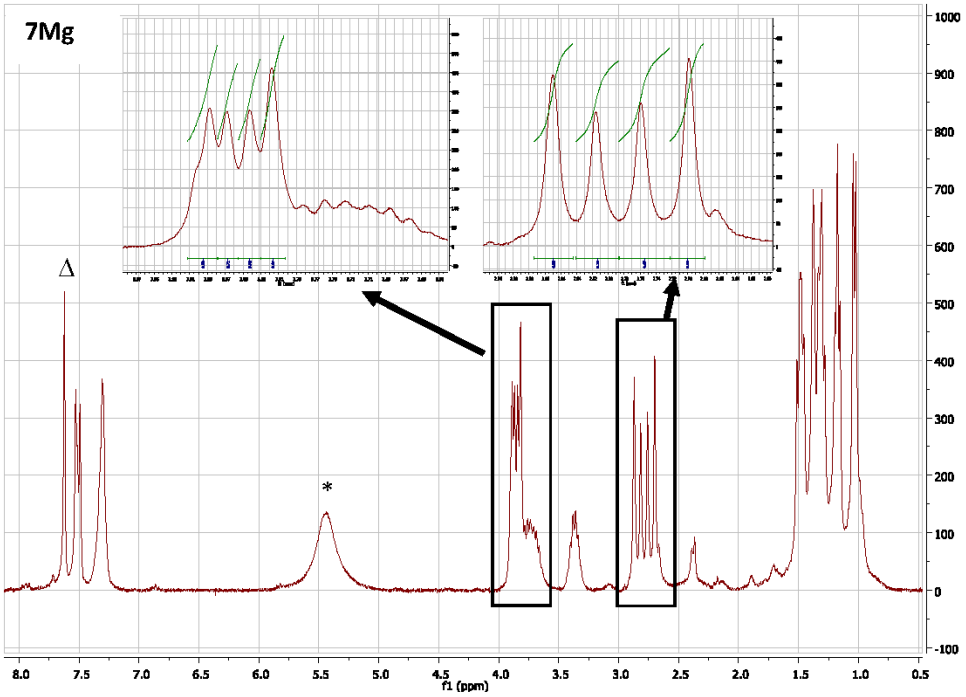

Figure S14. ^{1}H NMR spectrum of **7Mg** in $CDCl_3$/pyridine-d_5. Asterisk = signal of residual water. Triangle = residual signal of non-deuterated solvent.

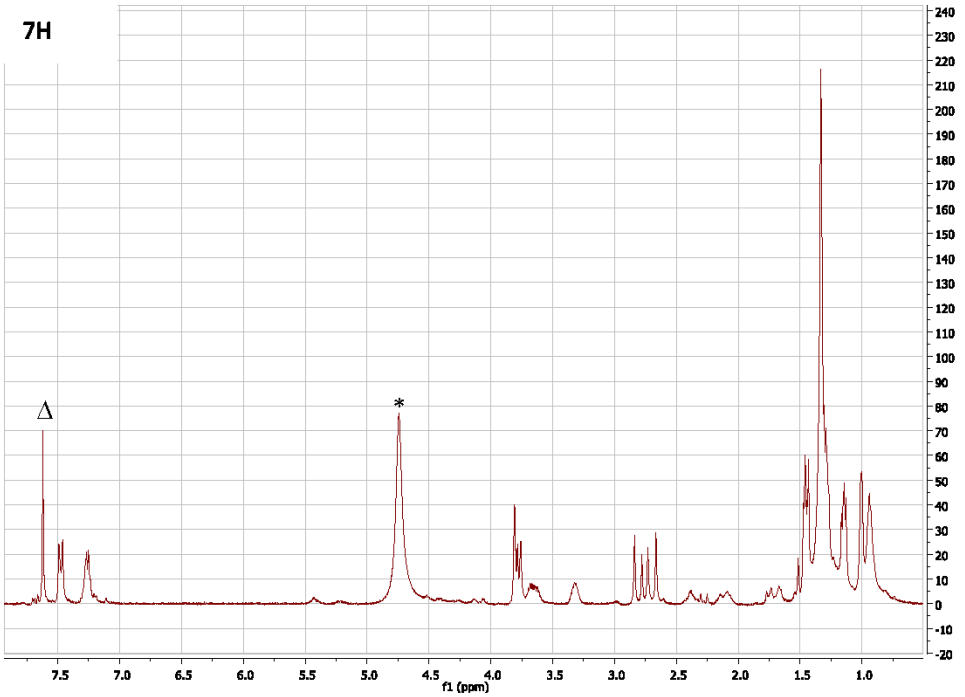

Figure S15. ^{1}H NMR spectrum of **7H** in $CDCl_3$/pyridine-d_5. Asterisk = signal of residual water. Triangle = residual signal of non-deuterated solvent.

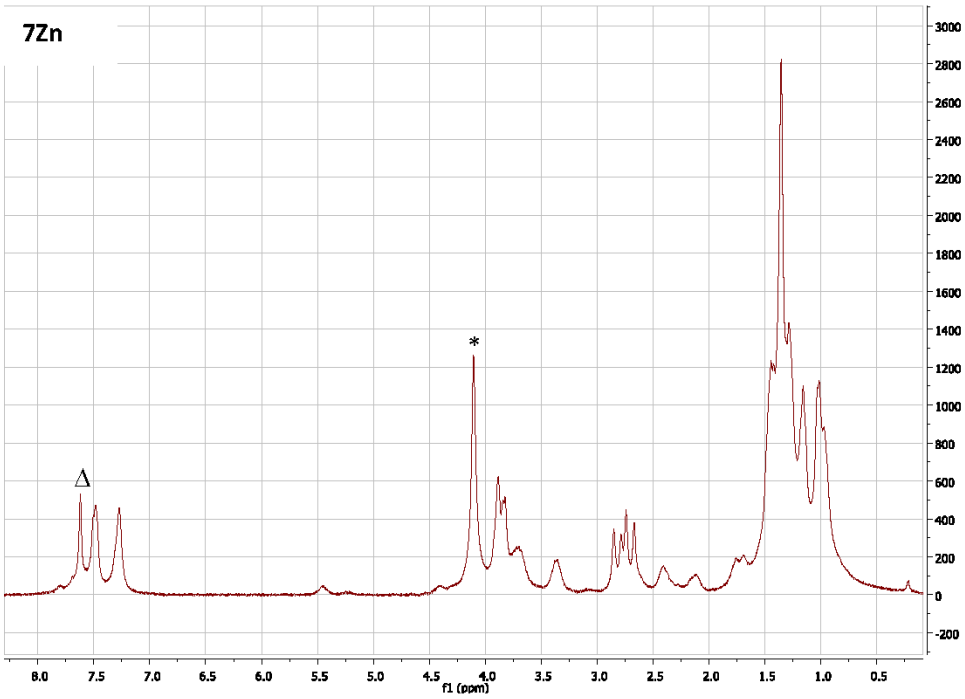

Figure S16. ^{1}H NMR spectrum of **7Zn** in $CDCl_3$/pyridine-d_5. Asterisk = signal of residual water. Triangle = residual signal of non-deuterated solvent.

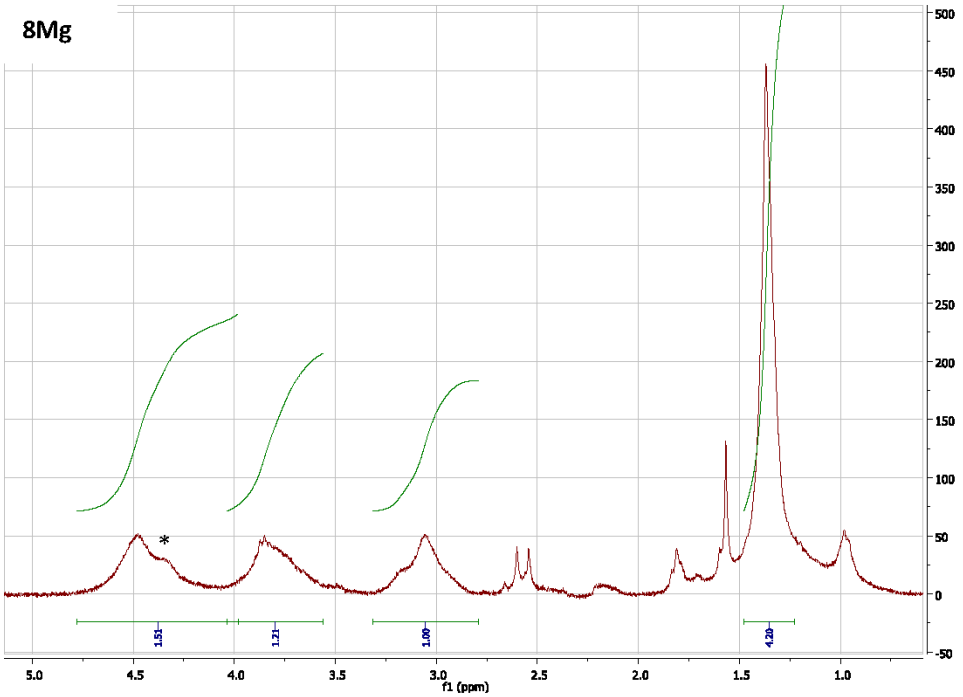

Figure S17. ^{1}H NMR spectrum of **8Mg** in $CDCl_3$/pyridine-d_5. Asterisk = signal of residual water.

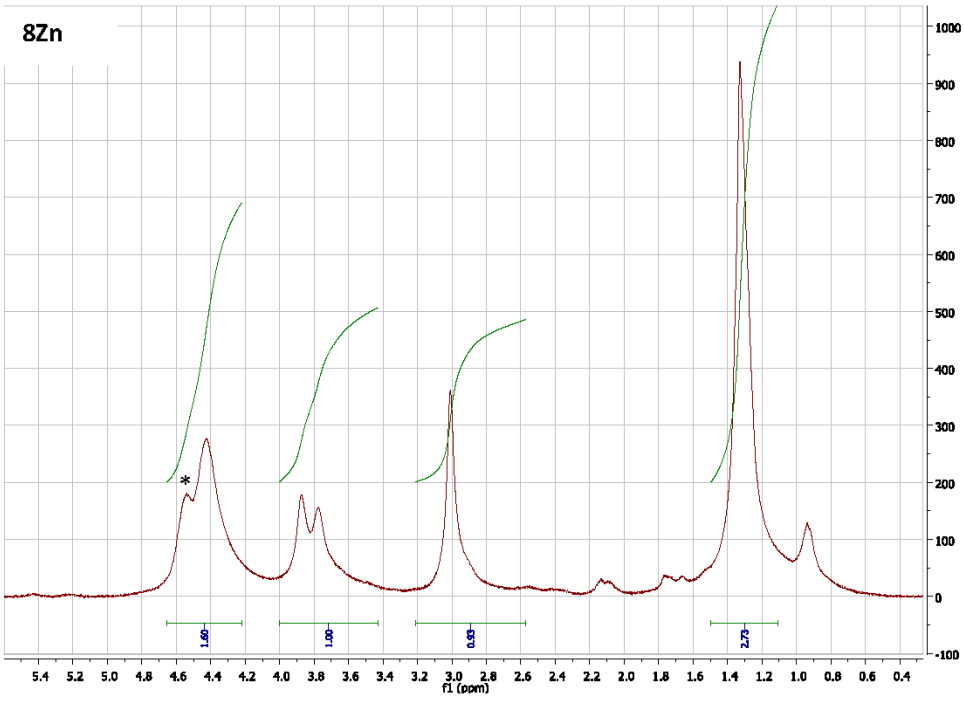

Figure S18. ^{1}H NMR spectrum of **8Zn** in $CDCl_3$/pyridine-d_5. Asterisk = signal of residual water.

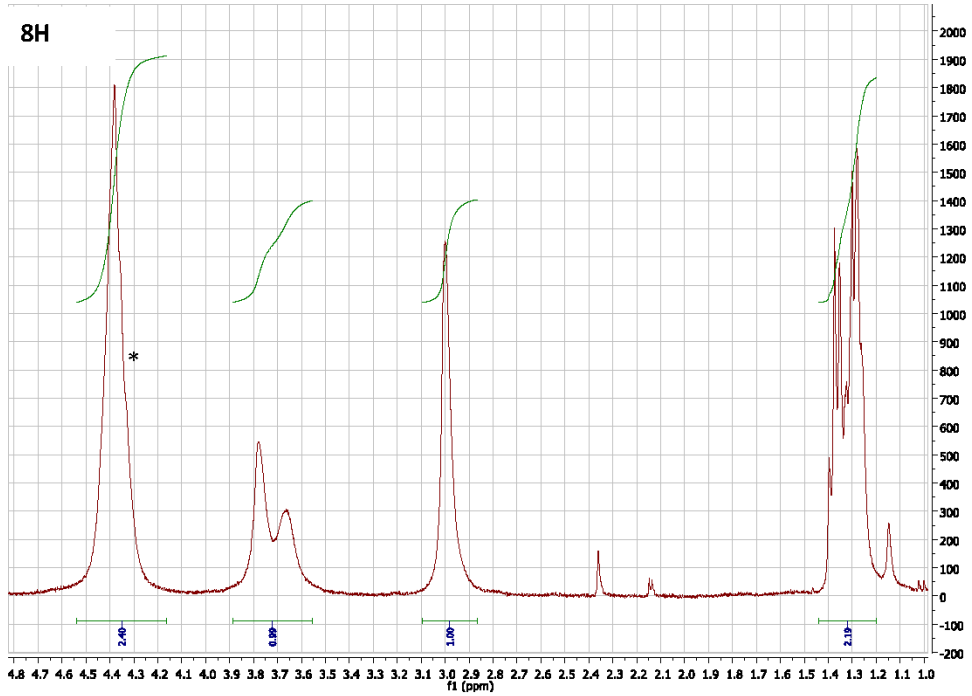

Figure S19. ^{1}H NMR spectrum of **8H** in $CDCl_3$/pyridine-d_5. Asterisk = signal of residual water.

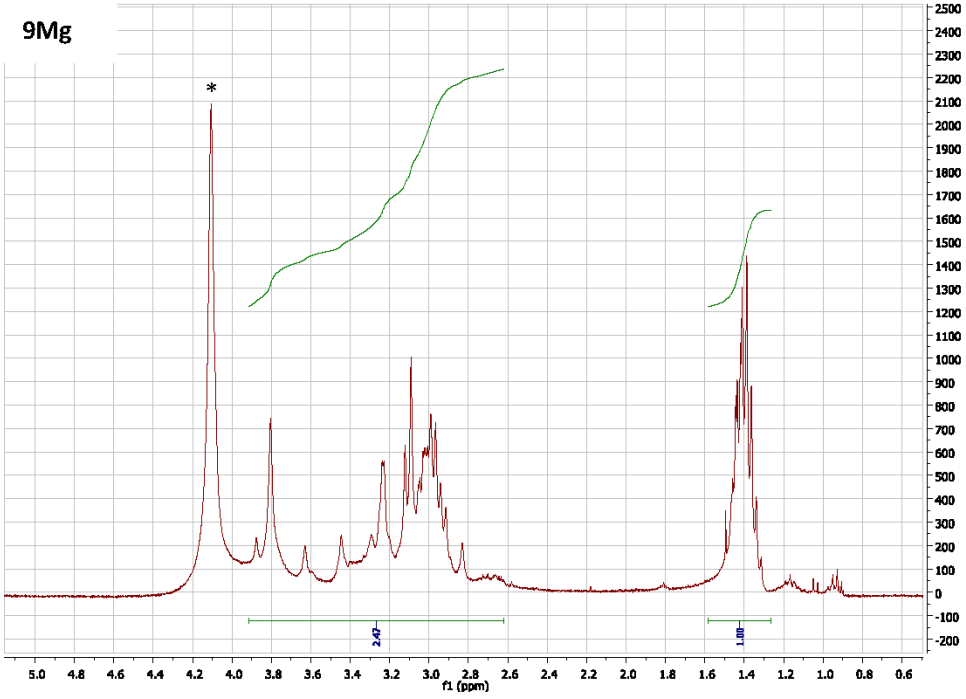

Figure 20. ^{1}H NMR spectrum of **9Mg** in $CDCl_3$/pyridine-d_5. Asterisk = signal of residual water.

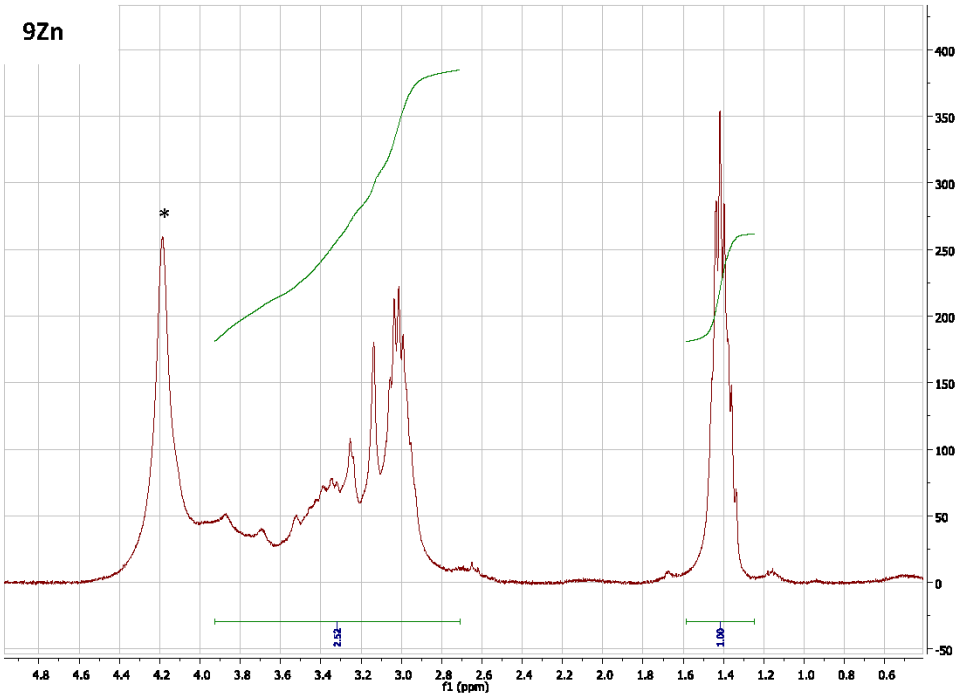

Figure S21. ^{1}H NMR spectrum of **9Zn** in $CDCl_3$/pyridine-d_5. Asterisk = signal of residual water.

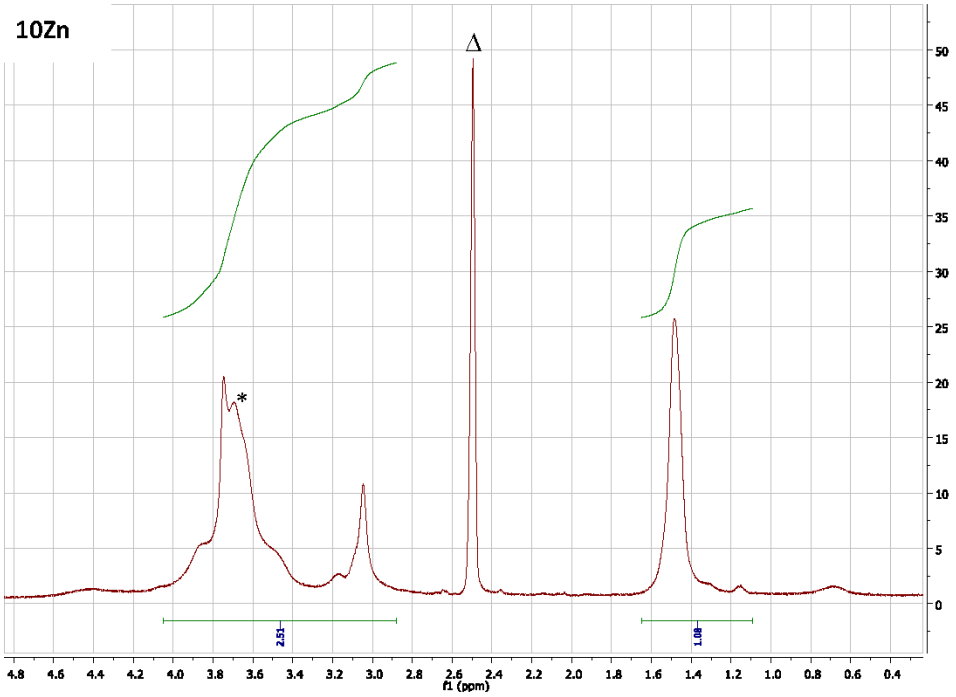

Figure S22. ^{1}H NMR spectrum of **10Zn** in DMSO-d_6/pyridine-d_5. Asterisk = signal of residual water. Triangle = residual signal of non-deuterated solvent.

MS spectra

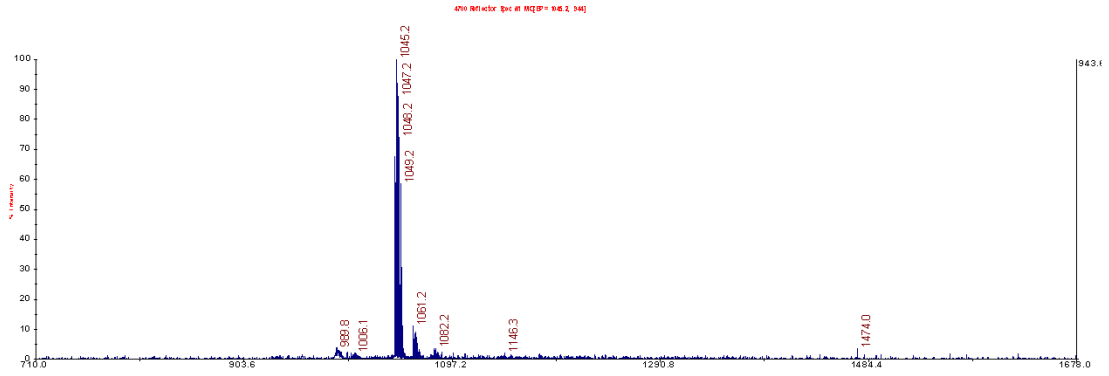

Figure S23. MALDI-TOF mass spectrum of **6Zn**.

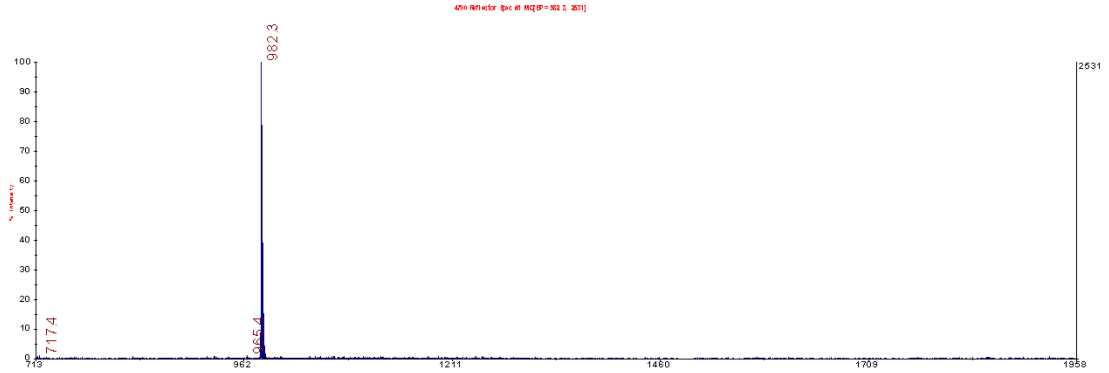

Figure S24. MALDI-TOF mass spectrum of **6H**.

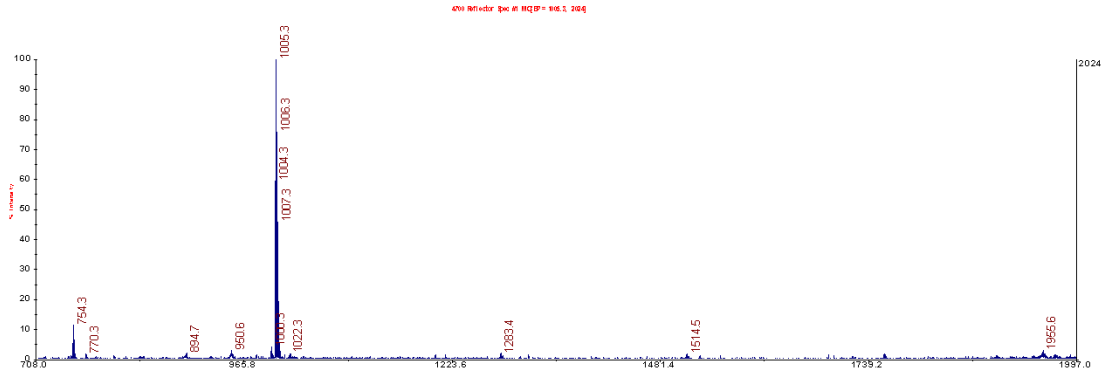

Figure S25. MALDI-TOF mass spectrum of **6Mg**.

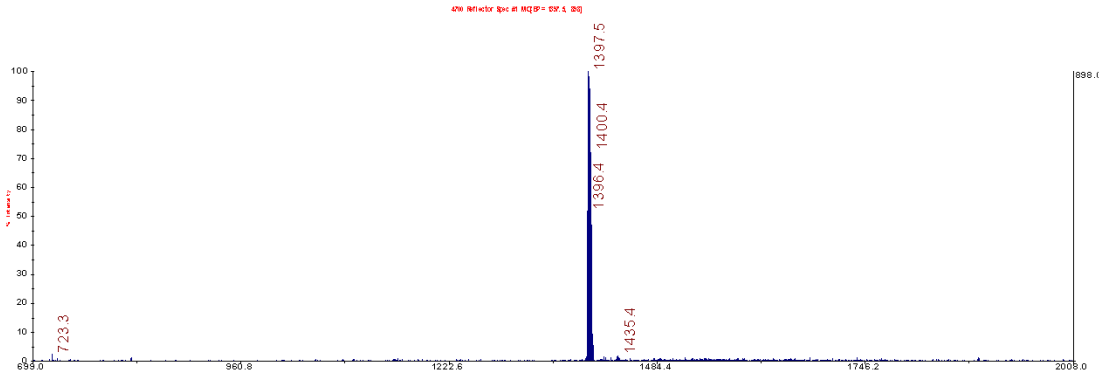

Figure S26. MALDI-TOF mass spectrum of **7Zn**.

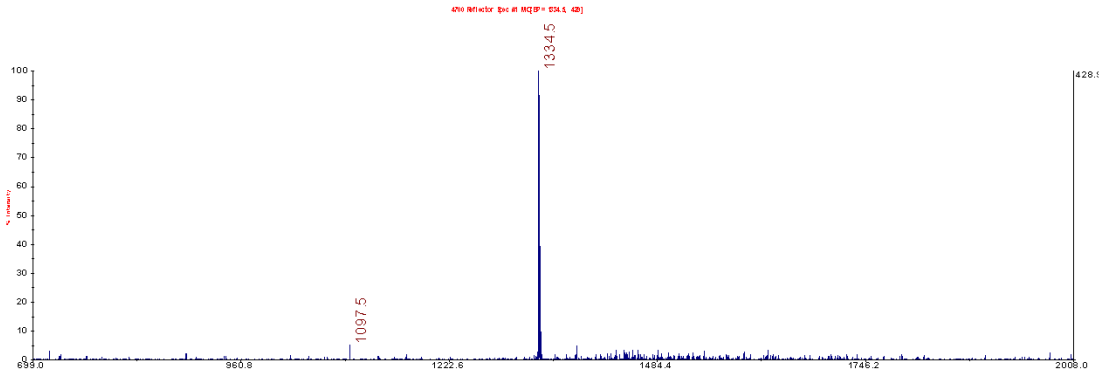

Figure S27. MALDI-TOF mass spectrum of **7H**.

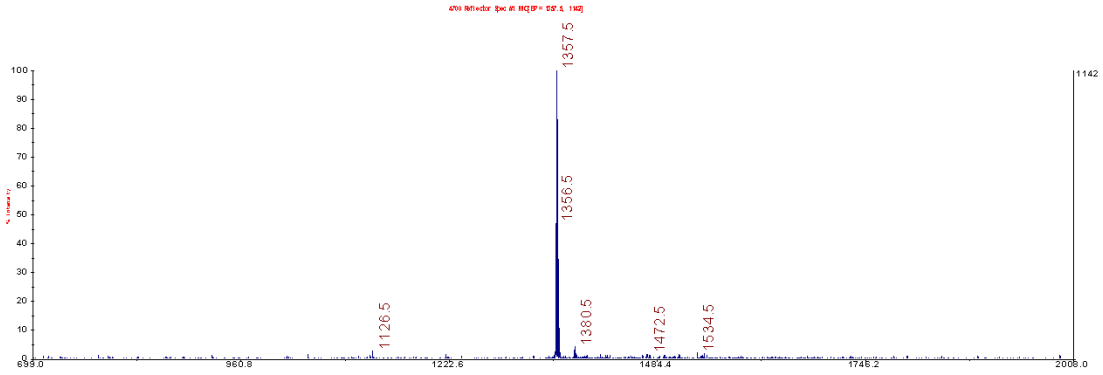

Figure S28. MALDI-TOF mass spectrum of **7Mg**.

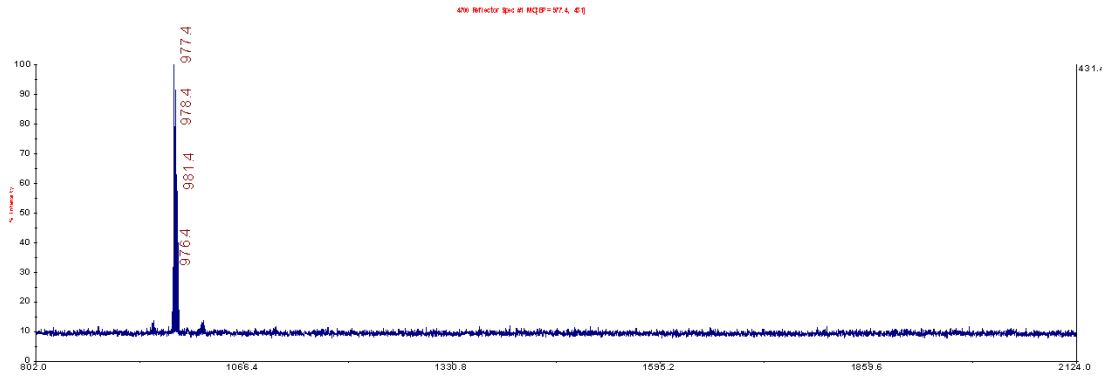

Figure S29. MALDI-TOF mass spectrum of **8Zn**.

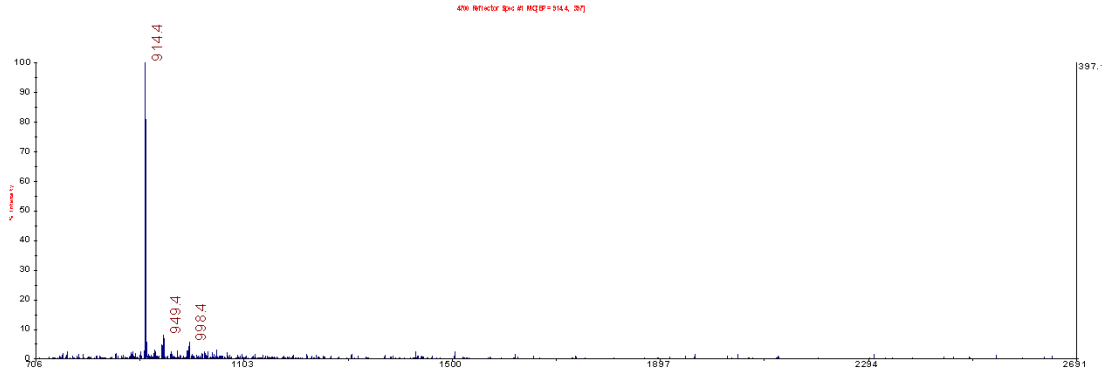

Figure S30. MALDI-TOF mass spectrum of **8H**.

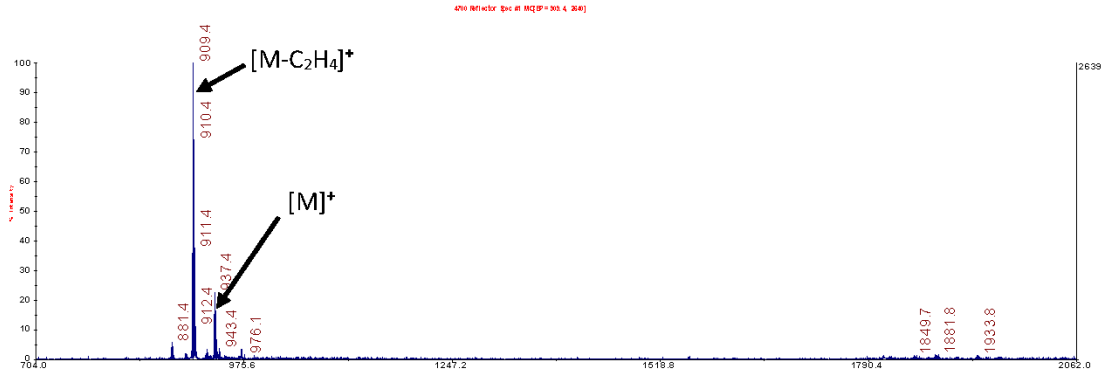

Figure S31. MALDI-TOF mass spectrum of **8Mg**.

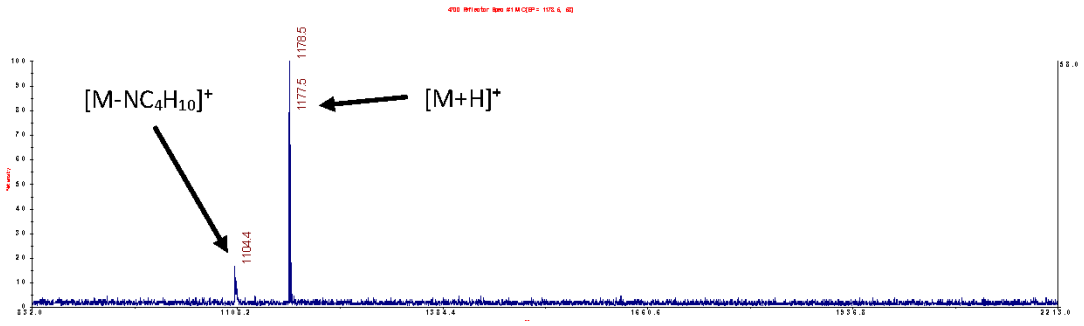

Figure S32. MALDI-TOF mass spectrum of **9Mg**.

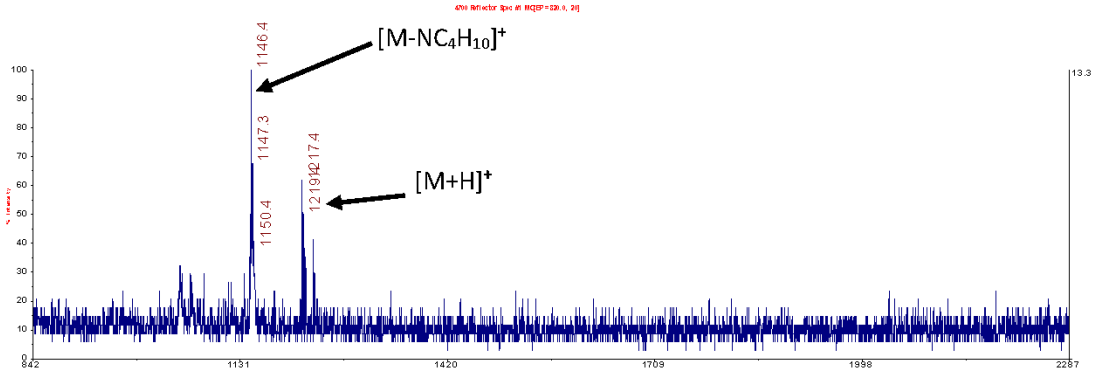

Figure S33. MALDI-TOF mass spectrum of **9Zn**.

HPLC separation

The analysis of the TPyPzs samples was accomplished by HPLC-DAD. The separation was performed on a Hypersil BDS C18 column (100 × 4.6 mm, particle size 2.4 μm) using a mobile phase consisting of acetonitrile, THF and water. The mobile phase A was water and mobile phase B contained acetonitrile-THF (1:1, v/v), both with addition of 0.025% triethylamine. The gradient program (except for **7Mg**) was set as follows: 0-20 min 60→90% B; 20-40 min 90% B; 40-40.5 min 90→60% B. The column was then equilibrated for 5 min under initial conditions (60% B). In order to achieve better separation of **7Mg** isomers the final concentration of mobile phase B in the gradient program was lowered to 83%. The column temperature was maintained at 40 °C and the flow rate was set at 1.0 mL/min. The chromatograms were recorded by a diode array detector at the wavelength corresponding to the absorbance maximum for each compound: **6Mg**, **6Zn** 730 nm; **7Mg**, **7Zn** 710 nm; **7H** 715 nm; **8Mg** 770 nm; **8Zn** 775 nm; **8H** 800 nm. Compound **6H** was not sufficiently soluble for HPLC analysis.

Quantitative HPLC analysis (*i.e.* percentual distribution of the isomers in the mixture) was performed only for the **6Mg**, **7Mg** and **8H** (Table S1), *i.e.* the compounds that originated directly from cyclotetramerization reaction and not from insertion/removal of the central metal. The reason is that some of the isomers could be removed or their amount reduced during next reaction steps. Nevertheless, the qualitative parameter, the retention time (t_R) of the isomers, is also mentioned in Experimental section for other complexes besides **6H**. Very low solubility of this compound did not allow HPLC analysis.

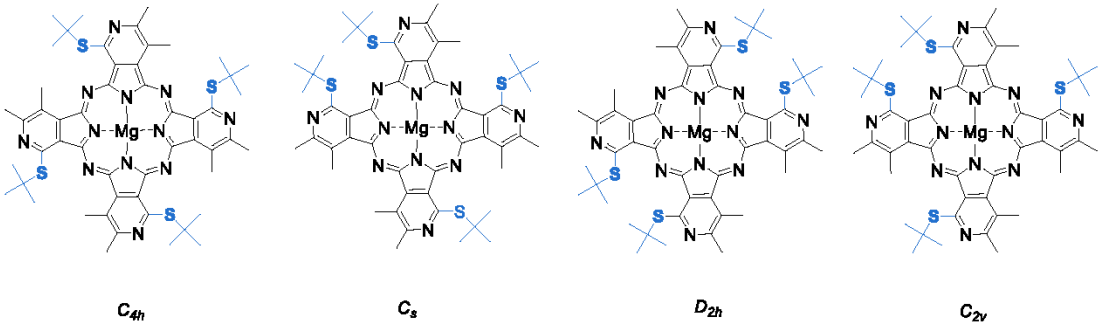

Figure S34. The possible positional isomers of synthesized TPyPz. Example for **6Mg**.

Table S1. Retention times (t_R, min) and percentual representation (in parentheses) of TPyPz isomers.

	Isomer A	Isomer B	Isomer C	Isomer D
5Mg	21.9 (61.5%)	22.77 (38.5%)	-	-
6Mg	28.8 (1%,) C_{2v}	29.2 (1.5%), D_{2h}	30.0 (30.5%), C_{4h}	30.5 (67%) C_s
7H	26.5 (16%)	28.5 (71%)	29.0 (13%)	-

Photophysical characterization

Fluorescence measurements

The samples were repurified using preparative TLC (except **10Zn**) before the photophysical measurements (both Φ_F and Φ_Δ) to ensure that they were highly pure. The fluorescence spectra were obtained using an AMINCO Bowman Series 2 luminescence spectrometer. All emission spectra were corrected for instrument response. The fluorescence quantum yields (Φ_F) were determined in THF (DMF for **10Zn**) *via* the comparative method using unsubstituted zinc phthalocyanine (ZnPc, Sigma-Aldrich) as a reference (Φ_F = 0.32 in THF[2]). Both the reference and sample were excited at 360 nm. The absorbance at the excitation wavelength and at the Q-band maximum was held below 0.05 to limit the inner filter effect. The value of Φ_F was calculated using Eq. S1[3]:

$$\Phi_F^S = \Phi_F^R \frac{F^S}{F^R}\left(\frac{1-10^{-A^R}}{1-10^{-A^S}}\right)\left(\frac{n^S}{n^R}\right)^2 \qquad \text{(Eq. S1)}$$

where F is the integrated area under the emission spectrum, n is refractive index of the solvent and A is the absorbance at the excitation wavelength. The superscripts R and S correspond to the reference and sample, respectively. All experiments were performed in triplicate with the data representing the mean (estimated error ±15%, for **8Mg**, **8Zn** and **8H** ±50% due to detection limit of the instrument).

Determination of the singlet oxygen production

The quantum yields of the singlet oxygen (Φ_Δ) were determined in THF (in DMF for **10Zn**) according to a previously published procedure[4] using the decomposition of a chemical trap 1,3-diphenylisobenzofuran (DPBF) with ZnPc as a reference (Φ_Δ = 0.53 in THF[5], Φ_Δ = 0.56 in DMF[6]) The detailed procedure was as follows: 2.5 mL of a DPBF stock solution in THF (or DMF) (5×10^{-5} M) was transferred into a 10 mm × 10 mm quartz optical cell and was saturated with oxygen for 1 min. A stock solution of the tested compound in THF (or DMF) (typically 20 μL) was then added to achieve an absorbance of the final solution in the Q-band

maximum of approximately 0.1. The solution was stirred and irradiated using a xenon lamp (100 W, ozone-free XE DC short-arc lamp, Newport). The incident light was filtered through a water filter (6 cm) and an OG530 cut-off filter (Newport) to remove the heat and the light below 523 nm, respectively. Decrease of DPBF in solution with irradiation time was monitored at 414 nm. All experiments were performed in triplicate, and the data presented herein represent the mean of the three experiments (estimated error: ±15%).

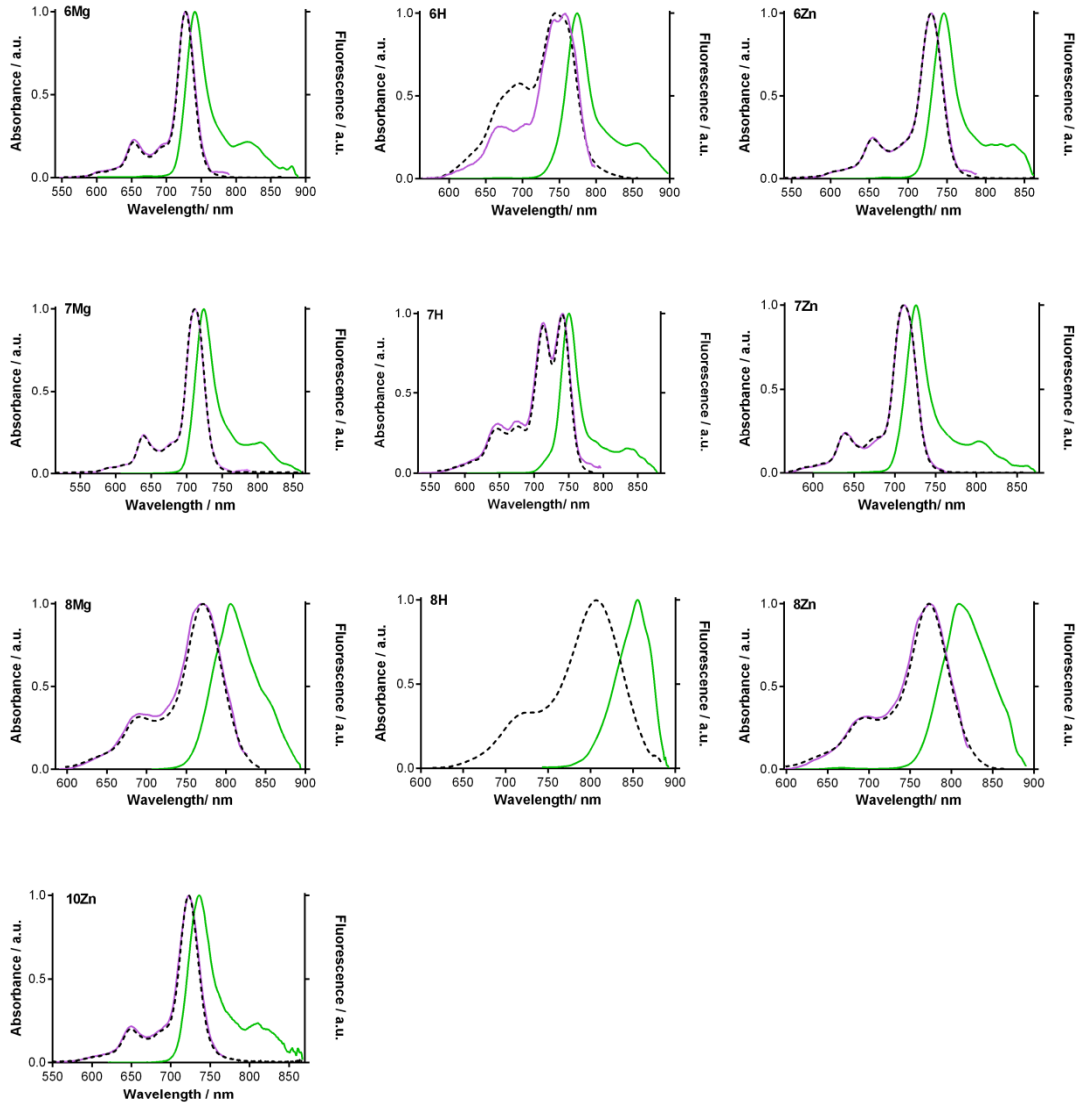

Figure S35. Absorption (black dashed), emission (green) and excitation (pink) spectra of **6M-8M** (M=Mg, 2H, Zn) in THF and **10Zn** in DMF. Absorption spectra of **6H** indicated aggregation. Fluorescence of **8H** was too weak to collect excitation spectra of sufficient quality. Emission spectra of compounds **8M** were influenced by fluorescence detector limit of the instrument (900 nm).

In vitro cytotoxicity assessments

Cell cultures

The HeLa cell line was obtained from the American Type Cell Culture Collection (ATCC, U.S.A.). Cells were cultured in Dulbecco's modified Eagle's medium (DMEM) without Phenol Red (Lonza, Belgium) supplemented with 10 % heat-inactivated fetal bovine serum (FBS, Lonza), 1 % penicillin/streptomycin solution (Lonza), 10 mM HEPES buffer (Sigma, Germany) and 4 mM L-glutamine (Lonza). The cells were cultured in 75 cm^2 tissue culture flasks (TPP, Switzerland) at 37 °C in a humidified atmosphere of 5% CO_2. Sub-confluent cells were subcultured every 3-4 days. For dark toxicity and photodynamic therapy experiments, cells were seeded in 96-well plates (TPP) at density of 7,500 cells per well (HeLa) 24 h prior an addition of the studied compound.

Uptake to the cells

To establish the time profile of intracellular accumulation of compound **10Zn**, HeLa cells were seeded in 6 cm petri dishes at density of 45,000 cells per dish. Cells had been left to attach for 24 h and then the medium was removed and 10 μM compound **10Zn** was added in 5 ml of cultivation medium in selected times prior harvesting (see Figure S36). After incubations, the cells were washed three times with 5 ml of phosphate buffered saline (PBS, Sigma) followed by addition of 5 ml of medium. Cells were scraped and transferred to 15 ml centrifugation tubes (TPP) and centrifuged 5 min at 70 × g. Supernatant was replaced with 2 ml of fresh medium, cell pellet was gently resuspended and centrifuged again. After the centrifugation, the medium was replaced with DMF (500 μL). Lysis of cells was performed overnight in -20°C. Trifluoracetic acid (10 μl of its 10% solution in DMF) was added and the fluorescence of **10Zn** (for spectrum see Figure S35) was measured (λ_{exc} = 354 nm and λ_{em} = 736 nm) using AMINCO-Bowman Series 2 luminescence spectrometer. Uptake experiments were performed in duplicate.

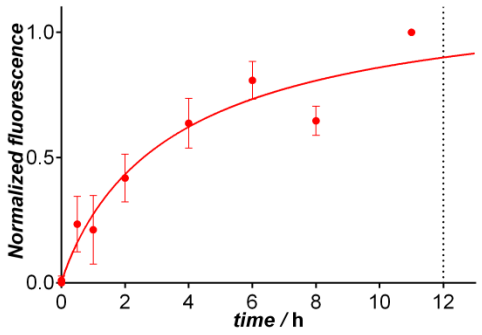

Figure S36. Uptake of compound **10Zn** by HeLa cells. Points represent mean of two independent experiments, curve is the best non-linear fit.

Subcellular localization.

Subcellular localization was performed by fluorescent microscopy method. Cells were seeded on glass-bottom 3 cm Petri dishes suitable for confocal microscopy (WillCo Wells B.V., Netherlands) at the concentration of 15 000 cells per dish. After 24 h medium was replaced with 10 μM solution of **10Zn** in fresh medium. Incubation time was set to 12 h. LysoTracker Blue DND-22 (2 μM, Molecular Probes) and MitoTracker Green FM (2 μM, Molecular Probes) were added for another 15 min to stain lysosomes and mitochondria, respectively. Cells were rinsed two times with pre-heated PBS (37°C) and 1 ml of medium was added. Photographs were obtained using Nikon Eclipse Ti (Nikon, Japan) fluorescence microscope equipped with CoolLED pE-300white fluorescence source (CoolLED Ltd., United Kingdom), cooled digital sCMOS camera Andor Zyla 5.5 (Andor Technology, United Kingdom) and NIS Elements AR 4.20 software (Laboratory Imaging, Czech Republic).

Dark toxicity experiments and photodynamic treatment.

The own toxicity of the **10Zn** without the presence of light (dark toxicity) was assayed at wide concentration range from 1 μM to 500 μM after 24 h incubations. Viabilities of HeLa cells were determined using neutral red (NR) uptake assay (Sigma) based on ability of living cells to incorporate NR in their intact lysosomes. Soluble NR was measured as its optical density at λ = 540 nm using Tecan Infinite 200M plate reader (Tecan, Austria). The viability of experimental groups was expressed as percentage of untreated controls (100%).

For photodynamic treatment experiments, HeLa cells were first loaded for 12 h with various concentrations (0.01 – 10 μM) of compound **10Zn**. After loading, the cells were washed with PBS and fresh medium was added. Irradiation of HeLa cells with light was performed using 450 W ozone-free Xe lamp (Newport) with intensity reduced to 400 W (λ > 570 nm, 12.4

mW/cm^2, 15 min, 11.2 J/cm^2), with long pass filter (Newport OG570) and water filter (8 cm) to eliminate undesirable wavelengths. After irradiation, the cells were incubated another 24 h before assaying their viability by NR as described before. At least five independent experiments, each in quadruplicate, were performed.

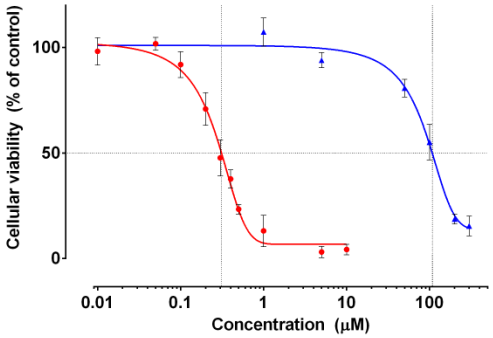

Figure S37. Phototoxicity (λ > 570 nm, 12.4 mW/cm^2, 15 min, 11.2 J/cm^2, red line) and dark toxicity (blue line) of **10Zn** on HeLa cells

References

1. K. V. Lipin, V. N. Maksimova, O. V. Ershov, A. V. Eremkin, Y. S. Kayukov and O. E. Nasakin, *Russ. J. Org. Chem.*, 2010, **46**, 617-618.
2. P. Zimcik, V. Novakova, K. Kopecky, M. Miletin, R. Z. Uslu Kobak, E. Svandrlikova, L. Váchová and K. Lang, *Inorg. Chem.*, 2012, **51**, 4215-4223.
3. J. R. Lakowicz, *Principles of fluorescence spectroscopy*, 3rd edn., Springer, New York, 2006.
4. V. Novakova, M. Miletin, T. Filandrová, J. Lenčo, A. Růžička and P. Zimcik, *J Org. Chem.*, 2014, **79**, 2082-2093..
5. L. Kaestner, M. Cesson, K. Kassab, T. Christensen, P. D. Edminson, M. J. Cook, I. Chambrier and G. Jori, *Photochem. Photobiol. Sci.*, 2003, **2**, 660-667.
6. U. Michelsen, H. Kliesch, G. Schnurpfeil, A. K. Sobbi and D. Wöhrle, *Photochem. Photobiol.*, 1996, **64**, 694-701.

1.4. **P4**

El-Betany A. M. M., VACHOVA L., Bezzu C. G., Pope S. J. A., McKeown N. B.: The synthesis and study of fluorescent PAMAM-based dendritic molecules. *Tetrahedron*, **2013**, 69, 8439-8445. IF_{2016} 2,651.

Podíl autorky: Studium fotofyzikálních parametrů a jejich stanovení při acidobazických titracích. Podíl na přípravě textu.

Tetrahedron 69 (2013) 8439–8445

Contents lists available at SciVerse ScienceDirect

Tetrahedron

journal homepage: www.elsevier.com/locate/tet

The synthesis and study of fluorescent PAMAM-based dendritic molecules

Alaa M.M. El-Betany [a,b], Lenka Vachova [a,c], C. Grazia Bezzu [a], Simon J.A. Pope [a], Neil B. McKeown [a,*]

[a] School of Chemistry, Cardiff University, PO Box 912, Cardiff CF10 3TB, UK
[b] Chemistry Department, Faculty of Science, Damietta University, New Damietta City 34517, Egypt
[c] Department of Pharmaceutical Chemistry and Drug Control, Faculty of Pharmacy in Hradec Kralove, Charles University in Prague, Heyrovskeho 1203, Hradec Kralove 50005, Czech Republic

ARTICLE INFO

Article history:
Received 26 April 2013
Received in revised form 27 June 2013
Accepted 15 July 2013
Available online 20 July 2013

Keywords:
PAMAM dendron
Water soluble fluorescent dendritic
Photoinduced electron transfer
Fluorescence lifetime
Fluorescent pH sensor

ABSTRACT

New water soluble and fluorescent PAMAM-based dendritic molecules based on the naphthalimide derivative 7*H*-benz[*de*]benzimidazo[2,1-*a*]isoquinoline-7-one as the fluorescent unit, have been prepared and their photophysical properties studied in aqueous solution over a wide pH range. The dendrons are all strongly fluorescent through an intramolecular charge transfer (ICT) excited state, but this can be modulated by photoinduced electron transfer (PeT) processes, which increases with higher PAMAM dendron generation.

1. Introduction

There is continuing interest in water-soluble fluorescent dendrimers for biological applications including visualization and diagnostic imaging.[1–6] Fluorescent labels are required to have high sensitivity, appropriate excitation and emission maxima, and specific functionality. Therefore, it is important to develop new fluorescent labels, which have high detection limits and appropriate fluorescent behaviour.[7] Self-quenching is a problem in aqueous media due to aggregation of the hydrophobic fluorophore, hence, it has been found beneficial to use bulky water-soluble dendritic structures to hinder self-association.[6] Fluorescent units can be incorporated within a dendrimer as peripheral groups, as branch points or as the core and it is clear that the resulting location of the fluorophore influences its properties. Importantly, the resulting position of the fluorescent unit has a major role in directing the method and complexity of the synthesis of the dendrimer.[6] The loading of fluorophores onto the periphery of dendrimers is still not trivial, with problems related to stoichiometric control of synthesis,[8,9] and intramolecular fluorescent quenching. These disadvantages may be avoided by loading the fluorophore as the core of a dendrimer or at the focal point of a dendritic molecule (dendron). The use of a single dendron substituent also allows the aromatic fluorophore to interact freely with biological systems (e.g., bind to DNA).

As well as being the first high-generation dendrimers and one of the most studied,[10] poly(amidoamine) (PAMAM) dendrimers are also considered one of the best potential drug delivery carriers due to their high biocompatibility. PAMAM dendrimers are very hydrophilic, can mimic globular proteins,[10] are readily transported across the epithelial barrier of the gut,[11–13] inhibit protein–protein binding,[14] and can be synthetically modified to possess fluorescent units at their core or peripheries. While in general PAMAM dendrimers are of biomedical interest, it is the anionic carboxylate-terminated PAMAM dendrimers, which are considered to be of greater potential as drug delivery vehicles because they have the important advantage of being non-cytotoxic in contrast to the cationic dendrimers,[11,15] whilst also being highly aqueous soluble and effective in transcellular transport and oral delivery applications.[15]

The objective of this work was the synthesis and study of the photophysical properties of novel PAMAM dendritic molecules that contain a single highly fluorescent unit at the focal point. Carboxylate-terminated PAMAM dendrons were selected to enhance solubility in water and, ultimately, biocompatibility.[16,17] Because of their strong fluorescence and good photostability, derivatives of 1,8-naphthalimide are used as fluorescent markers in biology,[18] light

* Corresponding author. Tel.: +44 (0)2920875851; fax: +44 (0)2920874030; e-mail address: mckeownnb@cardiff.ac.uk (N.B. McKeown).

0040-4020/$ – see front matter © 2013 Elsevier Ltd. All rights reserved.
http://dx.doi.org/10.1016/j.tet.2013.07.054

emitting diodes,[19 21] photoinduced electron transfer sensors,[22 26] fluorescent switches[27 29] and photo-chemotherapeutic inhibitors.[30 34] A number of 1,8-naphthalimide derivatives were screened for fluorescence and 7*H*-benz[*de*]benzimidazo[2,1-*a*]isoquinoline-7-one (BBIQ) selected for use as the fluorophore due to its strong fluorescence.[7,16,35 40]

2. Results and discussion

2.1. Synthesis

The precursor 3-bromo-7*H*-benz[*de*]benzimidazo[2,1-*a*]isoquinoline-7-one **1**, which was readily prepared from *o*-phenylenediamine and 4-bromo-1,8-naphthalenedicarboxylic anhydride using a literature procedure,[7,36] allows facile derivatisation of the BBIQ core by the replacement of the bromide via aromatic nucleophilic substitution. Hence, the introduction of the primary aliphatic amine functionality required for growth of the desired PAMAM dendrons was achieved by the reaction between **1** and ethylenediamine to give 3-(2-aminoethylamino)-7*H*-benz[*de*]benzimidazo[2,1-*a*]isoquinoline-7-one **2** (Scheme 2). Two different procedures were used (Methods A & B) both of which gave modest but adequate yields.

PAMAM synthesis, following a well-established method,[16,37] was instigated from **2** with exclusive Michael addition of methyl acrylate occurring at the aliphatic primary amine to yield **3**

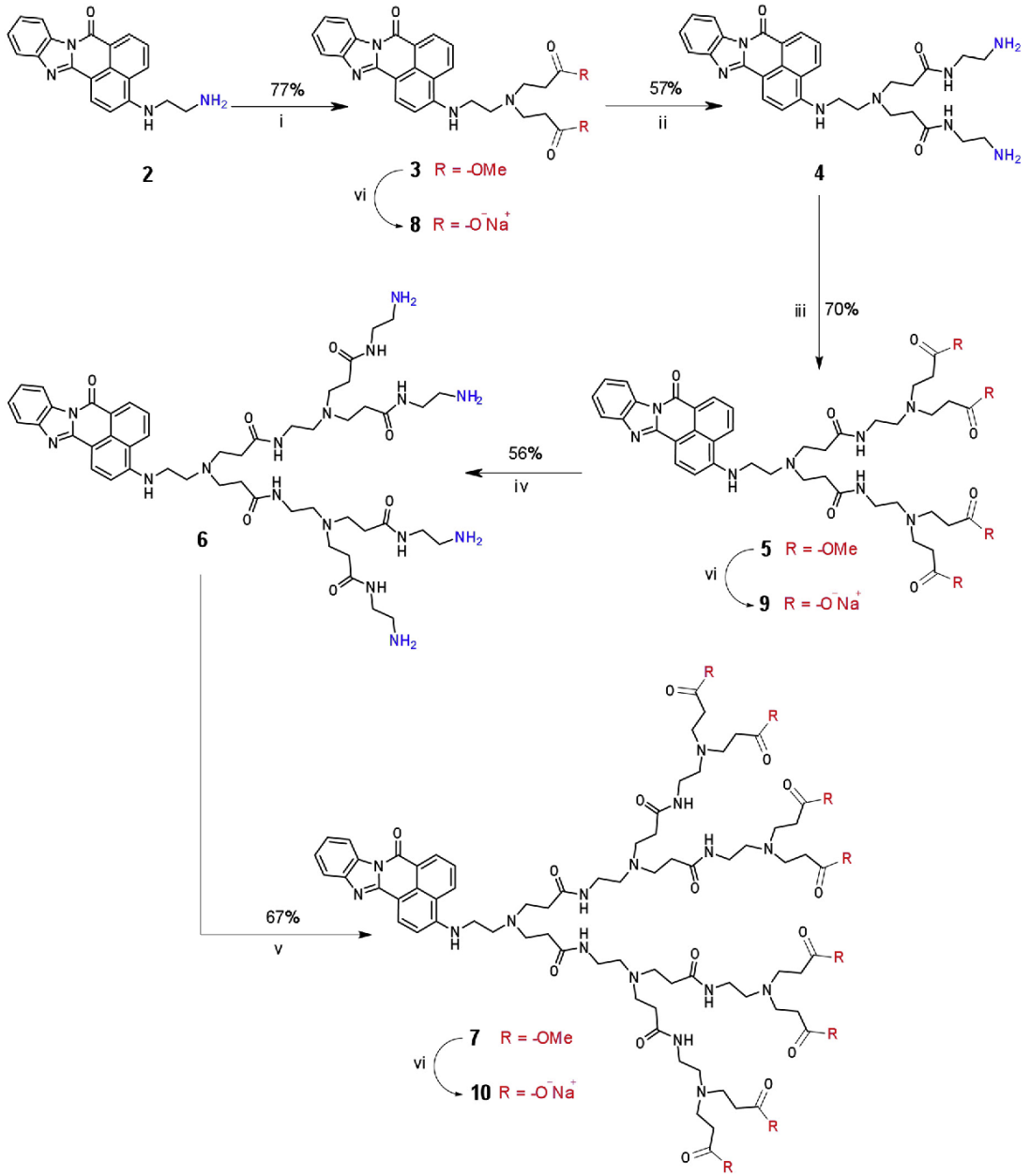

Scheme 1. Synthesis of **3**–**10**. Reagents and conditions: (i) Methyl acrylate, MeOH, reflux 6 h, stirring 16 h, rt; (ii) MeOH/DCM, EDA, stirring 2 days/N_2; (iii) Methyl acrylate, MeOH, reflux 24 h; (iv) MeOH/DCM, EDA, stirring 5 days/N_2; (v) Methyl acrylate, MeOH, reflux 2 days; (vi) Ethanolic NaOH, EtOH, (**8**) reflux 16 h; (**9**) and (**10**) stirring at rt for 24 h.

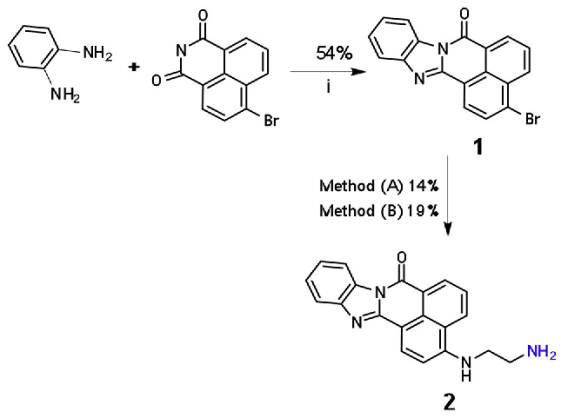

Scheme 2. Synthesis of **1** and **2**. Reagents and conditions: (i) AcOH, reflux 2 h; (A) MeCN, EDA, reflux 3 days; (B) EDA, heating 130 °C for 1 h.

(Scheme 1). Sequential amidations with ethylenediamine and Michael additions with methyl acrylate yielded dendritic molecules **4**–**7**. Alkaline hydrolysis of oligoesters **3**, **5** and **7**, by stirring with ethanolic NaOH at room temperature gave carboxylate terminated dendritic molecules **8**–**10**, respectively, in excellent yields (93–97%).

The dendritic molecules terminated with methyl esters were easily purified in good yield using column chromatography (eluent DCM/MeOH) (**3**=77%, **5**=70%, **7**=67%). The amine terminated dendritic molecules (**4**, **6**) proved more difficult to purify but were obtained sufficiently pure for further reaction by azeotropic removal of excess ethylenediamine (bp=118 °C) using a toluene/methanol mixture (9:1) followed by flash column chromatography using a mixture of DCM and MeOH/NH_4OH as eluent. The carboxylate terminated dendritic molecules **8**–**10** were purified by simple recrystallization from ethanol. The structures of **2**–**10** were verified by ^1H NMR, ^{13}C NMR and FTIR spectroscopy and electron ionization (EI) or matrix assisted laser desorption ionization (MALDI-TOF) mass spectrometry with all results agreeing with the proposed structures.[37]

2.2. Photophysical characterization

For compounds **2**–**10**, the λ_{max} from the absorption spectra together with the emission wavelength and lifetimes of the luminescence bands are presented in Table 1. The lowest energy absorption band (Fig. 1) associated with the chromophore is likely to have significant intramolecular charge transfer (ICT) character and are all in the range 500–511 nm.

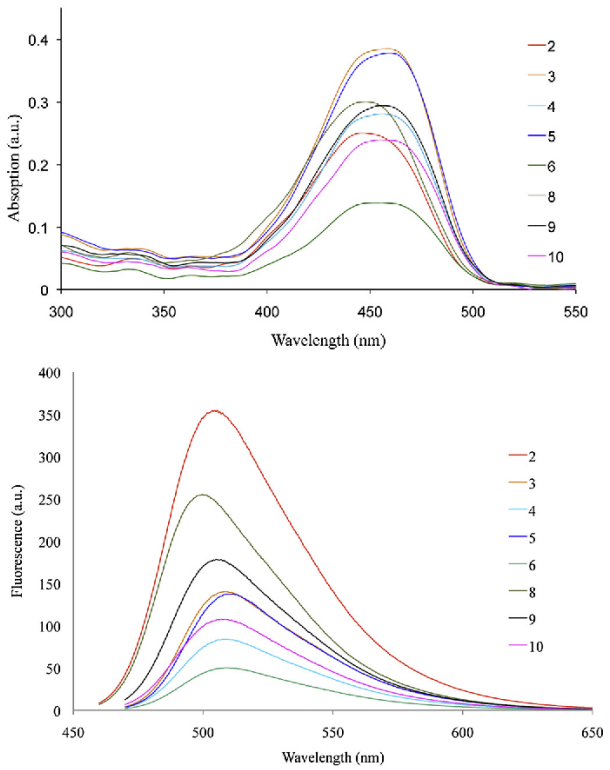

Fig. 1. UV/vis adsorption (top) and fluorescence spectra (bottom) of compounds **2**–**10** in methanol solution. See Table 1 for details.

The integrated emission intensities of compounds **2**–**10** are clearly influenced by the dendritic substituent at the C-3 position of the fluorophore. The emission lifetimes are all short (<10 ns) and characteristic of fluorescence in all cases. For the higher generation dendrimers the lifetime decay profiles do not fit satisfactorily to a single exponential decay and in these cases bi-exponential fits proved more appropriate (the relative weightings of each component are given in Table 1). The observation of dual component decay characteristics suggests that there are two distinct excited state environments for these higher generation species. Together with the observed trend in integrated intensity of fluorescence (**2**>>**3**~**4**>**5**>**6**>**10**), this effect is likely to be due to excited state quenching originating from photoinduced electron transfer (PeT) involving the multiple amine donors on the PAMAM dendrons,[38] with the tertiary amines being particularly efficient at PeT.[39–41]

Table 1
UV/vis and fluorescence data for selected compounds

Compound	Generation number	λ_{max} absorption[a]/nm	ε/M $^{-1}$ cm $^{-1}$	λ_{max} emission[b]/nm	τ/ns[c]
2	0	445	3.5×10^4	504	6.2
3	0.5	458	5.8×10^4	508	2.0
4	1	457	4.1×10^4	507	1.3
5	1.5	445	5.7×10^4	511	0.7, 2.7 (77%)[d]
6	2	450	2.3×10^4	509	1.1, 3.8 (58%)[d]
8	0.5	446	4.3×10^4	500	2.0, 5.3 (83%)[d]
9	1.5	455	4.3×10^4	506	1.4, 5.2 (73%)[d]
10	2.5	457	3.2×10^4	507	1.3, 4.8 (72%)[d]

[a] From MeOH solution.
[b] (**2**–**10**) excitation at 455 nm (MeOH).
[c] (**2**–**10**) excitation at 459 nm (MeOH).
[d] Relative weighting of longer lifetime component.

However, the retention of long lifetime components for **5**–**10** also suggests that a proportion of their excited states are relatively unperturbed and this may be due to conformational rigidity on the timescale of the lifetime experiments. Fluorescence intensity was also found to decrease in the carboxylate salts **8**>**9**>**10** due to the dendritic substituents (Fig. 1).[42] It was found that the emission intensity increased almost linearly with concentration for aqueous solutions of **8**, **9** and **10** indicating that there was no self-quenching due to aggregation over the concentration range $0.83-5.75\times10^{-4}$ mM L^{-1}.

The UV/vis absorption spectra of compounds **2**, **4** and **8** revealed similar pH dependence with a bathochromic shift of the main band below pH 5, presumably due to the protonation of the chromophore.[36] The pH dependence of the fluorescence spectra of the molecules **2**, **4** and **8** was also investigated over the pH range 1–13. For **2** the emission intensity is quenched at very low pH, but characterized by two maxima at 490 and 560 nm; increasing the pH 7–8 sees a single maximum intensity at 510 nm. The emission lifetimes at these pH values are relatively insensitive and all lie in the range 5.1–6.2 ns (Table 2). In contrast, **4** revealed two emission peaks at pH 1–4, an emission maximum intensity at pH 4, and a single emission peak at pH 6–12. The emission lifetimes at pH 1–4 were significantly extended (5.2–5.6 ns) and consistent with reduced quenching and suppression of PeT; at pH >6 the lifetime decays are dual component with very short (<0.5 ns) and short (<3 ns) contributions (Table 2), suggesting that excited state quenching is enhanced at such pH regimes and dependent upon conformational freedom. The behaviour of **8**, shown in Fig. 2, shows a maximum intensity of fluorescence at around pH=6–8 at 500 nm; at very low pH (<2) the emission is red-shifted to 560 and at very high pH emission is weak because the PeT is operative due to the lack of protonation of the amine groups within the dendritic substituent.

Table 2
Emission lifetimes (relative weightings in parentheses) of compounds **2**, **4** and **8** as a function of solution pH

Compound **2**		Compound **4**		Compound **8**	
pH	τ ns	pH	τns	pH	τ ns
1	5.29	1	5.17	1	4.68
3	5.39	2	5.39	2	4.74
5	5.68	4	5.60	3	5.11
7	6.24	6	1.03, 3.27 (69%)	4	6.32
8	6.20	8	0.45, 2.36 (80%)	5	6.24
10	5.15	10	0.20, 2.21 (82%)	6	6.35
12	3.50	12	0.38, 1.96 (82%)	8	6.30
				9	6.24
				10	6.31
				11	0.27, 5.09 (60%)

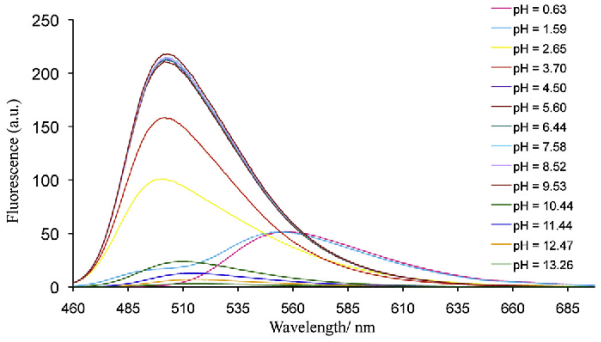

Fig. 2. Emission spectra for compound **8** obtained at pH 0.63–13.26.

3. Conclusions

A series of dendritic molecules that combine the highly fluorescent 7*H*-benz[*de*]benzimidazo[2,1-*a*]isoquinoline-7-one unit with small PAMAM side-groups were prepared. From a photophysical perspective, each of the compounds is visibly fluorescent in solution (including aqueous media) through an ICT excited state. The emission intensities and lifetimes are sensitive to the nature and generation of the dendritic architecture and this is ascribed to the well-understood PeT intramolecular quenching mechanism involving the amine groups. The pH dependence of the fluorescence behaviour is consistent with this mechanism. Lifetime measurements indicate that the PeT mechanism is likely to be conformationally dependent. Overall, the photophysical behaviour of these systems is roughly similar to that of the analogous 1,8-naphthalimide systems although the fluorescence for the later occurs at a significantly longer wavelength (~550 nm).[17]

4. Experimental

4.1. Photoluminescence measurements

Fluorescence spectra: Photophysical data were obtained on a JobinYvon–Horiba Fluorolog spectrometer fitted with a JY TBX picoseconds photodetection module as MeOH or aqueous solutions where appropriate. Emission spectra were uncorrected and excitation spectra were instrument corrected. The pulsed source was a Nano-LED configured for 372 nm output operating at 1 MHz. Luminescence lifetime profiles were obtained using the JobinYvon–Horiba FluoroHub single photon counting module and the data fits yielded the lifetime values using the provided DAS6 deconvolution software.

4.2. Materials and methods

Precursors were purchased from Sigma–Aldrich or Acros Organics/Fisher Scientific and were used without further purification. Anhydrous dichloromethane was obtained by distillation over calcium hydride under a nitrogen atmosphere. All reactions involving air/moisture sensitive reagents were performed in oven-dried glassware, under a nitrogen atmosphere. TLC analysis refers to analytical thin layer chromatography, using aluminium-backed plates coated with Merck Kieselgel 60 GF_{254}. Flash chromatography was performed on silica gel 60A (35–70 μ) chromatography grade (Fisher Scientific). Melting points were recorded using a Gallenkamp Melting Point Apparatus. Infrared spectra were recorded in the range 4000–600 cm^{-1} using a Perkin–Elmer 1600 series FTIR instrument either as a thin film or as a Nujol mull between sodium chloride plates. UV absorption spectra were recorded on a JASCO (V-570) UV/vis/NIR spectrophotometer. ^{1}H and ^{13}C NMR spectra were recorded in MeOD or $CDCl_3$ solution (as stated) using an Avance Bruker DPX 400 instrument (400 MHz) or an Avance Bruker DPX 500 (500 MHz). All chemical shifts (δ) are reported in parts per million with referenced to TMS (δ=0.0). Low-resolution mass spectrometric data were determined using a Fisons VG Platform II quadrupole instrument using electrospray (ES) ionization unless otherwise stated. High-resolution mass spectrometric data were obtained in electrospray (ES) mode on a Waters Q-TOF micromass spectrometer. Matrix Assisted Laser Desorption-time of flight Mass Spectrometry (MALDI-TOF) is available using a Waters Maldi Micro MX research grade instrument.

4.3. Synthetic details and characterization

*4.3.1. 3-Bromo-7H-benz[de]benzimidazo[2,1-a]isoquinoline-7-one (**1**).* The mixture of 4-bromo-1,8-naphthalic anhydride (0.277 g,

0.001 mol) and *o*-phenylenediamine (0.2 g, 0.002 mol) was dissolved in acetic acid (50 mL). The resulting solution was allowed to reflux for 2 h, the mixture was cooled to room temperature, and then poured into distilled water to precipitate the product as a bright yellow powder. Compound **1** (0.18 g, 54%) was obtained after twice recrystallized from toluene. R_f (20% MeOH/DCM) 0.86; mp: 253–254 °C (lit. mp: 253–254);[36] UV (λ_{max}, nm): 390 (MeOH, ε/L mol $^{-1}$ cm $^{-1}$ 1.2×10^4); IR (KBr, cm $^{-1}$): 1696 (C=O), 746 (C–Br); ^{1}H NMR (500 MHz, $CDCl_3$): δ 8.86 (dd, J=17.4, 7.3 Hz, 1H), 8.65 (dd, J=11.3, 8.2 Hz, 1H), 8.61–8.48 (m, 2H), 8.10 (dd, J=10.5, 7.9 Hz, 1H), 7.96–7.85 (m, 2H), 7.54–7.46 (m, 2H); ^{13}C NMR (125 MHz, $CDCl_3$): δ 193.3 (C=O), 144.0 (C), 143.4(C), 141.3 (CH), 138.4 (C), 133.7 (CH), 133.1 (CH), 131.4 (C), 131.2 (C), 130.5 (C), 130.2 (CH), 128.9 (CH), 128.6 (C), 127.5 (C–Br), 127.4 (CH), 123.2 (CH), 115.3 (CH); HRMS (EI$^+$): m/z=347.9909 (M^{79}Br$^+$, 100%), 349.9903 (M^{81}Br$^+$, 98%).

*4.3.2. 3-(2-Aminoethylamino)-7H-benz[de]benzimidazo[2,1-a]isoquinoline-7-one (**2**). Method A*: Compound **1** (0.6099 g, 1.747 mmol) and ethylenediamine (1.2 mL, 18.02 mmol) were stirred in refluxing MeCN (10 mL) for 3 days. The orange precipitate was collected by hot filtration and stirred in ether for 16 h, then filtered and dried. The orange solid was recrystallized from toluene to give (0.084 g, 14%) a pale orange powder **2** after flash column chromatography (DCM/MeOH; 10:0 to 8:2).

Method B: Compound **1** (0.6022 g, 0.002 mol) was suspended in ethylenediamine (6.68 mL, 0.1 mol) and the resulting suspension was heated to 130 °C for 1 h, the mixture was cooled to 95 °C and poured into distilled water at 90 °C. After stirring and cooling to room temperature, the deep red suspension was filtered and washed with water. The solid was dried and recrystallized from toluene twice to give (0.12 g, 19%) as deep red crystals **2** after flash column chromatography (DCM/MeOH; 10:0 to 8:2). R_f (20% MeOH/DCM) 0.26; mp: 212–213 °C; UV (λ_{max}, nm): 433 (MeOH, ε/L mol $^{-1}$ cm $^{-1}$ 3.5×10^4); IR (KBr, cm $^{-1}$): 3530 (–NH_2), 2900 (–CH_2–), 1677 (C=O); ^{1}H NMR (500 MHz, MeOD): δ 8.82 (d, J=7.3 Hz, 1H), 8.61 (dd, J=12.4, 7.9 Hz, 2H), 8.05 (d, J=8.4 Hz, 1H), 7.90 (d, J=6.3 Hz, 1H), 7.66 (t, J=7.9 Hz, 1H), 7.50–7.45 (m, 2H), 6.71 (d, J=8.5 Hz, 1H), 6.32 (s, 1H), 3.38 (dd, J=10.7, 5.1 Hz, 2H), 3.17 (t, J=5.7 Hz, 2H), 1.29 (s, 2H); ^{13}C NMR (125 MHz, MeOD): δ 142.5 (C), 141.4 (C), 141.1 (C), 135.2 (C), 133.7 (CH), 130.6 (C), 128.4 (C), 127.6 (CH), 124.5 (CH), 124.0 (CH), 123.9 (C), 123.1 (CH), 122.0 (CH), 121.8 (C), 116.1 (CH), 111.9 (CH), 45.7 (CH_2), 39.5 (CH_2); HRMS (ES$^+$): m/z=329.1401 (MH$^+$, 100%).

*4.3.3. General procedure for the synthesis of polyesters derivatives (**3**, **5**, **7**).* Methyl acrylate (75 equiv/NH_2 function) was added to a solution of conjugate with amine terminal groups and the mixture was heated to reflux. MeOH and the excess of methyl acrylate were eliminated to yield the polyester after chromatography using silica gel as substrate and a mixture of $CHCl_3$ and MeOH (10:0.1) as eluent.

*4.3.4. PAMAM dendron—G0.5 (**3**).* Methyl acrylate (6.75 mL, 0.075 mol) was added to a solution of **2** (0.328 g, 0.001 mol) in MeOH (40 mL) and the mixture was heated to reflux for 6 h, then stirred for 16 h at room temperature, filtered, washing with MeOH and dried. The orange solid was recrystallized from MeOH to give (0.084 g, 77%) a bright orange solid **3** after flash column chromatography (DCM/MeOH; 10:0 to 10:0.2). R_f (3% MeOH/DCM) 0.70; mp: 170–171 °C; UV (λ_{max}, nm): 445 (MeOH, ε/L mol $^{-1}$ cm $^{-1}$ 5.8×10^4); IR (KBr, cm $^{-1}$): 3413 (–NH), 3058 (Ar–H), 2950 (–CH_2–), 2848 (–OCH_3), 1734 (–$COOCH_3$), 1681 (N–C=O), 1581 (NH–C=O); ^{1}H NMR (400 MHz, $CDCl_3$): δ 8.55 (d, J=7.3 Hz, 1H), 8.47 (d, J=7.2 Hz, 1H), 8.24 (d, J=8.5 Hz, 1H), 7.94 (d, J=8.4 Hz, 1H), 7.74 (d, J=8.4 Hz, 1H), 7.38 (t, J=7.9 Hz, 1H), 7.34–7.30 (m, 2H), 6.29 (d, J=8.6 Hz, 1H), 6.08 (s, 1H), 3.40 (s, 6H), 3.08–3.01 (m, J=5.3 Hz, 2H), 2.62 (t, J=6.3 Hz, 4H), 2.56–2.49 (m, 2H), 2.30 (t, J=6.3 Hz, 4H); ^{13}C NMR (100 MHz, $CDCl_3$): δ 172.7 (COO), 160.5 (C), 150.6 (C), 149.8 (C), 143.7 (C), 134.9 (CH), 131.9 (C), 128.3 (C), 126.8 (CH), 124.9 (CH), 124.8 (CH), 124.5 (C), 120.5 (CH), 119.9 (CH), 119.3 (C), 115.9 (CH), 109.4 (CH), 104.3 (CH), 51.5 (Me), 51.4 (CH_2), 48.8 (CH_2), 40.1 (CH_2), 32.4 (CH_2); LRMS (ES$^+$): m/z=501.21 (MH$^+$, 100%), 502.22 (33%), 503.22 (6%); HRMS calcd for ($C_{28}H_{28}N_4O_5$): 500.2060, found 500.2139 (M$^+$, 100%).

*4.3.5. First generation PAMAM dendron (**4**).* A solution of **3** (0.5 g, 0.001 mol) in (MeOH/DCM; 5:15 mL) was added dropwise over 30 min to a cooled (0 °C) solution of ethylenediamine (13.38 mL, 0.2 mol) (100 equiv/COOMe) in MeOH (30 mL) and a small amount of DCM was added until the solution cleared. The reaction was stirred for 2 days under a nitrogen at room temperature. The bulk of the solvent and excess ethylenediamine were removed via rotary evaporation. Final traces of excess ethylenediamine were removed azeotropically using a mixture of toluene and MeOH (9:1) (this was repeated several times until all traces of ethylenediamine had been removed). The product was dried thoroughly under high vacuum (1 mmHg) then was purified by flash column chromatography (DCM/MeOH/NH4OH; 9:1:0.2) to obtain (0.32 g, 57%) of compound **4** as a pink oil. R_f (8:2:0.4 MeOH/DCM/NH_4OH) 0.32; UV (λ_{max}, nm): 445 (MeOH, ε/L mol $^{-1}$ cm $^{-1}$ 4.1×10^4); IR (Neat, cm $^{-1}$): 3284 (–NH_2), 3075 (Ar–H), 2942 (–CH_2–), 1675 (N–C=O), 1572 (NH–C=O); ^{1}H NMR (500 MHz, MeOD): δ 8.08 (d, J=7.8 Hz, 1H), 7.99 (d, J=7.3 Hz, 1H), 7.82 (d, J=8.3 Hz, 1H), 7.72 (d, J=8.5 Hz, 1H), 7.53 (d, J=7.7 Hz, 1H), 7.30 (dd, J=11.0, 4.1 Hz, 1H), 7.24 (dd, J=11.0, 4.1 Hz, 1H), 7.13 (t, J=7.8 Hz, 1H), 6.07 (d, J=8.8 Hz, 1H), 3.34–3.30 (m, 2H), 3.28 (t, J=6.1 Hz, 4H), 3.08 (s, 2H), 2.81–2.73 (m, 6H), 2.70 (t, J=6.2 Hz, 2H), 2.46 (t, J=6.7 Hz, 4H); ^{13}C NMR (125 MHz, MeOD): δ 173.6 (CONH), 159.5 (C), 150.9 (C), 149.0 (C), 142.5 (C), 134.4 (CH), 131.1 (C), 127.6 (C), 126.3 (CH), 125.1 (CH), 124.6 (CH), 123.8 (C), 123.7 (CH), 119.8 (CH), 118.2 (C), 115.4 (CH), 107.6 (CH), 103.6 (CH), 49.3 (CH_2), 48.5 (CH_2), 43.3 (CH_2), 41.6 (CH_2), 40.6 (CH_2), 33.3 (CH_2); HRMS calcd for ($C_{30}H_{36}N_8O_3$): 556.2983, found 556.2977 (M$^+$, 100%).

*4.3.6. PAMAM dendron—G1.5 [**5**].* Methyl acrylate (13.5 mL, 0.15 mol) was added to a solution of **4** (0.556 g, 0.001 mol) in MeOH (30 mL) and the mixture was heated to reflux for 24 h, then stirred for 16 h at room temperature. MeOH and excess of methyl acrylate were eliminated by heating under reduced pressure to yield the **5** as a deep orange oil (0.63 g, 70%) after purification by flash column chromatography (DCM/MeOH; 10:0–10:0.3). R_f (3% MeOH/DCM) 0.34; UV (λ_{max}, nm): 445 (MeOH, ε/L mol $^{-1}$ cm $^{-1}$ 5.7×10^4); IR (KBr, cm $^{-1}$): 3306 (–NH), 3039 (Ar–H), 2918 (–CH_2–), 2851 (–OCH_3), 1729 (–$COOCH_3$), 1674 (N–C=O), 1589 (NH–C=O); ^{1}H NMR (400 MHz, MeOD): δ 8.16 (d, J=7.5 Hz, 1H), 8.13 (d, J=7.5 Hz, 1H), 7.93 (d, J=0.54 Hz, 1H), 7.86 (d, J=8.5 Hz, 1H), 7.49 (d, J=8.5 Hz, 1H), 7.26–7.16 (m, 3H), 6.30 (d, J=8.8 Hz, 1H), 3.40 (s, 12H), 3.03 (t, J=6.1 Hz, 2H), 2.98 (t, J=6.4 Hz, 4H), 2.67 (t, J=6.6 Hz, 4H), 2.57 (t, J=5.7 Hz, 2H), 2.43 (t, J=6.7 Hz, 8H), 2.27–2.19 (m, 8H), 2.14 (t, J=6.6 Hz, 8H); ^{13}C NMR (100 MHz, MeOD): δ 173.2 (CONH), 173.1 (COO), 159.9 (C), 151.3 (C), 149.4 (C), 142.7 (C), 134.8 (CH), 131.3 (C), 128.0 (C), 126.6 (CH), 125.6 (CH), 124.8 (CH), 124.0 (C), 120.2 (CH), 118.6 (CH), 118.3 (C), 115.5 (CH), 107.9 (CH), 104.0 (CH), 52.2 (CH_2), 51.0 (CH_2), 50.7 (Me), 49.3 (CH_2), 48.9 (CH_2), 40.9 (CH_2), 37.0 (CH_2), 33.3 (CH_2), 32.0 (CH_2); HRMS (EI$^+$) calcd for ($C_{46}H_{60}N_8O_{11}$): 900.4454, found 900.4453 (M$^+$, 100%).

*4.3.7. Second generation PAMAM dendron (**6**).* A solution of **5** (0.9 g, 0.001 mol) in MeOH (30 mL) was added dropwise over 30 min to a cooled (0 °C) solution of ethylenediamine (26.76 mL, 0.4 mol) (100 equiv/COOMe) in MeOH (70 mL). The reaction was stirred for 5 days under nitrogen at room temperature. The bulk of the solvent

and excess ethylenediamine were removed via rotary evaporator. Final traces of excess ethylenediame were removed azeotropically using a mixture of toluene and MeOH (9:1) (this was repeated several times until all traces of ethylenediamine had been removed). The product was dried thoroughly under high vacuum (1 mmHg) then was purified by flash column chromatography (DCM/MeOH/NH_4OH; 9:1:0.2) to obtain (0.57 g, 56%) of polyamine **6** as a red oil. R_f (8:2:0.4 MeOH/DCM/NH_4OH) 0.08; UV (λ_{max}, nm): 433 (MeOH, ε/L mol $^{-1}$ cm $^{-1}$ 2.3×10^4); IR (Neat, cm $^{-1}$): 3262 (−NH_2), 3075 (Ar−H), 2929 (−CH_2−), 1675 (N−C=O), 1557 (NH−C=O); ^{1}H NMR (500 MHz, MeOD): δ 8.22 (d, J=6.7 Hz, 1H), 8.12 (d, J=6.6 Hz, 1H), 7.92 (d, J=7.6 Hz, 1H), 7.84 (d, J=7.0 Hz, 1H), 7.60 (d, J=7.0 Hz, 1H), 7.37–7.32 (m, 1H), 7.32–7.28 (m, 1H), 7.23–7.17 (m, 1H), 6.13 (d, J=7.1 Hz, 1H), 3.27–3.19 (m, J=5.9 Hz, 12H), 3.13–3.03 (m, 2H), 2.81 (t, J=29.7 Hz, 4H), 2.71 (t, J=6.2 Hz, 18H), 2.53–2.46 (m, 4H), 2.44–2.38 (m, 4H), 2.32–2.24 (m, 8H); ^{13}C NMR (125 MHz, MeOD): δ 173.5 (CONH), 173.0 (CONH), 164.4 (C), 159.6 (C), 151.1 (C), 149.2 (C), 142.8 (CH), 134.6 (C), 131.3 (C), 127.8 (CH), 126.5 (CH), 126.4 (CH), 124.7 (C), 124.0 (CH), 120.0 (CH), 118.4 (C), 115.5 (CH), 107.8 (CH), 103.8 (CH), 52.1 (CH_2), 49.7 (CH_2), 49.4 (CH_2), 48.6 (CH_2), 43.6 (CH_2), 41.7 (CH_2), 40.8 (CH_2), 37.3 (CH_2), 33.4 (CH_2); MALDI-TOF [LD$^+$] calcd for ($C_{50}H_{76}N_{16}O_7$): 1013.6170, found 1013.674 (M$^+$, 100%).

*4.3.8. PAMAM dendron—G2.5 (**7**).* Methyl acrylate (27 mL, 0.30 mol) was added to a solution of **6** (1.01 g, 0.001 mol) in MeOH (30 mL) and the mixture was heated to reflux for 2 days. MeOH and excess of methyl acrylate were eliminated by heating under reduced pressure to yield the **7** as a deep orange oil (1.3 g, 76%) after flash column chromatography (DCM/MeOH; 10:0 to 10:0.3). R_f (3% MeOH/DCM) 0.04; UV (λ_{max}, nm): 445 (MeOH, ε/L mol $^{-1}$ cm $^{-1}$ 1.6×10^4); IR (KBr, cm $^{-1}$): 3422 (−NH), 3043 (Ar−H), 2924 (−CH_2−), 2850 (−OCH_3), 1736 (−$COOCH_3$), 1681 (N−C=O), 1581 (NH−C=O); ^{1}H NMR (400 MHz, MeOD): δ 8.46 (d, J=7.3 Hz, 1H), 8.41 (d, J=7.2 Hz, 1H), 8.23 (dd, J=13.7, 8.5 Hz, 2H), 7.73 (d, J=7.3 Hz, 1H), 7.53–7.37 (m, 3H), 6.51 (d, J=8.8 Hz, 1H), 3.62 (s, 24H), 3.27–3.22 (m, 4H), 3.22–3.18 (m, 8H), 2.93–2.87 (m, 4H), 2.86–2.81 (m, 2H), 2.74 (t, J=6.8 Hz, 8H), 2.69 (t, J=6.6 Hz, 16H), 2.56–2.51 (m, 4H), 2.51–2.43 (m, 14H), 2.39 (t, J=6.6 Hz, 16H), 2.31 (t, J=6.8 Hz, 8H); ^{13}C NMR (100 MHz, MeOD): δ 173.2 (CONH), 173.1 (CONH), 173.0 (COO), 160.0 (C), 151.4 (C), 149.5 (C), 142.8 (C), 135.0 (CH), 131.4 (C), 128.3 (C), 126.8 (CH), 125.8 (CH), 124.9 (CH), 124.4 (C), 124.2(CH), 120.4 (CH), 118.9 (C), 115.6 (CH), 108.1 (CH), 104.2 (CH), 52.3 (CH_2), 52.0 (CH_2), 51.1 (Me), 50.8 (CH_2), 49.5 (CH_2), 49.0 (CH_2), 40.6 (CH_2), 37.2 (CH_2), 37.0 (CH_2), 33.4 (CH_2), 33.2 (CH_2), 32.1 (CH_2), 29.5 (CH_2); MALDI-TOF [LD$^+$] calcd for ($C_{82}H_{124}N_{16}O_{23}$): 1701.9554, found 1701.9690 (M$^+$, 100%).

*4.3.9. PAMAM dendron—G0.5 salt (**8**).* To NaOH (0.5 g, 12.5 mmol), dissolved in hot EtOH (40 mL), was added a solution of the **3** (1.2 g, 2.4 mmol) in EtOH (10 mL). The mixture was heated to reflux for 16 h. After cooling, the precipitate was collected by filtration and recrystallized from wet EtOH to yield **8** as a pale yellow solid (0.92 g, 95%). R_f (40% MeOH/H_2O) 0.66; mp>300 °C decomposed at 315 °C (TGA); UV (λ_{max}, nm): 445 (MeOH, ε/L mol $^{-1}$ cm $^{-1}$ 4.3×10^4); IR (KBr, cm $^{-1}$): 3380 (−NH), 3067 (Ar−H), 2956 (−CH_2−), 1666 (−COONa), 1681 (N−C=O), 1571 (NH−C=O); ^{1}H NMR (400 MHz, MeOD): δ 8.47 (dd, J=7.3, 0.7 Hz, 1H), 8.38 (d, J=7.3 Hz, 1H), 8.33 (d, J=8.7 Hz, 1H), 8.28 (d, J=8.6 Hz, 1H), 7.69 (d, J=7.7 Hz, 1H), 7.56 (dd, J=8.2, 7.6 Hz, 1H), 7.45–7.35 (m, 2H), 6.60 (d, J=8.8 Hz, 1H), 3.44 (t, J=6.4 Hz, 2H), 2.98–2.92 (m, 4H), 2.89 (t, J=6.5 Hz, 2H), 2.46–2.40 (m, 4H); ^{13}C NMR (100 MHz, MeOD): δ 179.9 (COO), 160.3 (C), 151.9 (C), 149.5 (C), 142.6 (C), 135.2 (CH), 131.3 (C), 128.3 (C), 126.8 (CH), 126.1 (CH), 124.8 (CH), 124.3 (C), 124.0 (CH), 120.5 (CH), 118.5 (C), 118.2 (CH), 115.5 (CH), 107.5 (CH), 50.7 (CH_2), 50.4 (CH_2), 40.5 (CH_2), 35.1 (CH_2); LRMS (ES$^+$): m/z=473.18 (MH$^+$, 100%); HRMS calcd for ($C_{26}H_{24}N_4O_5$): 472.1872, found 473.1840 (MH$^+$, 100%).

*4.3.10. PAMAM dendron—G1.5 salt (**9**).* To NaOH (1.0 g, 25 mmol), dissolved in absolute EtOH (100 mL), was added a solution of **5** (2.23 g, 2.4 mmol) in EtOH (10 mL). The mixture was stirred for 24 h at room temperature, and the precipitate was collected by filtration and recrystallized from wet EtOH to yield **9** as a deep orange solid (2.17 g, 97%). R_f (40% MeOH/H_2O) 0.46; mp: 283 °C; UV (λ_{max}, nm): 445 (MeOH, ε/L mol $^{-1}$ cm $^{-1}$ 4.3×10^4); IR (KBr, cm $^{-1}$): 3362 (−NH−), 3079 (Ar−H), 2968 (−CH_2−), 1655 (−COONa), 1681 (N−C=O), 1571 (NH−C=O); ^{1}H NMR (400 MHz, MeOD): δ 8.48 (d, J=7.3 Hz, 1H), 8.41 (d, J=7.2 Hz, 1H), 8.29 (d, J=3.5 Hz, 1H), 8.26 (d, J=8.7 Hz, 1H), 7.71 (d, J=6.8 Hz, 1H), 7.59–7.48 (m, 1H), 7.48–7.33 (m, 2H), 6.56 (d, J=8.8 Hz, 1H), 3.49–3.36 (m, 2H), 3.36–3.29 (m, 4H), 3.03–2.91 (m, 4H), 2.89–2.78 (m, 8H), 2.62 (t, J=5.9 Hz, 4H), 2.51 (t, J=6.1 Hz, 4H), 2.43–2.23 (m, 10H); ^{13}C NMR (100 MHz, MeOD): δ 181.4 (COO), 174.7 (CONH), 162.7 (C), 153.2 (C), 150.9 (C), 144.1 (C), 142.3 (CH), 137.6 (C), 132.7 (C), 129.7 (CH), 127.3 (CH), 126.3 (CH), 125.7 (C), 123.4 (CH), 120.1 (CH), 119.7 (C), 117.0 (CH), 108.9 (CH), 105.5 (CH), 58.3 (CH_2), 53.3 (CH_2), 52.4 (CH_2), 50.8 (CH_2), 41.6 (CH_2), 38.5 (CH_2), 36.4 (CH_2), 34.6 (CH_2); MALDI-TOF [LD$^+$] calcd for ($C_{42}H_{52}N_8O_{11}$): 845.3756, found 845.2874 (M$^+$, 100%).

*4.3.11. PAMAM dendron—G2.5 salt (**10**).* To NaOH (3.0 g, 75 mmol), dissolved in absolute EtOH (150 mL), was added a solution of **7** (4.23 g, 2.4 mmol) in EtOH (10 mL). The mixture was stirred for 24 h at room temperature and the precipitate was collected by filtration and was recrystallized from EtOH to yield **10** as a deep orange solid (3.9 g, 93%). R_f (40% MeOH/H_2O) 0.30; mp: 269 °C; UV (λ_{max}, nm): 445 (MeOH, ε/L mol $^{-1}$ cm $^{-1}$ 3.2×10^4); IR (KBr, cm $^{-1}$): 3412 (−NH−), 3091 (Ar−H), 2956 (−CH_2−), 1655 (−COONa), 1681 (N−C=O), 1571 (NH−C=O); ^{1}H NMR (500 MHz, MeOD): δ 8.52 (d, J=7.0 Hz, 1H), 8.44 (d, J=7.5 Hz, 1H), 8.36–8.31 (m, 2H), 7.72 (d, J=7.4 Hz, 1H), 7.59–7.53 (m, 1H), 7.45–7.40 (m, 2H), 6.60 (d, J=8.7 Hz, 1H), 3.30–3.25 (m, 14H), 2.83–2.77 (m, 28H), 2.58–2.53 (m, 14H), 2.34–2.30 (m, 28H); ^{13}C NMR (125 MHz, MeOD): δ 181.4 (COO), 174.7 (CONH), 174.6 (CONH), 161.9 (C), 153.4 (C), 151.1 (C), 144.3 (C), 142.5 (CH), 136.9 (C), 132.9 (C), 128.7 (CH), 127.6 (CH), 126.4 (CH), 125.6 (C), 122.2 (CH), 120.4 (CH), 119.9 (C), 117.0 (CH), 109.4 (CH), 105.8 (CH), 58.3 (CH_2), 53.3 (CH_2), 52.0 (CH_2), 50.9 (CH_2), 42.2 (CH_2), 38.5 (CH_2), 38.4 (CH_2), 36.5 (CH_2), 34.8 (CH_2), 34.5 (CH_2); MALDI-TOF [LD$^+$] calcd for ($C_{74}H_{108}N_{16}O_{23}$): 1588.7773, found 1588.27 (M$^+$, 100%).

Acknowledgements

The authors would like to acknowledge the EPSRC Mass Spectrometry Facility (Swansea University) and the Egyptian Cultural Affairs & Missions Sector (ECAMS) and Cardiff University for financial support.

Supplementary data

These data include the UV/vis adsorption spectra at different pH of compound **9** and **10**; corrected excitation spectra (λ_{em}=500 nm) for the compounds **1**–**10** obtained in MeOH and the MALDI-MS spectrum for compound **7**. Supplementary data related to this article can be found at http://dx.doi.org/10.1016/j.tet.2013.07.054.

References and notes

1. Tomalia, D. A.; Frechet, J. M. J. *J. Polym. Sci., A: Polym. Chem.* **2002**, *40*, 2719.
2. Lee, C. C.; MacKay, J. A.; Frechet, J. M. J.; Szoka, F. C. *Nat. Biotechnol.* **2005**, *23*, 1517.
3. Tekade, R. K.; Kumar, P. V.; Jain, N. K. *Chem. Rev.* **2009**, *109*, 49.
4. Tomalia, D. A.; Naylor, A. M.; Goddard, W. A. *Angew. Chem., Int. Ed. Engl.* **1990**, *29*, 138.

5. Bouit, P.-A.; Westlund, R.; Feneyrou, P.; Maury, O.; Malkoch, M.; Malmstrom, E.; Andraud, C. *New J. Chem.* **2009**, *33*, 964.
6. Caminade, A.-M.; Hameau, A.; Majoral, J.-P. *Chem.—Eur. J.* **2009**, *15*, 9270.
7. Nakaya, K.; Tanaka, T.; Shirataki, Y.; Shiozaki, H.; Funabiki, K.; Shibata, K.; Matsui, M. *Bull. Chem. Soc. Jpn.* **2001**, *74*, 173.
8. Hayek, A.; Ercelen, S.; Zhang, X.; Bolze, F.; Nicoud, J.-F.; Schaub, E.; Baldeck, P. L.; Mely, Y. *Bioconjugate Chem.* **2007**, *18*, 844.
9. Talanov, V. S.; Regino, C. A. S.; Kobayashi, H.; Bernardo, M.; Choyke, P. L.; Brechbiel, M. W. *Nano Lett.* **2006**, *6*, 1459.
10. Esfand, R.; Tomalia, D. A. *Drug Discovery Today* **2001**, *6*, 427.
11. Wiwattanapatapee, R.; Carreno-Gomez, B.; Malik, N.; Duncan, R. *Pharm. Res.* **2000**, *17*, 991.
12. El-Sayed, M.; Ginski, M.; Rhodes, C.; Ghandehari, H. *J. Controlled Release* **2002**, *81*, 355.
13. El-Sayed, M.; Ginski, M.; Rhodes, C. A.; Ghandehari, H. *J. Bioact. Compat. Polym.* **2003**, *18*, 7.
14. Chiba, F.; Hu, T. C.; Twyman, L. J.; Wagstaff, M. *Macromol. Symp.* **2010**, *287*, 37.
15. Malik, N.; Wiwattanapatapee, R.; Klopsch, R.; Lorenz, K.; Frey, H.; Weener, J. W.; Meijer, E. W.; Paulus, W.; Duncan, R. *J. Controlled Release* **2000**, *65*, 133.
16. Brana, M. F.; Dominguez, G.; Saez, B.; Romerdahl, C.; Robinson, S.; Barlozzari, T. *Eur. J. Med. Chem.* **2002**, *37*, 541.
17. Bojinov, V. B.; Georgiev, N. I.; Nikolov, P. S. *J. Photochem. Photobiol., A* **2008**, *197*, 281.
18. Stewart, W. W. *J. Am. Chem. Soc.* **1981**, *103*, 7615.
19. Bouche, C. M.; Berdague, P.; Facoetti, H.; Robin, P.; Le Barny, P.; Schott, M. *Synth. Met.* **1996**, *81*, 191.
20. Morgado, J.; Gruner, J.; Walcott, S. P.; Yong, T. M.; Cervini, R.; Moratti, S. C.; Holmes, A. B.; Friend, R. H. *Synth. Met.* **1998**, *95*, 113.
21. Zhu, W.; Hu, C.; Chen, K.; Tian, H. *Synth. Met.* **1998**, *96*, 151.
22. Tian, H.; Gan, J.; Chen, K.; He, J.; Song, Q. L.; Hou, X. Y. *J. Mater. Chem.* **2002**, *12*, 1262.
23. Grabchev, I.; Chovelon, J. M.; Qian, X. *J. Photochem. Photobiol., A* **2003**, *158*, 37.
24. Grabchev, I.; Chovelon, J.-M.; Qian, X. *New J. Chem.* **2003**, *27*, 337.
25. Grabchev, I.; Qian, X.; Xiao, Y.; Zhang, R. *New J. Chem.* **2002**, *26*, 920.
26. Tian, H.; Xu, T.; Zhao, Y.; Chen, K. *J. Chem. Soc., Perkin Trans. 2: Phys. Org. Chem.* **1999**, 545.
27. Gunnlaugsson, T.; McCoy, C. P.; Morrow, R. J.; Phelan, C.; Stomeo, F. *ARKIVOC* **2003**, 216.
28. Poteau, X.; Brown, A. I.; Brown, R. G.; Holmes, C.; Matthew, D. *Dyes Pigm.* **2000**, *47*, 91.
29. Jia, L.; Zhang, Y.; Guo, X.; Qian, X. *Tetrahedron Lett.* **2004**, *45*, 3969.
30. Chanh, T. C.; Lewis, D. E.; Judy, M. M.; Sogandares-Bernal, F.; Michalek, G. R.; Utecht, R. E.; Skiles, H.; Chang, S.-C.; Matthews, J. L. *Antiviral Res.* **1994**, *25*, 133.
31. Chang, S. C.; Archer, B. J.; Utecht, R. E.; Lewis, D. E.; Judy, M. M.; Matthews, J. L. *Bioorg. Med. Chem. Lett.* **1993**, *3*, 555.
32. Chang, S.-C.; Utecht, R. E.; Lewis, D. E. *Dyes Pigm.* **1999**, *43*, 83.
33. Lewis, D. E.; Utecht, R. E.; Judy, M. M.; Matthews, J. L. U.S. Patent 5,235,045, 1993.
34. Baughman, R. G.; Chang, S. C.; Utecht, R. E.; Lewis, D. E. *Acta Crystallogr., Sect. C: Cryst. Struct. Commun.* **1995**, *C51*, 1189.
35. Tao, Z.-F.; Qian, X. *Dyes Pigm.* **1999**, *43*, 139.
36. Podsiadły, R.; Kolińska, J.; Sokołowska, J. *Color. Technol.* **2008**, *124*, 79.
37. King, A. S.; Martin, I. K.; Twyman, L. J. *Polym. Int.* **2006**, *55*, 798.
38. Georgiev, N. I.; Bojinov, V. B.; Nikolov, P. S. *Dyes Pigm.* **2009**, *81*, 18.
39. Bissell, R. A.; Prasanna de Silva, A.; Gunaratne, H. Q. N.; Lynch, P. L. M.; Maguire, G. E. M.; Sandanayake, K. R. A. S. *Chem. Soc. Rev.* **1992**, *21*, 187.
40. Bissell, R. A.; Prasanna de Silva, A.; Gunaratne, H. Q. N.; Lynch, P. L. M.; Maguire, G. E. M.; McCoy, C. P.; Sandanayake, K. R. A. S. *Top. Curr. Chem.* **1993**, *168*, 223.
41. de Silva, A. P.; Gunaratne, H. Q. N.; Gunnlaugsson, T.; Huxley, A. J. M.; McCoy, C. P.; Rademacher, J. T.; Rice, T. E. *Chem. Rev.* **1997**, *97*, 1515.
42. Adronov, A.; Frechet, J. M. J. *Chem. Commun.* **2000**, 1701.

The synthesis and study of fluorescent PAMAM-based dendritic molecules

Alaa M. M. El-Betany[a,b], Lenka Vachova[a,c], C. Grazia Bezzu[a], Simon J.A. Pope[a] and Neil B. McKeown*[a]

[a]*School of Chemistry, Cardiff University, PO Box 912, Cardiff, CF10 3TB, UK.*

[b]*Chemistry Department, Faculty of Science, Damietta University, New Damietta City, 34517, Egypt..*

[c]*Department of Pharmaceutical Chemistry and Drug Control, Faculty of Pharmacy in Hradec Kralove, Charles University in Prague, Heyrovskeho 1203, Hradec Kralove, 50005, Czech Republic.*

Supplementary information

Contents:

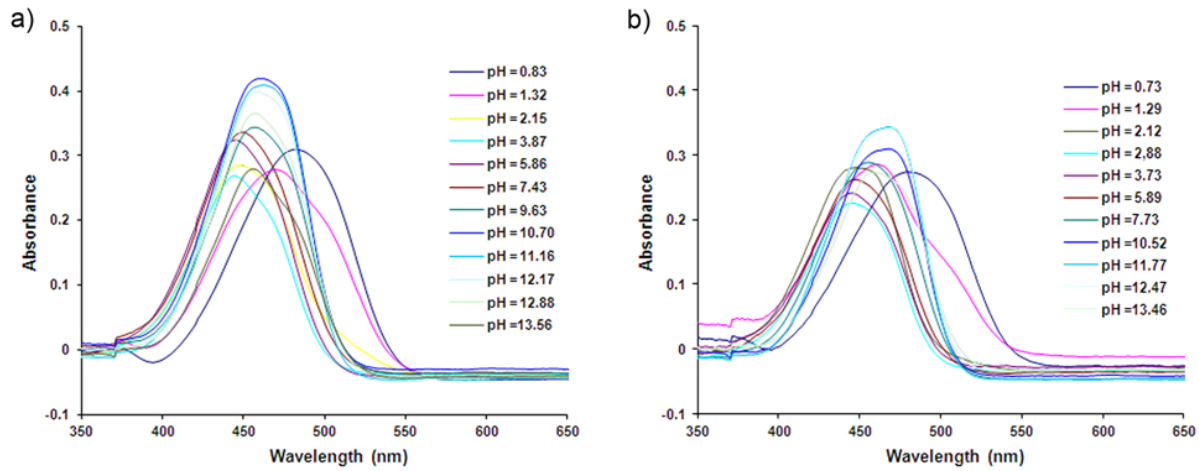

SI Fig. 1. The UV-Vis adsorption spectra at different pH of a) compound **9**; b) compound **10**.

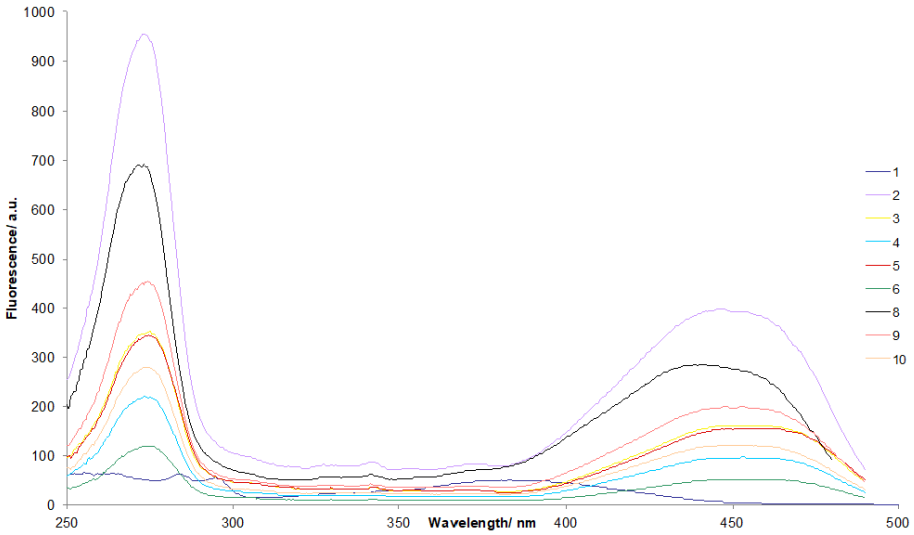

SI Fig. 2. The corrected excitation spectra (λ_{em} = 500 nm) for the compounds obtained in MeOH.

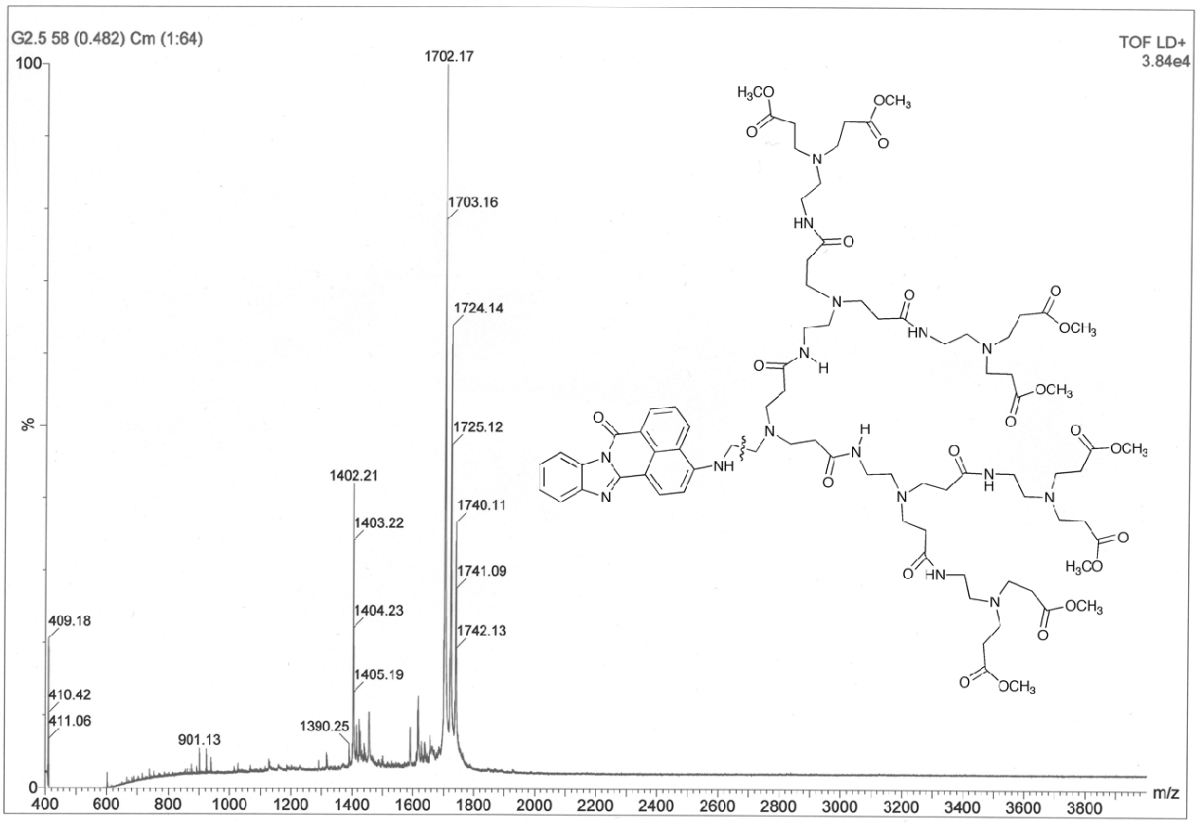

SI Fig. 3. MALDI-MS spectra of **7** showing the lack of potential defects that could be introduced during the divergent synthesis. The peak at 1402 appears to be due to fragmentation of the C-C bond at the position shown on the molecular structure. It does not correspond to any likely defect.